Millstone Power Station Unit 2
Safety Analysis Report

Chapter 3: Reactor

CHAPTER 3—REACTOR

Table of Contents

CHAPTER 3—REACTOR
Table of Contents (Continued)

CHAPTER 3—REACTOR
Table of Contents (Continued)

CHAPTER 3—REACTOR
Table of Contents (Continued)

CHAPTER 3—REACTOR

List of Tables

NOTE: REFER TO THE CONTROLLED PLANT DRAWING FOR THE LATEST REVISION.

CHAPTER 3—REACTOR

List of Figures

NOTE: REFER TO THE CONTROLLED PLANT DRAWING FOR THE LATEST REVISION.

CHAPTER 3-REACTOR
List of Figures (Continued)

CHAPTER 3 – REACTOR

3.1 SUMMARY DESCRIPTION

The reactor is of the pressurized water type using two reactor coolant loops. A vertical cross section of the reactor is shown in Figure 3.1–1. The reactor core is composed of 217 fuel assemblies, 73 control element assemblies (CEA) and up to four neutron source assemblies. The fuel assemblies are arranged to approximate a right circular cylinder with an equivalent diameter of 136 inches and an active length of 136.7 inches. The fuel assemblies are comprised of a structure and fuel and poison rods. The structure, which provides for 176 rod positions, consists of five guide tubes attached to spacer grids and is enclosed at the top and bottom by end fittings. Each of the guide tubes replaces four fuel rod positions and provides a channel which guides the control element over its entire length of travel. In selected fuel assemblies the central guide tube houses in-core instrumentation. The reactor is currently fueled by assemblies produced by AREVA.

The fuel is low enrichment UO_2 in the form of ceramic pellets and encapsulated in zirconium alloy tubes. These tubes are seal welded as hermetic enclosures.

Figure 3.1–2 shows a view of the reactor core cross section and some dimensional relations between fuel assemblies, fuel rods and CEA guide tubes.

The reactor internals support and orient the fuel assemblies and CEAs, absorb the static and dynamic loads and transmit the loads to the reactor vessel flange, provide a passage way for the reactor coolant, and guide in-core instrumentation.

The internals will safely perform their function during normal operating, upset and emergency conditions. The internals are designed to safely withstand the forces due to dead weight, pressure differential, flow impingement, temperature differential, vibrations and seismic acceleration. All reactor components are considered category 1 for seismic design. The reactor internals design limits deflection where required by function. Where necessary, components have been subjected to fatigue analysis. Where appropriate, the effect of neutron irradiation on the materials concerned is included in the design evaluation. The effects of shock loadings on the internals is included in the design analysis.

Reactivity control is provided by two independent systems: The control element drive system (CEDS) and the chemical and volume control system (CVCS). The CEDS controls short term reactivity changes and is used for rapid shutdown. The CVCS is used to compensate for long term reactivity changes and can make the reactor subcritical without the benefit of the CEDS. The design of the core and the reactor protective system (RPS) prevents fuel damage limits from being exceeded for any single malfunction in either of the reactivity control systems.

The CEAs consist of five poison rods (control elements) assembled in a square array, with one rod in the center. The rods are connected to a spider casting which is coupled to the control element drive mechanism (CEDM) shaft. There are a total of 73 CEAs. Some CEAs are mechanically connected in pairs and are known as dual CEAs.

Both dual and single CEAs are maneuvered by magnetic jack type CEDM's mounted on the reactor vessel head.

The maximum reactivity worth of the CEAs and the associated reactivity addition rate are limited by core, CEA and CEDS design to prevent sudden large reactivity increases. The design restraints are such that reactivity increases will not result in violation of the fuel damage limits, rupture of the reactor coolant pressure boundary (RCPB), or disruption of the core or other internals sufficient to impair the effectiveness of emergency cooling.

The fuel management scheme employed replaces approximately 40 percent of the core each refueling. Sufficient margin is provided to ensure that peak burnups of the individual fuel assemblies are within acceptable limits.

The nuclear design of the core will ensure that the combined response of all reactivity coefficients to an increase in reactor thermal power yields a net decrease in reactivity and that CEAs are moved in groups to satisfy the requirements of shutdown, power level changes and operational maneuvering. The control systems are designed to produce power distributions that are within the acceptable limits on overall nuclear heat flux factor (F^N_Q) and departure from nucleate boiling ratio (DNBR). The RPS and administrative controls ensure that these limits are not exceeded.

The reactor coolant enters the upper section of the reactor vessel through four inlet nozzles, flows downward between the reactor vessel shell and the core barrel, and passes through the flow skirt and into the lower plenum where the flow distribution is equalized. The coolant then flows upward through the core removing heat from the fuel rods, exits from the reactor vessel through two outlet nozzles and passes through the tube side of the vertical "U" tube steam generators where heat is transferred to the secondary system. The reactor coolant pumps (RCPs) return the coolant to the reactor vessel.

The principal objective of the thermal–hydraulic design is to avoid fuel damage during normal operation and anticipated transients. It is recognized that there is a small probability of limited fuel damage in certain situations as discussed in Chapter 14.

In order to meet the objective of the thermal–hydraulic design the following design limits are established, but violation of either is not necessarily equivalent to fuel damage:

a. There is a high confidence level that departure from nuclear boiling (DNB) is avoided during normal operation and anticipated transients. This is achieved by confirming the minimum DNBR calculated according to the HTP correlation (Reference 3.1-1) is greater than the 95/95 limit for the correlation;

b. The melting point of the UO_2 fuel is not reached during normal operation or anticipated transients.

The RPS and the reactor control system (RCS) provide for automatic reactor trip or corrective actions before these design limits are exceeded.

The core design bases are presented in Section 3.2; the core mechanical design is discussed in Section 3.3; the nuclear design of the core is discussed in Section 3.4; and the thermal and hydraulic design is discussed in Section 3.5.

3.1.1 REFERENCES

3.1-1 EMF-92-153(P)(A) Rev. 1, “HTP: Departure From Nucleate Boiling Correlation for High Thermal Performance Fuel,” Siemens Power Corporation, January 2005.

FIGURE 3.1–1 REACTOR VERTICAL ARRANGEMENT

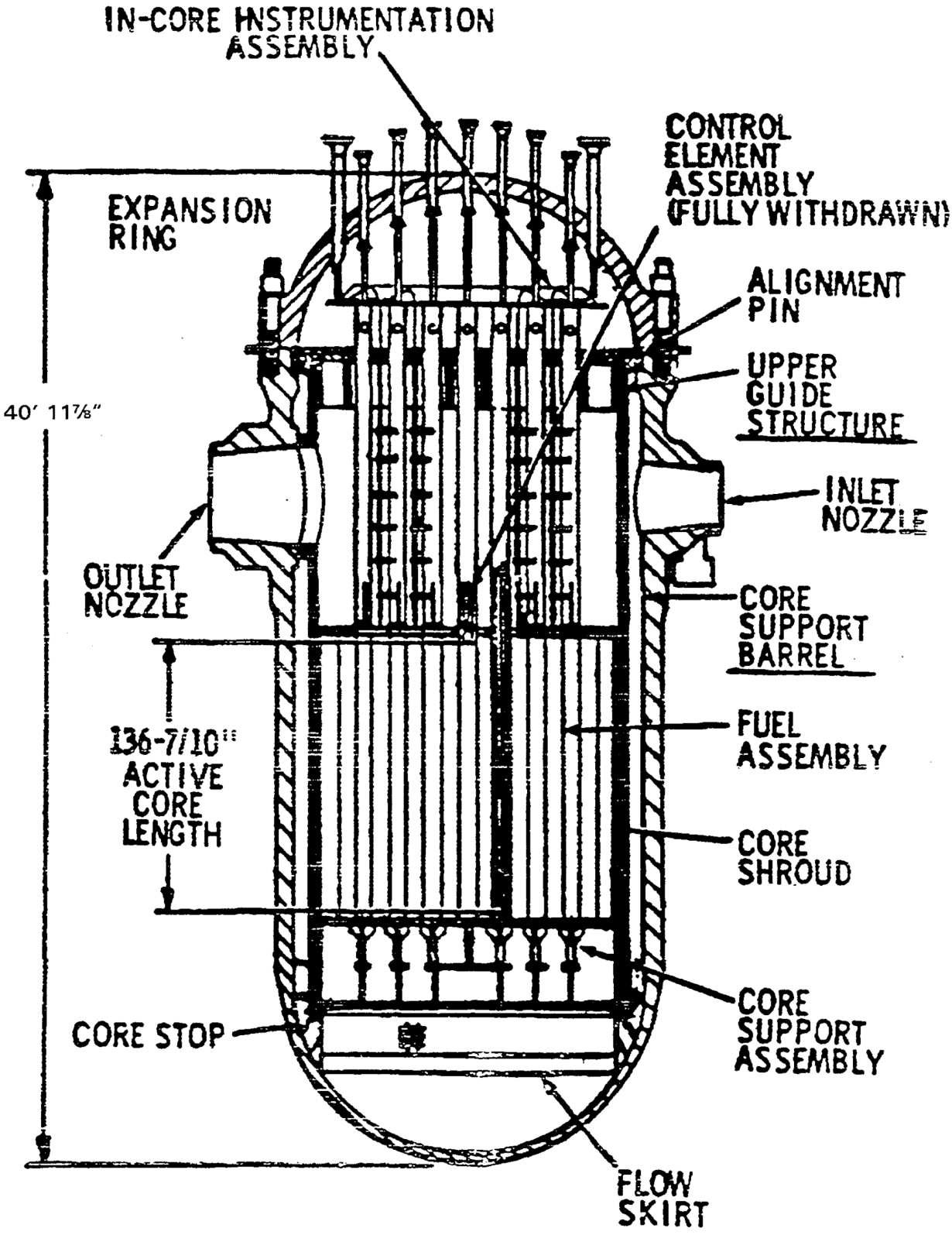

FIGURE 3.1–2 REACTOR CORE CROSS SECTION

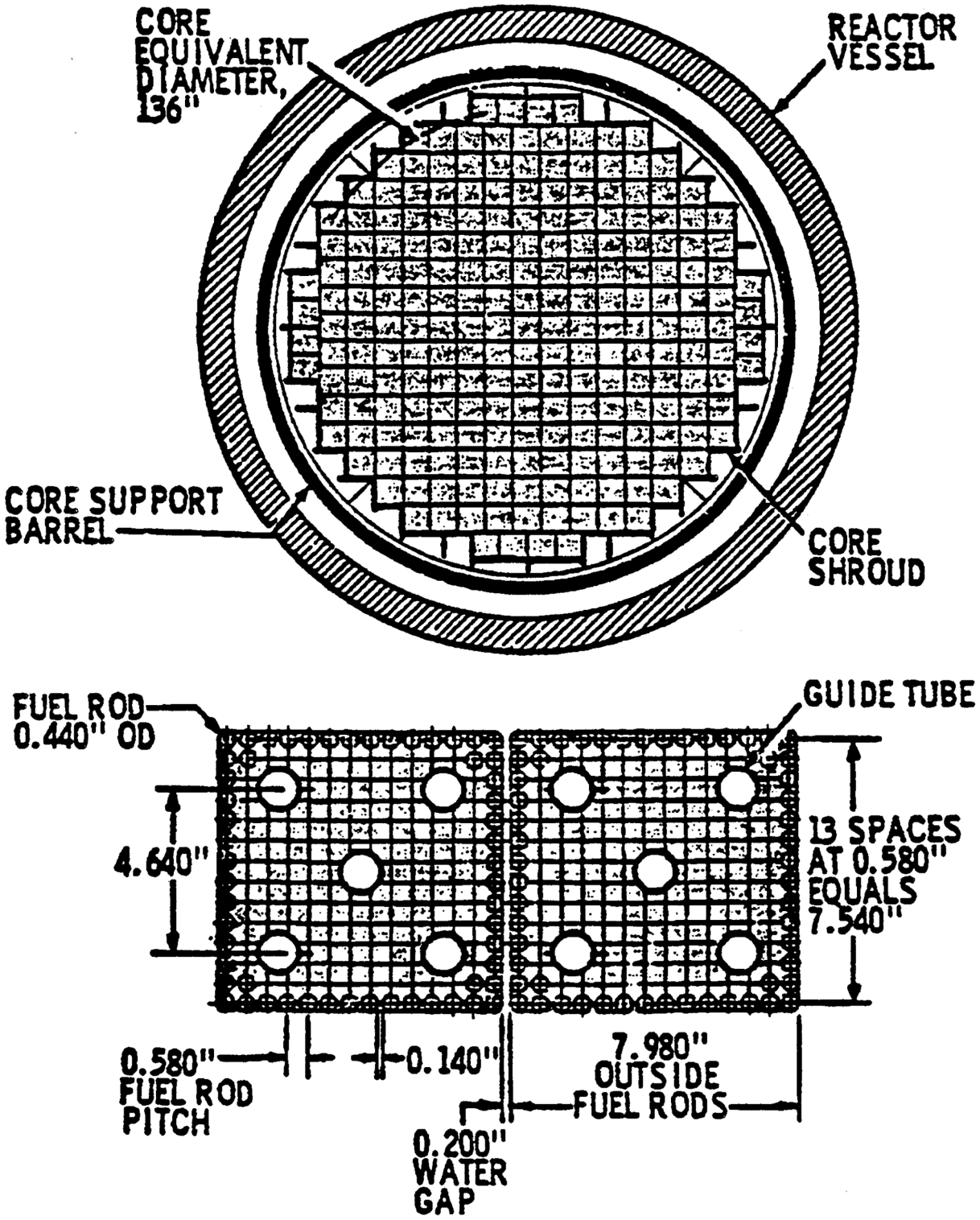

3.2 DESIGN BASES

The full power thermal rating of the core is 2,700 MWt. The physics and thermal and hydraulic information presented in this section is based on this core power level.

3.2.1 MECHANICAL DESIGN BASES

3.2.1.1 Fuel Assembly Design Bases

The design bases for evaluating the structural integrity of AREVA fuel assemblies are:

A. Fuel Assembly Handling

The fuel assembly is evaluated for dynamic axial loads of approximately 2.5 times the fuel assembly weight.

B. For All Applied Loads for Normal Operation and Anticipated Operational Events

Fuel assembly component strength is evaluated against either prototype testing or elastic stress analysis. When the stress analysis method is used, the stress limits presented in the ASME Boiler and Pressure Vessel Code, Section III, Division 1, are used as a guide.

The stress design limits for structural components are:

$$P_m \leq 1.0S_m$$
$$P_m + P_b \leq 1.5S_m$$
$$P + Q \leq 3.0S_m$$

where:

P_m is the primary membrane stress intensity
P_b is the primary bending stress intensity
P is the primary stress intensity
Q is the secondary stress intensity

The design stress, S_m is identified in the ASME Boiler and Pressure Vessel Code for austenitic stainless steel as a function of temperature. In the case of Zircaloy, which is not specifically identified in the ASME Boiler and Pressure Vessel Code, the design stress is identified as the lesser of two-thirds the yield stress, S_y, or one-third the ultimate stress, S_u.

The ASME Boiler and Pressure Vessel Code defines the stress intensity based on the maximum shear stress theory. The stress intensity is equal to one-half the largest algebraic difference between two principal stresses.

Primary stresses are developed by the imposed loading which is necessary to satisfy the laws of equilibrium between external and internal forces and moments. The basic characteristic of a primary stress is that it is not self-limiting. If a primary stress exceeds the yield strength of the material through the entire wall thickness, the prevention of failure is entirely dependent on the strain-hardening properties of the material.

Secondary stresses are developed by the self-constraint of a structure. It must satisfy an imposed strain pattern rather than being in equilibrium with an external load. The basic characteristic of a secondary stress is that it is self-limiting. Local yielding and minor distortions can satisfy the discontinuity conditions due to thermal expansions which cause the stress to occur.

C. Loads during Postulated Accidents

Deflection or failure of components shall not interfere with reactor shutdown or emergency cooling of the fuel rods.

The fuel assembly structural component stresses under faulted conditions are evaluated using primarily the methods outlined in Appendix F of the ASME Boiler and Pressure Vessel Code, Section III. The current methods utilize the limits provided for elastic system analysis.

The design stress intensity value (S_m) is defined the same as for normal operating conditions.

Spacer grid crush load strength is based on the 95% confidence level on the true mean as taken from test measurements on unirradiated production grids at (or corrected to) operating temperature.

3.2.1.2 AREVA Fuel Rod Cladding Design Bases

A discussion of the AREVA fuel rod cladding is given as part of the AREVA fuel rod discussion in Section 3.3.1.1.

3.2.1.3 Control Element Assembly Design Bases

The CEA has been designed to ensure that the stress intensities in the individual structural components do not exceed the allowable limits for the appropriate material established in Section III of the ASME Boiler and Pressure Vessel Code. The exceptions to this criterion are that (a) the Inconel 625 cladding is permitted to sustain plastic strain up to 3 percent due to irradiation induced expansion of the filler materials, and (b) because the ASME Code does not apply to springs, the allowable stresses for the CEA springs are based on values which have been proven in practice.

The CEA stress analyses consider the following load sources:

a. Internal pressure build up due to the effect of irradiation on B_4C (production of helium).

b. External pressure of reactor coolant (in the computation for determining the maximum stress in the cladding due to internal pressure, no internal pressure is assumed).

c. Dynamic stresses produced by seismic loading.

d. Dynamic loads produced by stepping motion of the magnetic jack.

e. Mechanical and hydraulic loads produced during SCRAM.

f. Cladding loads produced by differential expansion between clad and filler materials.

In addition to the comparison of calculated stress levels with allowable stresses, the fatigue damage produced by significant cyclic stresses is also determined. It is a design requirement that the calculated cumulative damage factor for any location may not be equal to or greater than 1.0. The fatigue usage factor calculations are based on the fatigue curves (stress range vs. number of cycles) contained in Section III of the ASME Boiler and Pressure Vessel Code.

3.2.1.4 Reactor Internals Design Bases

The reactor vessel internals are designed to meet the loading conditions and the design limits specified below. The materials used in fabrication of the reactor internal structures are primarily Type 304 stainless steel. The flow skirt is fabricated from Inconel. Welded connections are used where feasible; however, in locations where mechanical connections are required, structural fasteners are used which are designed to remain captured in the event of a single failure. Structural fastener material is typically a high strength austenitic stainless steel; however, in less critical applications, Type 316 stainless steel is employed. Hardfacing, of Stellite material, is used at wear points. The effect of irradiation on the properties of the materials is considered in the design of the reactor internal structures.

A. Categorization and Combination of Loadings

1. Normal Operating and Upset Conditions

The reactor vessel internals are designed to perform their functions safely without shutdown. The combination of design loadings for these conditions are the following:

Normal operating temperature differences

Normal operating pressure differences

Low impingement loads

Weights, reactions and superimposed loads

Vibration loads

Shock loads (including OBE)

Transient loadings of frequent occurrences not requiring shutdown

Handling loads

2. Emergency Conditions

The internals are designed to permit an acceptable amount of local yielding while experiencing the loadings listed above with the SSE load replacing the OBE load.

3. Faulted Conditions

Permanent deformation of the reactor internal structures is permitted. The loadings for these conditions include all the loadings listed for emergency conditions plus the loadings resulting from the postulated LOCA.

B. Design Limits

Reactor internal components are designed to ensure that the stress levels and deflections are within an acceptable range. The stress values for core support structures are not greater than those given in the May 1972 draft of Section III of the ASME Boiler and Pressure Vessel Code, Subsection NG, including Appendix F, “Rules for Evaluation of Faulted Conditions.” Stress limits for the reactor vessel core support structures are presented in Table 3.2-1. In addition, to properly perform their functions, the reactor internal structures will satisfy the deformation limits listed below.

1. Under design loadings plus operating basis earthquake forces or normal operating loadings plus SSE forces, deflections will be limited so that the CEAs can function and adequate core cooling is preserved.

2. Under normal operating loadings plus SSE forces plus pipe rupture loadings resulting from a break of the largest line connect to the primary system piping, deflections will be limited so that the core will be held in place, adequate core cooling is preserved, and all CEAs can be inserted. Those deflections which would influence CEA movement will be limited to less than 80 percent of the deflections required to prevent CEA insertion.

3. Under normal operating loadings plus SSE forces plus the maximum pipe rupture loadings resulting from the full spectrum of pipe breaks, deflections will be limited so that the core will be held in place and adequate core cooling is preserved. Although CEA insertion is not required for a safe and orderly shutdown for break sizes greater than the largest line connected to the primary system piping, calculations show that the CEAs will be insertable for larger breaks except for a

few CEAs located near the vessel outlet nozzle which is feeding the postulated rupture.

3.2.1.5 CEDM/RVLMS (HJTC) Pressure Housing Design Bases

The control element drive mechanism and Reactor Vessel Level Monitoring System (RVLMS) pressure housings form part of the reactor coolant boundary and are, therefore, designed to meet the stress requirements consistent with those of the reactor vessel closure head. The limiting stresses in the CEDM's and RVLMS pressure boundary components due to the design, Level A, Level B, Level C, Level D and Test conditions satisfy ASME Boiler Pressure Vessel Code, Section III, Subsection NB plus Appendix 1 and Section II, Part D, 1998 Edition through 2000 Addenda, including Code Case N-4-12 for the CEDM motor housing material.

The CEDMs and the RVLMs are designed to function normally during and after exposure to normal operating conditions plus the design basis earthquake (DBE). Under normal operating conditions, plus DBE, plus pipe rupture loadings, deflections of the CEDM will be limited so that the CEAs can be inserted after exposure to these conditions. Those deflections, which could influence CEA movement, will be limited to less than 80 percent of the deflections required to prevent CEA movement. The RVLMS and the adjacent CEDMs do not contact each other with maximum lateral displacement of the pressure housings.

Loading Combinations		**ASME Code Subsection**
Design Condition	$P_m \leq S_m$	NB-3221
	$P_l \leq 1.5S_m$	
	$P_l + P_b < 1.5S_m$	
Level A and Level B	$P_l + P_b + Q \leq 3S_m$	NB-3222 and NB3223
(Normal and Upset)	$U \leq 1$	
Level C Condition	$P_m \leq$ greater of $[1.2S_m, S_y]$	NB-3224
(Emergency)	$P_l + P_b \leq$ greater of $[1.8S_m, 1.5S_y]$	
Level D Condition	$P_m \leq$ lesser of $[2.4S_m, 0.7S_u]$	Paragraph F-1330 or F-1340, Appendix F
(Faulted)	$P_l + P_b \leq$ lesser of $[3.6S_m, 1.05S_u]$	
Test Conditions	$P_m \leq 0.9S_y$	NB-3226
	$P_m + P_b \leq 1.35S_y$ when $P_m \leq 0.67S_y$ or $P_m + P_b \leq (2.15\ S_y - 1.2P_m)$ when $0.67S_y < P_m \leq 0.9S_y$	
Design Condition	$P_m \leq S_m$	NB-3221
Shear Stress	$\leq 0.6S_m$	NB-3227.2

where

P_m = General primary membrane stress intensity
P_l = Primary local membrane stress intensity
$P_l + P_b$ = Primary membrane plus bending stress intensity
$P_l + P_b + Q$ = Primary plus secondary stress intensity
S_m = Design stress intensity
S_y = Yield strength
S_u = Tensile strength
U = Cumulative fatigue usage factor

3.2.2 NUCLEAR DESIGN BASES

The initial full power thermal rating of the core is 2700 MWt. It is upon this power level that the physics and thermal and hydraulic information presented in this section are based. The design basis for the nuclear design of the fuel and reactivity control systems are:

a. Excess Reactivity and Fuel Burnup

The excess reactivity provided for each cycle is based on the depletion characteristics of the fuel and burnable poison and the desired burnup for each cycle. The desired burnup is based on the economic analysis of both the fuel cost and the projected operating load demand cycle for the plant. The average burnup in the core is chosen so as to insure that the peak assembly burnup is not greater than 56,000 MWD/MTU for Batch N, 52,500 MWD/MTU for Batch P, and 57,400 MWD/MTU for Batch R and later.

b. Core Design Lifetime and Fuel Replacement Program

The core design lifetime and fuel replacement program are based on a three region core with approximately 40 percent of the fuel assemblies replaced at each refueling.

c. Negative Reactivity Feedback and Reactivity Coefficients

The negative reactivity feedback provided by the design is based on the requirement of General Design Criterion (GDC) 11. In the power operating range, the inherent combined response of the reactivity feedback characteristics (fuel temperature coefficient (FTC), moderator temperature coefficient (MTC), moderator void coefficient (MVC), and moderator pressure coefficient (MPC)) to an increase in reactor thermal power will be a decrease in reactivity.

d. Burnable Poison Requirements

The burnable poison reactivity worth provided in the design will be sufficient to ensure that moderator coefficients of reactivity have magnitudes and algebraic signs consistent with the requirements for negative reactivity feedback and acceptable consequence in the event of postulated accidents or anticipated operational occurrences, viewed in conjunction with the supplied protective equipment.

e. Stability Criteria

The design of the reactor and the instrumentation and control systems is based on meeting the requirements of GDC 12 with respect to spatial oscillations and stability. Sufficient CEA rod worth will be available to suppress xenon-induced power oscillations.

f. Maximum Controlled Reactivity Insertion Rates

The maximum reactivity addition rates are limited by core, CEA, and reactor regulating system (RRS) design based on preventing increases in reactivity which would result in the violation of specified acceptable fuel design limits, damage to the reactor pressure boundary, or disruption of the core or other internals sufficient to impair the effectiveness of emergency core cooling.

g. Power Distribution Control

Acceptable operation of the reactor in the absence of an accidental transient depends on maintaining a relationship among many parameters, some of which depend on the power distribution. In the absence of an accidental transient the power distribution is controlled such that in conjunction with other controlled parameters, limiting conditions of operation (LCO) are not violated. LCO are not less conservative than the initial conditions used in the accident analyses in Chapter 14. LCO and limiting safety system settings (LSSS) are determined such that specified acceptable fuel design limits are not violated as a result of anticipated operational occurrences and such that specified predicted acceptable consequence are not exceeded for other postulated accidents.

h. Shutdown Margins and Stuck Rod Criteria

The amount of reactivity available from insertion of withdrawn CEAs is required to be sufficient, under all power operating conditions, to ensure that the reactor can be brought to at least 3.6 percent $\Delta\rho$ subcritical from the existing condition, including the effects of cooldown to an average coolant temperature of 532°F, even when the highest worth CEA fails to insert. This criteria is exclusive of any safety allowance and is consistent with the most pessimistic analysis in Chapter 14.

i. Chemical Shim Control

The chemical and volume control system (CVCS) (Section 9.2) is used to adjust dissolved boron concentration in the moderator. After a reactor shutdown, this system is able to compensate for the reactivity changes associated with xenon decay and reactor coolant temperature decrease to ambient temperature. It also provides adequate shutdown margin during refueling. This system also has the capability of controlling long term reactivity changes due to fuel burnup, and reactivity changes during xenon transients resulting from changes in reactor load independently of the CEAs. In particular, any xenon transient may be accommodated at any time in the fuel cycle.

3.2.3 THERMAL AND HYDRAULIC DESIGN BASIS

Avoidance of thermally induced fuel damage during normal steady state and anticipated transient operation is the principal thermal and hydraulic design basis. It is recognized that there is a small probability of limited fuel damage in certain unlikely accident situations discussed in Chapter 14.

The following corollary design basis are established, but violation of them is not necessarily equivalent to fuel damage.

a. A limit corresponding to 95% probability with 95% confidence (Reference 3.2-1) is set on the departure from nucleate boiling ratio (DNBR) during normal operation and any anticipated transients as calculated according to the HTP correlation.

b. The peak temperature of the fuel will be less than the melting point during normal operation and anticipated transients.

The reactor control and protection system will provide for automatic reactor trip or other corrective action before these design limits are exceeded.

The core hydraulic resistance was considered in establishing the operational limits curves provided in Figures 4.5–4 and 4.5–5, and the Low Temperature Overpressure Protection (LTOP) System described in Section 7.4.8. The effect on the RCS flow resistance due to changes in fuel design will be evaluated to determine the impact.

3.2.4 REFERENCES

3.2-1 EMF-92-153(P)(A) Rev. 1, “HTP: Departure From Nucleate Boiling Correlation for High Thermal Performance Fuel,” Siemens Power Corporation, January 2005.

TABLE 3.2-1 STRESS LIMITS FOR REACTOR VESSEL INTERNAL STRUCTURES

Operating Conditions	Stress Categories and Limits of Stress Intensities
1. Normal and Upset	Figure NG 3221.1 including notes
2. Emergency	Figure NG 3224.1 including notes
3. Faulted	Appendix F, Rules for Evaluating Faulted Conditions

3.3 MECHANICAL DESIGN

The reactor core and internals are shown in Figure 3.3–1A. A cross section of the reactor core and internals is shown in Figure 3.1–2. Mechanical design features of the reactor internals, the control element drive mechanisms (CEDM) and the core are described below. Mechanical design parameters are listed in Table 3.3-1.

3.3.1 CORE MECHANICAL DESIGN

The core approximates a right circular cylinder with an equivalent diameter of 136 inches and an active height of 136.7 inches. It is made up of zirconium alloy clad fuel rods containing slightly enriched uranium in the form of sintered UO_2 pellets and UO_2-Gd_2O_3 pellets. The fuel rods are grouped into 217 assemblies.

Short term reactivity control is provided by 73 control element assemblies (CEA). The CEAs are guided within the core by the guide tubes which are integral parts of the fuel assemblies.

3.3.1.1 AREVA Fuel Rod

The detailed fuel rod design (see Figures 3.3–1A and 3.3–1B) establishes such parameters as pellet diameter and length, density, cladding-pellet diametral gap, fission gas plenum size, and rod pre-pressurization level. The design also considers effects and physical properties of fuel rod components which vary with burnup.

The integrity of the fuel rods is ensured by designing to prevent excessive fuel temperatures, excessive internal rod gas pressures, and excessive cladding stresses and strains. This end is achieved by designing the fuel rods to satisfy the design criteria (Reference 3.3-12) during normal operation and anticipated operational occurrences over the fuel lifetime. For each design criteria, the performance of the most limiting fuel rod shall not exceed the specified limits.

Fuel rods are designed to function throughout the design life of the fuel based upon the reactor operating conditions designated below without loss of mechanical integrity, significant dimensional distortion, or release of fuel or fission products.

The assemblies were evaluated for a peak assembly burnup of 56,000 MWD/MTU for Batch N, 52,500 MWD/MTU for Batch P, and 57,400 MWD/MTU for Batch R and later.

The Millstone Unit 2 Cycle 19 reload core included four fuel assemblies with natural uranium replacement fuel rods with an anti-rotation feature designed to prevent spinning of the rod during operations. The four assemblies containing replacement rods, and the conditions under which they were evaluated for use, are discussed in Section 3.3.1.3.1, "Design Summary".

3.3.1.1.1 Fuel Rod Mechanical Criteria

The cladding primary and secondary stresses shall meet the 1977 ASME Boiler and Pressure Vessel Code Section III (Reference 3.3-1) requirements summarized below:

Stress Intensity Limits

Zircaloy-4 Fuel Rod Cladding		
(*Parameter*)	Yield Strength	Ultimate Tensile Strength
Primary Membrane (P_m)	$< 2/3\ S_y$	$< 1/3\ S_u$
Primary Membrane Plus Primary Bending ($P_m + P_b$)	$< 1.0\ S_y$	$< 0.5\ S_u$
Primary Plus Secondary ($P + Q$)	$< 2.0\ S_y$	$< 1.0\ S_u$
M5® Fuel Rod Cladding		
(*Parameter*)	Yield Strength	
Primary Membrane (P_m)	$< 1.0\ S_y$ (Compression) $< 2/3\ S_y$ (Tension)	
Primary Membrane Plus Primary Bending ($P_m + P_b$)	$< 1.0\ S_y$	
Primary Plus Secondary ($P + Q$)	$< 2.0\ S_y$	
The M5® cladding stress intensity limits are based on hoop yield strength per Reference 3.3-11.		

Primary stresses are developed by the imposed loading which is necessary to satisfy the laws of equilibrium between external and internal forces and moments. The basic characteristic of a primary stress is that it is not self-limiting. If a primary stress exceeds the yield strength of the material through the entire thickness, the prevention of failure is entirely dependent on the strain-hardening properties of the material.

Secondary stresses are developed by the self constraint of a structure. It must satisfy an imposed strain pattern rather than being in equilibrium with an external load. The basic characteristic of a secondary stress is that it is self-limiting. Local yielding and minor distortions can satisfy the discontinuity conditions due to thermal expansions which cause the stress to occur.

Cladding circumferential strain shall not exceed the design limit through end-of-life (EOL).

The total uniform strain, elastic and plastic shall not exceed the design limit during a transient. The strain analysis was performed with the RODEX2 (Reference 3.3-2) RAMPEX codes benchmarked to available power ramp test data, i.e., INTERRAMP, OVERRAMP, and SUPERRAMP.

The fuel rod shall be designed such that at a rod average burnup when substantial axial consolidation has occurred, the total clad creep deformation shall not exceed the initial minimum diametral fuel cladding gap. This will prevent pellet hangups allowing the plenum spring to close axial gaps until densification is substantially complete, thus preventing the formation of pellet column gaps of sufficient size for clad flattening.

The fuel rod pressure at EOL shall not exceed the criteria approved by the NRC (Ref. 3.3-3). A review of departure from nucleate boiling ratio (DNBR) limits for condition III or IV postulated accidents events is required for fuel rods that exceed nominal system pressure. When fuel rod pressure is predicted to exceed system pressure, the pellet-cladding gap shall not increase for steady or increasing power conditions. Analysis approved by the NRC has shown that the fuel rod gas pressure can safely exceed system pressure without causing any damage to the cladding.

Total cladding wall thinning due to generalized external and internal corrosion shall not exceed a value which will impair mechanical performance over the projected fuel rod design lifetime under the most adverse projected power conditions within coolant chemistry limits recommendations of Table 3.3-2. It will also assure that the metal/oxide interface temperature will remain well below the level where large increases in corrosion, due to the insulating effect of the oxide, would adversely affect the mechanical behavior of the cladding.

The cumulative usage factor for cyclic stresses for all important cyclic loading conditions shall not exceed the design limit.

The clearance between the upper and lower tie plate shall be able to accommodate the maximum differential fuel rod and fuel assembly growth to the designed burnup.

The centerline temperature of the hottest pellet shall be below the melting temperature. Fuel centerline temperature is calculated at overpower conditions to verify that fuel pellet overheating does not occur during normal operation and anticipated operational occurrences.

3.3.1.1.2 Fuel Rod Design Analyses

Each design analysis was performed with Framatome methodology which involves a well defined selection of appropriate data and parameters, and the latest approved versions of computer codes. This methodology, as required, has been submitted to the Nuclear Regulatory Commission (NRC) and approved. The analysis is performed in accordance with the methods described in Framatome’s “Qualification of Exxon Nuclear Fuel For Extended Burnup” (Reference 3.3-3) and “Qualification of Advanced Nuclear Fuels' PWR Design Methodology for Rod Burnups of 62 GWd/MTU” (Reference 3.3-13).

The impact of fuel thermal conductivity degradation (TCD) with burnup has been considered and included in the fuel rod analyses consistent with the NRC's approval of Framatome treatment of fuel TCD in Reference 3.3-12.

The cladding steady state stress analysis was performed by considering primary and secondary membrane and bending stresses due to hydrostatic pressure, flow-induced vibration, spacer contact, pellet cladding interaction (PCI), thermal and mechanical bow and thermal gradients. Stresses were calculated for the various combinations of the following conditions:

a. beginning of life (BOL) and EOL

b. cold and hot conditions

c. at mid-span and at spacer locations

d. at both the inner and outer surfaces of the cladding

The analysis was performed for the various sources of stress, including pressure, thermal, spacer contact, PCI, and rod bow. The applicable stresses at each orthogonal direction were combined to calculate the maximum stress intensities which are compared to the ASME design criteria. The results of the analysis indicate that all stress values are within acceptable design limits for both BOL and EOL, hot and cold conditions. The EOL stresses have ample margin for both the hot and cold condition stresses.

The cladding steady state strain is evaluated with the RODEX2 code, which has been approved by the NRC (Reference 3.3-2). The code considers the thermal-hydraulic environment at the cladding surface, the pressure inside the cladding, and the thermal, mechanical and compositional state of the fuel and cladding. Pellet density, swelling, densification, and fission gas release or absorption models, and cladding and pellet diameters are input to RODEX2 to provide the most conservative strain calculation or subsequent ramping or collapse calculations for the reference fuel rod design. The major fuel rod performance characteristics modeled by the RODEX2 code are:

a. Radial Thermal Conduction and Gap Conductance

b. Fuel Swelling, Densification, Cracking, and Crack Healing

c. Gas Release and Absorption

d. Cladding Creep Deformation and Irradiation-Induced Growth

e. Cladding Corrosion

f. PCI

g. Free Rod Volume and Gas Pressure

The calculations are performed on a time incremental basis with conditions updated at each calculated increment so that the power history and path dependent processes can be modeled. The axial dependence of the power and burnup distributions are handled by dividing the fuel rod into a number of axial and radial regions. Power distributions can be changed at any desired time, and the coolant and cladding temperatures are readjusted in all the regions. All the performance models, e.g., giving the deformations of the fuel and cladding and gas release, are calculated at successive times during each period of assumed constant power generation. The calculated cladding strain is reviewed throughout the life of the fuel and both the maximum circumferential strain and the maximum strain increment are compared with the design criteria. The calculated strain did not exceed the strain limit. Both the maximum strain and the positive strain increment are below the design limit strain.

The ramping strain and the fatigue evaluation of the fuel rod were evaluated. The ramps are assumed to occur anytime during the irradiation and may reach the maximum peaking factor allowed by the limits of operation. The ramps are analyzed either from cold shutdown or from a variety of hot powered starting conditions. The approach to rated power at the beginning of each reactor cycle is performed to satisfy the AREVA maneuvering and conditioning recommendations. The clad response during ramping power changes is calculated with the RAMPEX code. This code calculates the PCI during a power ramp for one axial node at a time. The initial conditions are obtained from RODEX2 output. The RAMPEX code considers the thermal condition of the rod in its flow channel, and the mechanical interactions that result from fuel and cladding creep at any desired axial section in the rod during the power ramp. As compared to RODEX2, RAMPEX additionally models the pellet cladding axial stress interaction, primary creep with strain hardening, the effects of pellet chips, and localized stresses due to ridging.

The RAMPEX code provides the hoop stress and the stress intensity. The stress results of the ramping analysis are used to evaluate the cladding fatigue damage through life due to the cyclic power variations. The fatigue analysis is based on the O'Donnel and Langer (Reference 3.3-4) design curve. The cyclic amplitudes of the maximum local stress intensity, as determined by RAMPEX over the power cycling range, are compared with this curve to determine the allowed cycles for each stress range. This result is combined with the projected number of duty cycles to determine a fatigue usage factor. All of the reactor cycle (startup) ramp stresses were within the design limit.

Creep collapse calculations are performed with RODEX2 and COLAPX codes. The RODEX2 code determines the cladding temperature and internal pressure history based on a model which accounts for changes in fuel rod volumes, fuel densification and swelling, and fill gas absorption. The reactor coolant, fuel rod internal temperature, and pressure histories generated by the RODEX2 analysis are input to the COLAPX code along with a conservative statistical estimate of initial cladding ovality and the fast flux history. The COLAPX code calculates, by large deflection theory, the ovality of the cladding as a function of time while the uniform cladding creepdown is obtained by the RODEX2 analysis. The cladding ovality increase and creepdown are summed, at a rod average burnup when substantial axial consolidation has occurred, to show that they remain less than the initial minimum pellet clad gap. Measurements of highly densifying irradiated fuel have demonstrated that pellet densification is essentially complete by the time the fuel has attained this burnup so that further creepdown after this phase will not result in significant pellet to pellet gaps. The combined radial creepdown was shown to meet the design criteria. This will prevent pellet hangups due to cladding creep, allowing the plenum spring to close axial gaps until densification is substantially complete, and thus assures that clad collapse will not occur. The pitch of the plenum spring is less than the spacing calculated for stiffening rings in a cylindrical shell under external pressure which will prevent clad collapse in the plenum area.

Calculation of the gas pressure within a fuel rod is performed with the RODEX2 code. The initial fill gas is found by calculating the initial free volume and using the ideal gas law, along with input values for fill gas pressure and reference fill gas temperature. The free gaseous fission product yield is calculated for each axial region and the total yield obtained by summing the axial region contributions. The power of each history used was multiplied for each cycle by a factor required

for the highest projected rod power to reach the F_r limit plus uncertainties. The calculations show that for all power histories analyzed, the rod internal gas pressure will remain below the criteria approved by the NRC (Reference 3.3-3) for use in extended burnup gas pressure analysis.

The waterside corrosion of fuel rods is evaluated with the MATPRO-11 (Reference 3.3-5) correlation. The MATPRO-11 model is a two-stage corrosion rate model which is cubic in dependence on oxide thickness until a transition to a subsequent linear dependence occurs. To calculate the rate changes as a function of both oxide thickness and the operating conditions of the fuel rod, the MATPRO model is incorporated into AREVA's RODEX2 fuel performance code. The RODEX2 code determines the temperature increase of the water along the fuel rod assuming heat balance within a channel for the prescribed mass flow and inlet temperature. The radial temperature drops are evaluated successively between the water, the oxide surface, the metal/ oxide interface, and the inside of the cladding using RODEX2 correlations and methods. To account for the change in corrosion rate due to the changing oxide layer and thermal conditions, the code includes an update in cladding temperature at every calculation step. This is an iterative process due to the continuously changing oxide thickness. Conditions are also revised at times where new power or flow conditions are prescribed. The MATPRO model incorporated in RODEX2 is benchmarked via an overall enhancement factor to oxide thickness data from assemblies in seven separate reactors. Each data point represents the maximum thickness measured along a rod length. The enhancement factor is based on a best fit regression analysis of the data. A final multiplier is also applied which envelopes the data. The waterside corrosion in the cladding was evaluated with RODEX2 for the steady state strain analysis. A best-fit corrosion amplification factor was applied to the MATPRO model along with a final multiplier to bound the measured data on AREVA standard cladding. The maximum calculated oxide thickness was below the design limit.

Fuel rod and fuel assembly growth projected to occur during irradiation was based on conservative design curves established from measured irradiation growth data. The rod growth minus the assembly growth plus tolerances was compared with the clearance within the assembly for fuel rod growth. Differential thermal expansion between the fuel rods and guide tubes was also considered. There is space between the upper and lower tie plates to accommodate the maximum differential growth out to a rod burnup of 62,000 MWd/MTU.

The pellet centerline temperature calculation was performed with the RODEX2 code. Fuel pellet centerline temperatures were calculated at overpower conditions. The high power cycle of each power history was modified to include a spike in each cycle. This spike increased the maximum power of a pellet in the rod up to F^T_Q. Pellet melting temperature is a function of burnup. Considering a conservative peak pellet burnup to determine the minimum pellet melting temperature at EOL, the maximum pellet centerline temperature is well below both BOL and EOL limits.

3.3.1.2 (Deleted)

3.3.1.3 AREVA Fuel Assembly

3.3.1.3.1 Design Summary

The AREVA fuel assemblies are 14 by 14 arrays containing 176 fuel rods in a cage structure of 5 guide tubes and 9 spacer grids. Both the guide tubes and the fuel rod cladding are made of zirconium alloy for low neutron absorption and high corrosion resistance. The fuel assembly upper tie plates are stainless steel castings with Nickel Alloy X-750 holddown springs. The fuel assembly upper tie plate is mechanically locked to the guide tubes and may be easily removed to allow inspection of irradiated fuel rods. For Reload T (Cycle 15) and beyond, lower tie plates are the FUELGUARD™ debris resistant design.

In Reloads M, N, and P (Cycles 10-12), eight of the nine spacers in each fuel assembly are made of a Zircaloy-4 structure with Nickel Alloy 718 springs (i.e., bi-metallic spacer). The ninth spacer, located just above the lower tie plate, is made of Nickel Alloy 718 and, using features of the AREVA High Thermal Performance (HTP) spacer design, has been adapted to provide fuel assembly debris resistance.

The fuel assembly design for Reloads R and S (Cycles 13 and 14) has all nine spacers of the bimetallic design. Additionally, in this design a longer solid fuel rod lower end cap is used. The longer end cap serves to raise the fuel rod cladding above the debris trapping region of the ninth (bottom) spacer.

In Reloads T through X (Cycles 15-18), the High Thermal Performance (HTP) fuel assembly design was implemented in which all nine spacers are of the Zircaloy-4 HTP design. This design retained the longer, solid fuel rod lower end cap.

The fuel assembly design for Reload Y (Cycle 19) and later utilized eight Zircaloy-4 HTP spacers and replaces the ninth, bottom spacer with an Inconel High Mechanical Performance (HMP) spacer. The HMP spacer is similar to the HTP spacer, except that it is constructed of Nickel Alloy 718 and the flow channels are parallel to the fuel.

Drawings of the AREVA fuel assemblies are given in Figure 3.3–2A and Figure 3.3–3A. Fuel assembly drawings for Reload T (Cycle 15) and beyond are included in Figures 3.3–2B and 3.3–3B.

The fuel assembly design for Reload EE (Cycle 25) and later changes to the AREVA Standard CE-14 HTP™ fuel design. This design features M5® clad fuel rods with increased uranium loading (larger diameter pellet and increased theoretical density) and Zircaloy-4 MONOBLOC™ corner guide tubes.

The analysis has shown that the AREVA reload fuel assemblies will meet the design criteria:

a. The maximum steady state cladding strain is well below the design limit.

b. The maximum steady state cladding stress meets the ASME Boiler and Pressure Vessel Code requirements.

c. The transient strain is within the circumferential limit.

d. Cladding creep collapse is precluded.

e. The fuel rod internal pressure at the EOL remains below the criteria approved by the NRC (Ref. 3.3-3).

f. The maximum clad oxidation is below the design limit.

g. The cladding fatigue usage factor is well below the design limit.

h. There is space between the upper and lower tie plate to accommodate fuel rod growth.

i. Pellet centerline temperatures remain below the design criteria.

j. The fuel assembly growth is within the space available between the upper and lower core plates in the reactor core.

k. The assembly holddown springs will prevent bundle lift-off.

The fuel rods consist of short cylindrical UO_2 pellets or UO_2-Gd_2O_3 pellets contained in zirconium alloy tubular cladding. Zirconium alloy end caps are welded to each end to give a hermetic seal.

The fuel rod upper plenum contains a high strength alloy compression spring to prevent fuel column separation during fabrication and shipping, and during incore operation. The rods are pressurized with helium to improve heat transfer and reduce clad creep ovality.

The fuel assembly structure consists of an upper tie plate assembly, lower tie plate, guide tubes and spacer grids, which together provide the support for the fuel rods.

The lower tie plate is a machined stainless steel casting which provides the lower end support for the guide tubes. The zirconium alloy guide tubes are attached to the lower tie plate by means of Nickel Alloy X-750 cap screws. The FUELGUARD™ lower tie plate, included in Reload T and beyond provides protection to the fuel from debris in the primary coolant.

The upper tie plate assembly latches to and provides the upper end support for the guide tubes. The upper tie plate assembly consists of a stainless steel grid structure and reaction plate containing five Nickel Alloy X-750 holddown springs. The springs are located around Nickel Alloy X-750 locking nuts and sleeves which mechanically attach to the guide tubes and pilot into the reactor alignment plate. The springs are partially shrouded on the outside diameter by stainless steel cups to prevent flow induced spring vibration.

The guide tubes, in conjunction with the spacers and tie plates, form the structural skeleton of the fuel assembly and provide channels for insertion of the control rods. The guide tubes are fabricated from Zircaloy-4 tubing and are fully annealed. The center tube is of uniform diameter whereas the outer four guide tubes have a reduced diameter section at the bottom which produces a dashpot action to decelerate the dropped CEAs.

An end plug is welded to the lower end of the guide tube and is drilled and threaded to accept the lower cap screws. At the upper end, the guide tube is crimped into an external stainless steel locking sleeve which engages the upper tie plate assembly. The upper tie plate assembly is locked to the guide tube end fittings and can be unlocked for reconstitution or for fuel examination using special tools.

A stainless steel sleeve assembly with a chrome plated inside diameter is inserted in the top end of the guide tube assembly. This sleeve protects the guide tube from control rod fretting and wear when the rod is in the withdrawn/ready position. The sleeve is mechanically captured by the upper tie plate.

Fuel rod pitch and position is maintained by nine spacer grids. The spacers are axially positioned so that the assemblies will be compatible with existing fuel assemblies.

The bi-metallic spacers used in Reloads M through S (Cycles 10-14) are formed by an interlocking rectangular grid of Zircaloy-4 structural strips (see Figure 3.3–4A). Inconel-718 spring strips are mechanically secured within these strips. The Zircaloy-4 structural strips are welded at all intersections and to the side plates. Dimples formed in the structural strips center the fuel rod within the cell and along with the springs provide a positive but compliant support for each rod, sufficient to prevent fretting vibration.

In Reloads M, N, and P (Cycles 10-12), the debris resistant Nickel Alloy 718 HTP spacer grid in the ninth, bottom location is located just above the lower tie plate. It is formed by an interlocking rectangular grid of Nickel Alloy 718 strips. The strips are welded at all intersections and to the side plates. The spacer is positioned on top of the lower tie plate with the strip intersections directly above the tie plate flow holes. This reduces the size of debris that may pass through the flow holes thereby reducing the possibility of fretting against the cladding. Reloads R and S (Cycles 13 and 14) use a similar debris resistant concept with the Nickel Alloy 718 HTP spacer replaced by a bimetallic spacer coupled with a longer lower end cap on the fuel rods.

The HTP spacers for Reloads T through X (Cycles 15-18) are all Zircaloy-4 (Figure 3.3–4B). The strips are welded at the intersections and side plates. The structure of the Zircaloy-4 strips provides the rod support.

In Reload Y (Cycle 19) and later, all Zircaloy-4 HTP spacers are used in eight locations. The Nickel Alloy 718 HMP spacer is used in the ninth, bottom location. The Nickel Alloy 718 HMP bottom spacer is similar in design to the HTP spacers except for the flow channels, which are not canted.

The Millstone Unit 2 Cycle 19 reload core included four fuel assemblies with natural uranium replacement fuel rods with an anti-rotation feature designed to prevent spinning of the rod during operations. The four assemblies containing replacement rods were installed in symmetric, peripheral core locations against the baffle as shown in Figure 3.3–19 (Reference 3.3-9). The core locations into which the assemblies were placed where P–1, A–8, H–21, and Y–14 (see Figure 3.4–1). The replacement rods installed under these conditions were evaluated against established mechanical, nuclear, and thermal/hydraulic design criteria for Millstone Unit 2 fuel, and were determined to be compliant with their design and licensing bases (Reference 3.3-10).

The fuel assembly design for Reload EE (Cycle 25) and later is updated to the AREVA Standard CE-14 HTP™ design by implementing an M5® clad fuel rod and the MONOBLOC™ corner guide tube design. The M5® clad fuel rod increases the nominal pellet OD from 0.377 inches to 0.3805 inches and increases the nominal pellet theoretical density from 95.35% to 96.00%. The cladding material changes from Zircaloy-4 to M5® for improved corrosion resistance and reduced hydrogen pickup. The cladding ID also changes from 0.384 inches to 0.387 inches to accommodate the larger fuel pellet. The axial position of the fuel column is slightly lowered and the rod length is increased from 146.25 inches to 146.67 inches.

The AREVA Standard CE-14 HTP design utilizes Zircaloy-4 MONOBLOC™ corner guide tubes. The MONOBLOC™ guide tube design maintains a constant outer diameter whereas the inner diameters change between the dashpot region and the non-dashpot region (the wall thickness increases in the dashpot region). As compared to the previous design, the inner diameters of the non-dashpot and dashpot regions are unchanged and the outer diameters of the guide tube in the non-dashpot region are unchanged. The interface with the fuel assembly lower tie plate is also unchanged.

The bottom HMP™ spacer grid on the AREVA Standard CE-14 HTP fuel design is modified at the corner guide tube locations to accommodate the larger MONOBLOC™ guide tube outer diameters. All of the rod positions, interfaces with the fuel rods, and side plates are the same as the previous design. The HTP™ spacer grid design, the FUELGUARD™ lower tie plate, and the reconstitutable upper tie plate are unchanged from the previous design.

3.3.1.3.2 Fuel Assembly Mechanical Criteria

The structural integrity of the fuel assemblies is assured by setting design limits on stresses and deformations due to various handling operational and accident loads. These limits are applied to the design and evaluation of upper and lower tie plates, grid spacers, guide tubes, holddown springs, and locking hardware.

The design bases for evaluating the structural integrity of the fuel assemblies are:

a. Fuel Assembly Handling - Dynamic axial loads approximately 2.5 times assembly weight.

b. For All Applied Loads for Normal Operation and Anticipated Operational Events - The fuel assembly component structural design criteria are established for the two primary material categories, austenitic stainless steels (tie plates), and Zircaloy (guide tubes, grids, spacer sleeves). The stress categories and strength theory for austenitic stainless steel presented in the ASME Boiler and Pressure Vessel Code, Section III (Reference 3.3-1) are used as a general guide.

   Steady state stress limits are given in FSAR Section 3.3.1.1.1. Stress nomenclature is per the ASME Boiler and Pressure Vessel Code, Section III.

c. Loads During Postulated Accidents - Deflection or failure of components shall not interfere with reactor shutdown or emergency cooling of the fuel rods during postulated seismic and loss of coolant accident (LOCA) occurrences.

   The assembly structural component stresses under faulted conditions are evaluated using primarily the methods outlined in Appendix F of the ASME Boiler and Pressure Vessel Code, Section III.

The design basis for the guide tube wear sleeves is that the fuel assembly shall not be damaged by CEA induced fretting-wear. Flow tests at reactor conditions of prototypic fuel and guide tube wear sleeve assemblies have been used in establishing the performance of the CEA wear sleeve combination.

The holddown springs, as compressed by the upper core plate during reactor operation, shall provide a net positive downward force during steady state operation, based on the most adverse combination of component dimensional and material property tolerances. In addition, the holddown springs are designed to accommodate the additional load associated with a pump overspeed transient (resulting in possible temporary liftoff of the fuel assemblies), and to continue to ensure fuel assembly holddown following such an occurrence.

The fuel assembly growth plus BOL length shall not exceed the minimum space between the upper and lower core plates in the reactor cold condition (70°F). The reactor cold condition is limiting since the expansion coefficient of the stainless steel core barrel is greater than the coefficient of expansion of the Zircaloy guide tubes.

The spacer assembly is designed to withstand the thermal and irradiation induced differential expansion between the fuel rods and guide tubes and to withstand the design handling and accident loads discussed above. The debris resistant Nickel Alloy 718 HTP spacer used in the ninth, bottom location for reloads M, N and P (Cycles 10-12) was positioned such that the internal strip intersections are directly above the lower tie plate flow holes, thus reducing the size of debris which could pass through the lower tie plate.

In Reloads R and S (Cycles 13 and 14), the Nickel Alloy 718 HTP spacer grid at the ninth, bottom location was replaced with a bimetallic spacer which is raised off the upper surface of the lower tie plate. The gap between the upper surface of the lower tie plate and the lower surface of the bimetallic spacer is spanned by a long fuel rod end cap of solid Zircaloy-4.

The Zircaloy-4 HTP spacer grid is used in all nine locations in Reloads T through X (Cycles 15-18). This design is typically referred to as the 'HTP Fuel Assembly'. This spacer grid design provides improved DNB performance, structural strength, and fretting resistance. The long fuel rod end cap is maintained in the HTP Fuel Assembly.

In Reload Y (Cycle 19) and later, the Zircaloy-4 HTP spacer grid is used in eight locations and a Nickel Alloy 718 HMP spacer grid is used in the ninth, bottom location. This design retains the long fuel rod lower end cap and is typically referred to as the 'HTP+HMP Fuel Assembly'. The HTP+HMP design has improved structural strength, and fretting resistance compared to the HTP design.

In Reload EE (Cycle 25) and later, the fuel design is updated to the AREVA CE-14 HTP™ design by implementing the M5® clad fuel rod design and the MONOBLOC™ corner guide tube design. See Section 3.3.1.3.1 for additional details on the updated design.

The design analysis is based upon reactor operating conditions. Typically, these conditions are:

Nominal Core Thermal Power	= 2700 MW
Nominal Coolant Pressure	= 2250 psia
Maximum Flow for Fuel Assembly Liftoff	= 422,466 gallons per minute (at 380°F)
Maximum Core Coolant Inlet Temperature at Nominal Power	= 549°F
Total Average Linear Power	= 6.206 kW/ft

The power histories used in the design analysis are designed to achieve a peak assembly burnup of 56,000 MWD/MTU for Batch N, 52,500 MWD/MTU for Batch P, and 57,400 MWD/MTU for Batch R and later.

Conservative rod local peaking factors are used which result in a peak rod burnup of 62,000 MWd/MTU. Each of the rod design histories follows the single hottest rod in the first cycle operation, the hottest rod in second cycle operation, etc.

Fuel assembly components must be able to withstand anticipated seismic and LOCA forces. These may result from bundle vibration and impact due to a seismic or LOCA event. An analysis was performed for the previous reloads to determine the maximum bundle displacements and the maximum spacer grid forces expected during postulated accidents for Millstone 2. The loads and displacements analysis, which was performed by CE (Reference 3.3-6), considered the safe shutdown earthquake (SSE) and limiting Branch Line LOCA events, and the dynamic properties of the AREVA reload fuel assemblies. The resulting fuel assembly displacements and the combined seismic and LOCA grid spacer impact forces were provided to AREVA.

The loads and displacements were conservatively adjusted for the Batch R design due to the optimization of the fuel rod. The fuel weight was increased and the assembly stiffness was decreased. The spacer impact loads and the fuel assembly maximum deflections were conservatively recalculated from the reference analysis values. The spacer strength margin, the guide tube stresses, and the fuel rod stresses were calculated for the adjusted loads.

Calculated stresses at the appropriate deflections were combined with the steady state stresses and compared with the ASME Design Criteria for faulted conditions. This limit is 0.7 times the ultimate strength for the primary stress combinations as compared to 0.5 times ultimate for steady state loadings. This criteria was met for both the fuel rods and the guide tubes.

The calculated grid spacer loads during each accident and the combined loads were compared with the allowable grid spacer strength at operating temperature. The loads evaluated were the maximum projected one-sided impact load and the maximum through grid load. The maximum allowable crushing load is the 95 percent confidence lower limit of the true mean of the distribution of crush test measurements. The allowable through grid strength is well above the maximum through grid load. It is also above the maximum one-sided impact load. For Reload R through Reload DD, the seismic/LOCA calculations were reviewed and determined to be bounding. For Reload EE and beyond, the seismic/LOCA calculations were re-evaluated for the upgraded fuel design and produced acceptable margins.

design and produced acceptable margins.

3.3.1.4 Fuel Assembly Holddown Device

A fuel assembly holddown device has been incorporated to prevent the possibility of lifting the fuel assembly by hydraulic forces under all normal flow conditions with temperature greater than 500°F. The holddown device consists of a spring-loaded plate which is integral to the fuel assembly. The springs are compressed as the upper guide structure is lowered into place. The added spring load, together with the weight of the fuel assembly, prevents possible axial motion of the fuel assembly during operating conditions.

The holddown device is incorporated into the upper end fitting and features a movable holddown plate which acts on the underside of the fuel alignment plate (refer to Figure 3.3–5). The movable plate is loaded by coil springs which are located around the upper end fitting posts. The springs are positioned at the upper end of the assembly so that the spring load combines with the assembly weight in counteracting the upward hydraulic forces. The springs are sized and the spring preload selected, such that a net downward force will be maintained for all normal and anticipated transient flow and temperature conditions. It should be noted that the movable plate also serves as the lifting surface during handling of the fuel assembly.

Assembly holddown was previously analyzed in Section 3.6.1 of Reference 3.3-8. The analysis has been reperformed for Batch T and beyond fuel and is conservative.

3.3.1.5 Control Element Assembly

CEAs are provided by Combustion Engineering (CE) and AREVA. The CEA (shown in Figure 3.3–6) is comprised of five Inconel tubes 0.948 inch in diameter. All tubes contain neutron poison materials with the distribution of the poison materials as depicted in Figure 3.3–7. Each tube is sealed by welded end caps. A gas expansion space is provided to limit maximum tube stress due to internal pressure developed by the release of gas and moisture from the boron carbide. The overall length of the CEA is provided in Table 3.3-1. Four tubes are assembled in a

square array around the centrally located fifth tube. The tubes are welded to an upper end fitting. The upper end fittings are attached to a spider hub which couples the CEA to the drive mechanism through the extension shaft.

Mechanical reactivity control is achieved by operational maneuvering of groups of single CEAs. The dual CEA is made up of two single CEAs connected to separate grippers attached to single extension shaft. The arrangement of the CEAs in the core is shown in Figures 3.3–8 and 3.3–9.

There are 49 single CEAs and 12 dual CEAs all operated by a total of 61 CEDMs. Considering the 12 dual CEAs as 24 single CEAs gives an overall number of 73 CEAs in the core.

A buffer (deceleration dashpot) system is used for slowing down the CEAs at the end of a reactor trip. The buffering action is accomplished by guide tubes which have a reduced diameter in the lower section. When the tip of a CEA falls into the buffer region, the pressure buildup in the lower guide tube supplies the force to slow down the CEA. The velocity is decreased to a level which will minimize impact. The final impact is further cushioned by a coil spring arrangement mounted around the center CEA finger.

The four outer guide tubes have the reduced diameter lower section (dashpot). There is no dashpot in the center guide tube. There are four bleed holes above the dashpot region for the four outer guide tubes. For the center guide tube, these four bleed holes are at a lower elevation. For all guide tubes, there is a small drain hole at the bottom. The CEA tip is filled with a Silver-Indium-Cadmium alloy. This replaces the B_4C to avoid the change of buffer characteristics that B_4C radiation-induced swelling might bring about.

The design parameters have been optimized to establish the best combination of buffer stroke and buffer annulus. A significant analytical effort has shown that the pressure buildup and the impact loads are not damaging to the system. In addition, a test program has confirmed the feasibility of the system. It has demonstrated that the buffer will work under the worst expected tolerance condition.

3.3.1.6 Neutron Source Design

For Cycle 18 and beyond, the reactor core will not utilize neutron sources. It has been determined that during startups without neutron sources, there will continue to be a sufficient neutron count rate at each of the four Wide Range (WR) Excore fission detectors due to the high burnup fuel assemblies that will be positioned on the core periphery.

For Cycle 17 and earlier, four neutron sources were installed in the reactor core. They were held in vacant CEA guide tubes by means of an externally loaded spring reacting between the upper fuel alignment plate and the top of the fuel assembly. The cladding of the neutron source rods is of a free standing design. The internal pressure is always less than reactor operating pressure. Internal gaps and clearances are provided to allow for differential expansion between the source material and cladding.

3.3.1.7 In-Core Instruments

The in-core instruments (refer to Section 7.5.4) are located in the in-core instrumentation assembly (Figure 3.3–10). The in-core instrumentated thimble support frame and guide tubes are supported by the upper guide structure (UGS) assembly. The tubes are conduits which protect the in-core instruments and guide them during removal and insertion operations. The thimble support frame supports the 43 in-core thimble assemblies and acts as an elevator to lift the thimbles from the core into the UGS during the refueling operation.

3.3.1.8 Heated Junction Thermocouples

The heated junction thermocouple (HJTC) system is composed of two channels of HJTC instruments. Each HJTC instrument channel is manufactured into a probe assembly consisting of eight HJTC sensors, a seal plug, and electrical connectors (Figure 7.5–6). The eight HJTC sensors are physically independent and located at eight levels from the reactor vessel head to the fuel alignment plate.

The probe assembly is housed in a stainless steel support tube structure that protects the sensors from flow loads and serves as the guide path for the sensors. Figure 3.3–18 describes the locations of the HJTC probe assemblies.

HJTC Probes and Support Tubes in Upper Guide Structure

The HJTC probes and support tubes are installed inside two-part length CEA shrouds which protect the support tubes from normal operating cross-flow loads as well as blowdown loads. The support tubes are latched to the bottom of the CEA shroud and permanently tensioned by means of a threaded spanner nut at the top. Operating loads are far less than the preload developed by the tensioning operation. Therefore, the support tubes will not be affected by thermal or flow loads. The support tubes are designed to account for all tolerance conditions so that proper clearances will be assured. Physically, the support tubes are similar in mass and size to a typical control element assembly drive shaft, which would reside in the same area of the upper guide structure. The presence or absence of the HJTC probes within the support tubes will in no way affect the integrity of the support tubes, the UGS, the pressure boundary, and will have no significant effect upon the hydraulic conditions within the reactor vessel head.

3.3.2 REACTOR INTERNAL STRUCTURES

The reactor internals are designed to support and orient the reactor core fuel assemblies and CEAs, absorb the CEA dynamic loads and transmit these and other loads to the reactor vessel flange, provide flow paths for the reactor coolant, and guide in-core instrumentation.

The internals are designed to safely perform their function during all steady state conditions and during normal operating transients. The internals are designed to safely withstand the forces due to deadweight, handling, system pressure, flow impingement, temperature differential, vibration and seismic acceleration. All reactor components are considered Class 1 for seismic design. The reactor internals design limits deflection where required by function. In most cases the design of

reactor internals components is limited by stress, not deflection. For the CEA shroud which is the most limiting internal component for deflection, the allowable design deflection limit is 0.5 inch. This limit is two-thirds of the conservatively established loss-of-function deformation limit, 0.75 inch and applies to a break whose equivalent diameter is no larger than the largest line connected to the primary coolant line. The structural components satisfy stress values given in Section III of the ASME Pressure Vessel Code. Certain components have been subjected to a fatigue analysis. Where appropriate, the effect of neutron irradiation on the materials concerned is included in the design evaluation.

The components of the reactor internals are divided into four major parts consisting of the core support barrel, the lower core support structure (including the core shroud), the UGS (including the CEA shrouds, the in-core instrumentation guide tubes and the HJTC support tubes). The flow skirt, although functioning as an integral part of the coolant flow path is separate from the internals and is affixed to the bottom head of the pressure vessel. These components are shown in Figure 3.1–1 and 3.3–11. The in-core instrumentation is described in Section 7.5.4.

Dynamic system analysis methods and procedures which have been used to determine dynamic responses of reactor internals have been provided in CE, Report CENPD-42, “Topical Report of Dynamic Analysis of Reactor Vessel Internals under Loss-of-Coolant Accident Conditions with Application of Analysis to CE 800 MWe Class Reactors”.

3.3.2.1 Core Support Assembly

The major support member of the reactor internals is the core support assembly. This assembled structure consists of the core support barrel, the lower support structure, and the core shroud. The major materials for the assembly is Type 304 stainless steel.

The core support assembly is supported at its upper end by the upper flange of the core support barrel which rests on a ledge in the reactor vessel flange.

The lower flange of the core support barrel supports and positions the lower support structure. The lower support structure provides support for the core by means of a core support plate supported by columns resting on beam assemblies. The core support plate provides support and orientation for the fuel assemblies. The core shroud which provides lateral support for the fuel assemblies is also supported by the core support plate. The lower end attaches the core barrel to the pressure vessel.

3.3.2.2 Core Support Barrel

The core support barrel is a right circular cylinder with a nominal inside diameter of 148 inches and a minimum wall thickness of 1.75 inch. It is suspended by a 4 inch thick flange from a ledge on the pressure vessel. The core support barrel, in turn, supports the lower support structure upon which the fuel assemblies rest. Press fitted into the flange of the core support barrel are four alignment keys located 90 degrees apart. The reactor vessel, closure head and upper guide structure assembly flanges are slotted in locations corresponding to the alignment key locations to provide proper alignment between these components in the vessel flange region.

Since the core support barrel is over 27 feet long and is supported only at its upper end, it is possible that coolant flow could induce vibrations in the structure. Therefore, amplitude limiting devices, or snubbers are installed on the outside of the core support barrel near the bottom end. The snubbers consist of six equally spaced double lugs around the circumference and are the grooves of a “tongue-and groove” assembly; the pressure vessel lugs are the tongues. Minimizing the clearance between the two mating pieces limits the amplitude of any vibration. During assembly, as the internals are lowered into the vessel, the pressure vessel tongues engage the core support grooves in an axial direction. With this design, the internals may be viewed as a beam with supports at the furthest extremities. Radial and axial expansion of the core support barrel are accommodated, but lateral movement of the core support barrel is restricted by this design. The pressure vessel tongues have bolted, lock welded Inconel X shims and the core support barrel grooves are hardfaced with Stellite to minimize wear. The snubber assembly is shown in Figure 3.3–12.

3.3.2.3 Core Support Plate and Support Columns

The core support plate is a 147 inch diameter, 2 inch thick, Type 304 stainless steel plate into which the necessary flow distributor holes for the fuel assemblies have been machined. Fuel assembly locating pins (four for each assembly) are shrunk-fit into this plate. Columns and support beams are located between this plate and the bottom of the core support barrel in order to provide support for this plate and transmit the core load to the bottom flange of the core support barrel.

3.3.2.4 Core Shroud

The core shroud provides an envelope for the core and limits the amount of coolant bypass flow. The shroud (Figure 3.3–13) consists of two Type 304 stainless steel ring sections, aligned by means of radial shear pins and attached to the core support plate by Type 348 stainless steel tie rods. A gap is maintained between the core shroud outer perimeter and the core support barrel in order to provide some coolant flow upward between the core shroud and core support barrel, thereby minimizing thermal stresses in the core shroud and eliminating stagnant pockets.

3.3.2.5 Flow Skirt

The Inconel flow skirt is a right circular cylinder, perforated with 2-11/16 inch diameter holes, and reinforced at the top and bottom with stiffening rings. The flow skirt is used to reduce inequalities in core inlet flow distributions and to prevent formation of large vortices in the lower plenum. The skirt provides a nearly equalized pressure distribution across the bottom of the core support barrel. The skirt is supported by nine equally spaced machined sections which are welded to the bottom of the pressure vessel.

3.3.2.6 Upper Guide Structure Assembly

This assembly (Figure 3.3–14) consists of the upper support structure, 69 CEA shrouds, a fuel assembly alignment plate and an expansion compensating ring. The UGS assembly aligns and laterally supports the upper end of the fuel assemblies, maintains the CEA spacing, prevents fuel

assemblies from being lifted out of position during a severe accident condition and protects the CEAs from the effect of coolant crossflow in the upper plenum. The UGS is handled as one unit during installation and refueling.

The upper end of the assembly is a structure consisting of a support plate welded to a grid array of 24 inch deep beams and a 24 inch deep cylinder which encloses and is welded to the ends of the beams. The periphery of the plate contains four accurately machined and located alignment keyways, equally spaced at 90 degree intervals, which engage the core barrel alignment keys. The reactor vessel closure head flange is slotted to engage the upper ends of the alignment keys in the core barrel. This system of keys and slots provides an accurate means of aligning the core with the closure head. The grid aligns and supports the upper end of CEA shrouds.

The CEA shrouds extend from the fuel assembly alignment plate to an elevation about three feet above the UGS support plate. There are 57 single-type shrouds. These consist of cylindrical upper sections welded to integral bottom sections, which are shaped to provide flow passages for the coolant passing through the alignment plate while shrouding the CEAs from cross-flow. There are also 12 dual-type shrouds which in configuration consist of two single-type shrouds connected by a rectangular section shaped to accommodate the dual CEAs. The shrouds are bolted to the fuel assembly alignment plate. At the UGS support plate, the single shrouds are connected to the plate by spanner nuts which permit axial adjustment. The spanner nuts are tightened to proper torque and lockwelded. The dual shrouds are attached to the upper plate by welding.

The fuel assembly alignment plate is designed to align the upper ends of the fuel assemblies and to support and align the lower ends of the CEA shrouds.

Precision machined and located holes in the fuel assembly alignment plate align the fuel assemblies. The fuel assembly alignment plate also has four equally spaced slots on its outer edge which engage with Stellite hardfaced pins protruding from the core shroud to limit lateral motion of the UGS assembly during operation. The fuel alignment plate bears the upward force of the fuel assembly holddown devices. This force is transmitted from the alignment plate through the CEA shrouds to the UGS support plate and hence to the expansion compensating ring.

The expansion compensating ring bears on the flange at the top of the assembly to accommodate axial differential thermal expansion between the core barrel flange, UGS flange and pressure vessel flange support edge and head flange recess.

The UGS assembly also supports the in-core instrumentation thimble support frame, guide tubes, and HJTC support tubes.

All integral connections in the reactor internals are designed within the stress intensity limits listed in Tables N-422 and N-416.1 of Section III of the ASME code for normal and upset conditions. For emergency and faulted conditions, the design limits are as given in Table 3.2-1.

3.3.3 CONTROL ELEMENT DRIVE MECHANISM

3.3.3.1 Design

The CEDM is of the magnetic jack type drive. Each CEDM is capable of withdrawing, inserting, holding or tripping the CEA from any point within its 137-inch stroke. The design of the CEDM is shown in Figure 3.3–15 and is identical to that for Maine Yankee (AEC Docket Number 50-309) and Calvert Cliffs Units 1 and 2 (AEC Docket Numbers. 50-317 and 50-318).

The CEDM drives the CEA within the reactor core and indicates the position of the CEA with respect to the core. The speed at which the CEA is inserted or withdrawn from the core is consistent with the reactivity change requirements during reactor operation. For conditions that require a rapid shutdown of the reactor, the CEDM coils of the shutdown and regulating CEAs are deenergized, allowing the CEA and the supporting CEDM components to drop into the core by gravity. The CEA drop time is 2.75 seconds, where drop time is defined as the interval between the time power is removed from the CEDM coils and the time the CEA has reached 90 percent of its fully inserted position. The reactivity is reduced during such a drop at a rate sufficient to control the core under any operating transient or accident condition. The CEA accelerates to about 11 ft/sec and is decelerated at the end of the drop by the buffer section of the CEA guide tubes. Drive down capability following a reactor trip is not required for safety purposes. The safety analyses of Chapter 14 assume the CEA of highest reactivity worth sticks in the fully withdrawn position. A drive down feature would introduce the possibility of a failure which would prevent power from being removed from the CEDMs during a trip, which would lead to a reduction in plant safety.

There are 69 CEDM nozzles on top of the reactor vessel closure head. Eight of the 69 nozzles were used for the part length CEAs in Cycle 1, six of which are no longer used, and two of which are used for HJTC/RVLMS instrumentation. There are 61 CEDMs in current use. The six spare nozzles are capped with adapters. Each CEDM is connected to a CEA by a locked coupling. The weight of the CEAs and CEDMs is carried by the vessel head.

The CEDM is designed to handle dual, single or part length CEAs. The maximum operating speed capability of the CEDMs is 40 inches per minute for single CEAs and 20 inches per minute for dual CEAs.

3.3.3.2 Control Element Drive Mechanism Pressure Housing

The CEDM housing is attached to the reactor vessel head nozzle by means of a threaded joint and seal welded. The CEDM nozzles are made of Inconel Alloy 690 to minimize Primary Water Stress Corrosion Cracking. The CEDM pressure housings including the magnetic coil jack assemblies were replaced as part of the replacement reactor vessel closure head project.

The CEDM upper housing design and fabrication conform to the requirements of the ASME Boiler and Pressure Vessel Code, Section III, 1998 Edition through 2000 Addenda. The housing is designed for steady state conditions as well as all anticipated pressure and thermal transients.

Once the CEDM housing is seal welded to the head nozzle, it need not be removed since all servicing of the CEDM is performed from the top of the CEDM housing. This opening is closed by means of an upper housing and an omega seal weld. The CEDM pressure housing is capable of being vented after major coolant refills of the reactor coolant system (RCS), such as after a refueling and after reactor coolant pump (RCP) maintenance. However, venting of the CEDM pressure housing is no longer necessary after major refills of the Reactor Coolant System (RCS), since a vacuum refill method is used. The vacuum refill process involves a partial vacuum in the RCS while at mid-loop level and then slowly refilling the RCS.

3.3.3.2.1 Heated Junction Thermocouple Pressure Boundary

The HJTC probe assemblies are located at the two original locations (CEDMs 11 and 13) on the replacement reactor vessel closure head. The HJTC pressure boundary also known as the Reactor Vessel Level Monitoring System (RVLMS) pressure housing assembly consists of upper pressure housing tube, upper flange type Grayloc connection and lower housing. The lower housing is joined to the reactor vessel head nozzle by means of a threaded joint and an omega seal weld. The pressure boundary at the top of the RVLMS pressure housing is maintained by a quick disconnect Grayloc type flange (See Figure 3.3–17). The components are designed to ASME Section III, B&PV Code 1998 Edition through 2000 Addenda.

The pressure and thermal loads associated with normal operation and transient conditions have been included in stress analyses performed in accordance with ASME BPVC criteria. All stresses are within allowable limits.

3.3.3.3 Magnetic Jack Assembly

The magnetic jack motor assembly is an integral unit which fits into the CEDM housing through an opening in the top of the housing. This unit carries the motor tube, lift and hold pawls and magnets. The drive power is supplied by electrical coils positioned around the CEDM housing. The CEDMs are cooled by air supplied at 900 CFM at 95°F (maximum) to each CEDM. The design of the control element drive mechanism is such that loss of cooling air will not prevent the CEDM from releasing the CEA. The ability of the CEDM to release the rods is not dependent on the cooling flow provided by the CEDM Cooling System. Cooling function is only to ensure reliability of the CEDM coil stack. Following insertion of the CEDM motor assembly, the upper pressure housing is threaded into the CEDM motor housing and seal welded. This upper pressure housing encloses the CEDM extension shaft and supports the shroud assembly. The reed switch assembly is supported by the shroud assembly.

The lifting operation consists of magnetically operated step movements. Two sets of mechanical latches (one holding, one lifting) are utilized engaging a notched drive shaft. To prevent excessive latch wear, a means has been provided to unload the lifting latches during the engaging and disengaging operations.

The magnetic force is obtained from large DC magnet coils mounted on the outside of the motor tube.

Power for the electromagnets is obtained from one of two separate supplies. A control programmer actuates the stepping cycle and obtains the CEA location by a forward or reverse stepping sequence. CEDM hold for shutdown and regulating CEAs is obtained by energizing a hold coil at a reduced current while all other coils are deenergized. The full length CEAs are tripped upon interruption of electrical power to all coils.

3.3.3.4 Position Indication

Three separate means are provided for transmitting CEA position indication.

The first method utilizes the electrical pulses from the magnetic coil power programmer. The second method utilizes reed switches and a voltage divider network mounted on the CEDM to provide an output voltage proportional to CEA position. The third method utilizes three pairs of reed switches spaced at discrete locations within a position transmitter assembly. A permanent magnet built into the drive shaft actuates the reed switches one at a time as it passes by them. CEA position instrumentation is discussed in detail in Section 7.5.3.

3.3.3.5 Control Element Assembly Disconnect

The CEA is connected to the drive shaft extension with an internal collet-type coupling at its lower end. (Coupling is performed before the vessel head is installed). In order to disengage the CEA from the drive shaft extension, a tool is attached to the top end of the drive shaft when the reactor vessel head has been removed.

By pulling up on the spring-loaded operating rod in the center of the drive shaft, a tapered plunger is withdrawn from the center of the collet-type gripper causing it to collapse due to axial pressure from the CEA, thus permitting removal of the coupler from the CEA. Releasing the operating rod plunger after the coupler has been withdrawn from the CEA expands the coupler to a diameter that prevents recoupling to the CEA.

3.3.3.6 Test Program

A test program has been conducted to verify the adequacy of the magnetic jack CEDM. The program is described in Section 1.5.4.

3.3.4 REFERENCES

3.3-1 ASME Boiler and Pressure Vessel Code, Section III, 1977 Edition, ASME New York, NY.

3.3-2 K. R. Merckx, “RODEX2 - Fuel Rod Thermal-Mechanical Response Evaluation Model,” XN-NF-81-58 (NP)(A), Revision 2, March 1985 and Supplements.

3.3-3 “Qualification of Exxon Nuclear Fuel for Extended Burnup (PWR),” XN-NF-82-06 (NP)(A), Revision 1, Supplements 2, 4, 5, October 1985.

3.3-4 W. J. O'Donnell and B. F. Langer, “Fatigue Design Basis for Zircaloy Components,” Nuclear Science and Engineering, Volume 20, January 1964.

3.3-5 MATPRO Version, “A Handbook of Material Properties for Use in the Analysis of Light Water Reactor Fuel Rod Behavior,” TREE-NUREG 1008, December 1976.

3.3-6 J. C. Winslow (CE) to T. J. Honan (NU), CE Letter, “Seismic and Branch Line LOCA Analysis of SPC Reload Fuel for Millstone 2,” NU-88-043 (March 31, 1988).

3.3-7 “PWR Primary Water Chemistry Guidelines,” Revision 2, Electric Power Research Institute (EPRI) Final Report, EPRI NP7077, dated November 1990.

3.3-8 ANF-88-88(P), Rev. 1, “Design Report for Millstone Point Unit 2 Reload ANF-1,” August 29, 1988.

3.3-9 AREVA Contract Requirements Document Number 89-9070921-001-AREVA Contract No. J37MIL219B, January 28, 2008.

3.3-10 AREVA Document 51-9074000-000, “Compliance Document - Replacement Fuel Rod - Millstone 2 Fuel Failure Mitigation,” March 5, 2008.

3.3-11 BAW-10240(P)-A, Revision 0, “Incorporation of M5™ Properties in Framatome ANP Approved Methods,” Framatome ANP, Inc., May 2004.

3.3-12 EMF-92-116(P)(A), Revision 0, Supplement 1(P)(A), Revision 0, “Generic Mechanical Design Criteria for PWR Fuel Designs,” AREVA Inc., February 2015.

3.3-13 ANF-88-133(P)(A) and Supplement 1, “Qualification of Advanced Nuclear Fuels' PWR Design Methodolody for Rod Burnups of 62 GWd/MTU”, Advanced Nuclear Fuels Corporation, December 1991.

TABLE 3.3-1 MECHANICAL DESIGN PARAMETERS *

Fuel Assembly	
Geometry	14 x 14
Assembly Pitch, inches	8.180
Assembly Envelope, inches	8.160
Rod Pitch, inches	0.580
Number of Grids per Assembly	9
Approximate Assembly Weight, lb.	1280 (batches N and P) 1313 (batches R through DD) 1337 (batches EE and subsequent)
Fuel Rod to Fuel Rod Outside Dimension, inches	7.980
Fuel Rod and Pellet	
Active Stack Length, Cold, inches	136.7
Pellet Diameter, inches	0.3700 (batches N and P) 0.3770 (batches R through DD) 0.3805 (batches EE and subsequent)
Pellet Length, inches	0.425 (batches N and P) 0.435 (batches R through DD) 0.476 (batches EE and subsequent)
Pellet Density (% Theoretical)	94.0 (batches N and P) 95.0 (batches R and S) 95.35 (batches T through DD) 96.00 (batches EE and subsequent)
Clad Material	Zircaloy-4 (batches N through DD) M5™ (batches EE and subsequent)
Clad OD, inches	0.440
Clad Thickness, inches	0.031 (batches N and P) 0.028 (batches R through DD) 0.0265 (batches EE and subsequent)
Diametrical Gap, nominal, cold, inches	0.008 (batches N and P) 0.007 (batches R through DD) 0.0065 (batches EE and subsequent)

TABLE 3.3-1 MECHANICAL DESIGN PARAMETERS * (CONTINUED)

Control Rod Guide Tube	
Number per Assembly	4
Tube ID, above dashpot, inches	1.035
Wall Thickness, above dashpot, inches	0.040
Wall Thickness, dashpot, inches	0.040 (batches N through D) 0.0735 (batches EE and subsequent)
Instrumentation Tube	
Number per Assembly	1
Tube ID, inches	1.035
Wall Thickness, inches	0.040
Spacer Grid	
Material	Zircaloy-4 / Nickel Alloy 718 (bottom grid)
Number per Assembly	8 / 1 (batches N and P) 9 / 0 (batches R through X) 9 / 1 (batches Y and subsequent)
Sleeves (Wear)	
Material	SS, Chrome Plate
Burnable Poison Rod	
Active Length, inches	124.7 + UO_2 blankets
Pellet Material	Gd_2O_3 / UO_2
Pellet Diameter, inches	0.3700 (batches N and P) 0.3770 (batches R through DD) 0.3805 (batches EE and subsequent)
Pellet Length, inches	0.435 (batches R through DD) 0.476 (batches EE and subsequent)
Clad Material	Zircaloy-4 (batches N through DD) M5™ (batches EE and subsequent)
Clad ID, inches	0.378 (batches N and P) 0.384 (batches R through DD) 0.387 (batches EE and subsequent)
Clad OD, inches	0.440

TABLE 3.3-1 MECHANICAL DESIGN PARAMETERS * (CONTINUED)

Clad Thickness, nominal, inches	0.031 (batches N and P) 0.028 (batches R through DD) 0.0265 (batches EE and subsequent)
Diametral Gap, nominal, cold, inches	0.008 (batches N and P) 0.007 (batches R through DD) 0.0065 (batches EE and subsequent)
Control Element Assembly	
Number	73
Number of Absorber Elements per Assembly	5
Type	Cylindrical Rods
Clad Material	Nickel Alloy 625
Clad Thickness, inches	0.036
Clad OD, inches	0.948
Poison Material	B_4C / Ag-In-Cd
Corner Element Pitch, inches	4.64
Total CEA Length, inches	161.31- CE 161.25 - AREVA
Poison Length, inches	132 -CE 133.5 - AREVA
CEA Dry Weight, lb.	95 - CE 85 - AREVA
Total Operating Assembly Dry Weight, lb.	
Single	210 - CE 200 - AREVA
Dual	334 - CE 314 AREVA
Core Arrangement	
Number of Fuel Assemblies in Core Total	217
Number of Single CEAs	49
Number of Dual CEAs	12
CEA Pitch, minimum, inches	11.57

TABLE 3.3-1 MECHANICAL DESIGN PARAMETERS * (CONTINUED)

Spacing Between Fuel Assemblies, Fuel Rod Surface to Surface, inches	0.200
Spacing, Outer Fuel Rod Surface to Core Shroud, inches	0.18
Hydraulic Diameter, Nominal Channel, feet	0.04445
Total Flow Area (Excluding Guide Tubes), square feet	53.5
Total Core Area, square feet	101.1
Core Equivalent Diameter, inches	136
Core Circumscribed Diameter, inches	143.1
Core Volume, liters	32,526
Total Fuel Loading, MTU (Typical)	83.65
Total Heat Transfer Area, square feet	50,117

TABLE 3.3-2 PRESSURIZED WATER REACTOR PRIMARY COOLANT WATER CHEMISTRY RECOMMENDED SPECIFICATIONS

Conductivity (μS/cm at 25°C)	Relative to Lithium and Boron concentration.
pH at 25°C	Determined by the concentration of boric acid and lithium present. Consistent with the Primary Chemistry Control Program.(4)
Dissolved Oxygen, at power	< 0.1 ppm (1) (2) (3)
Chloride	< 0.15 ppm
Fluoride	< 0.10 ppm
Hydrogen	25-50 cc (STP)/KgH_2O
Suspended Solids	≤ 0.35 ppm prior to reactor startup
Li	Consistent with the Primary Chemistry Control Program.(4)
Boron, as boric acid	0-2620 ppm (5)

NOTES:

(1) The temperature at which the Oxygen limit applies is > 250°F.

(2) The at power operation residual Oxygen concentration control value is ≤ 0.005 ppm.

(3) During plant startup, Hydrazine may be used to control dissolved Oxygen concentration at ≤ 0.1 ppm.

(4) During power operation lithium is coordinated with boron to maintain a $pH_{(t)}$ of ≥ 7.0, but ≤ 7.4, consistent with the Primary Chemistry Control Program. Lithium is added to the RCS during plant startup, but prior to reactor criticality, and is in specification per the Primary Chemistry Control Program within 72 hours after criticality. Lithium may be removed from the reactor coolant immediately before, or during, shutdown periods to aid in the cleanup of corrosion products. By evaluation, a maximum lithium concentration of 4.5 ppm is permissible with a target lithium concentration of 4.3 ppm for 100% power operations.

(5) RCS boron concentration is maintained as necessary to ensure core reactivity or shutdown margin requirements are met. Although the RCS and related auxiliary systems containing reactor coolant are designed for a maximum concentration of 2620 ppm boron, it should be noted the design basis for the TSP baskets in the containment sump assumes the RCS, SITs, and RWST are at a maximum boron concentration of 2400 ppm.

FIGURE 3.3–1A FUEL ROD ASSEMBLY (BATCH "DD" AND PRIOR)

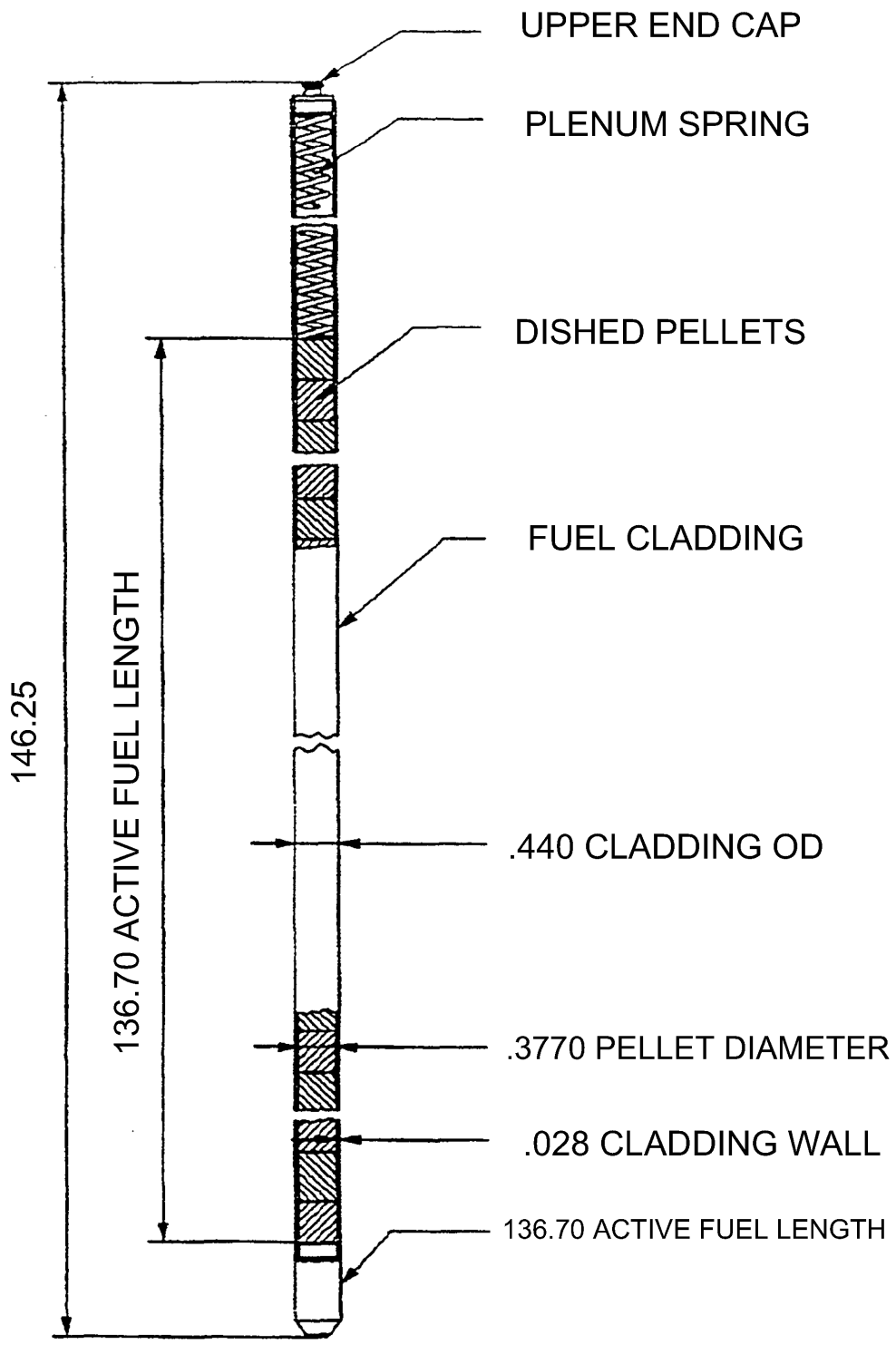

FIGURE 3.3–1B FUEL ROD ASSEMBLY (BATCH "EE" AND LATER)

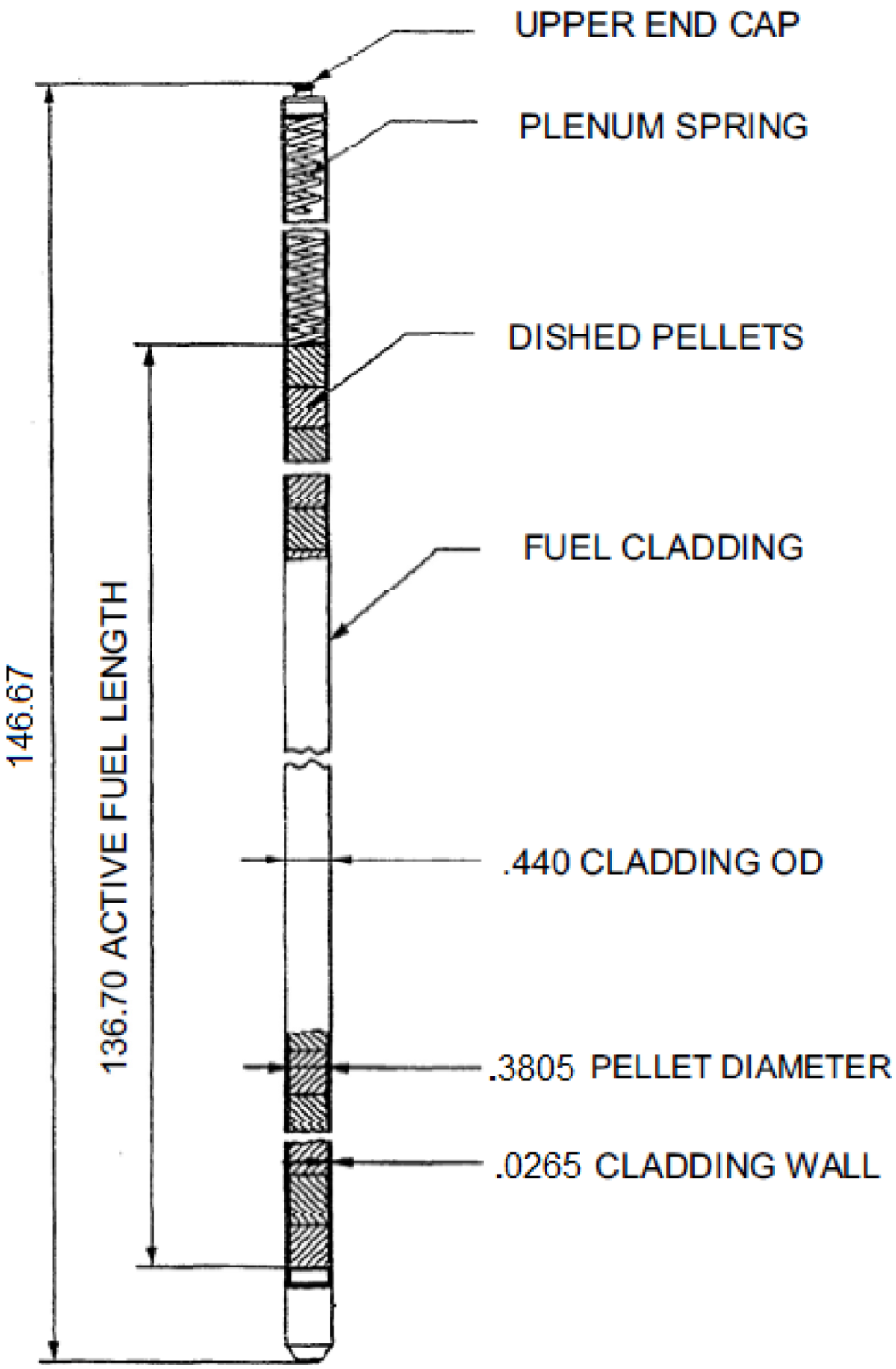

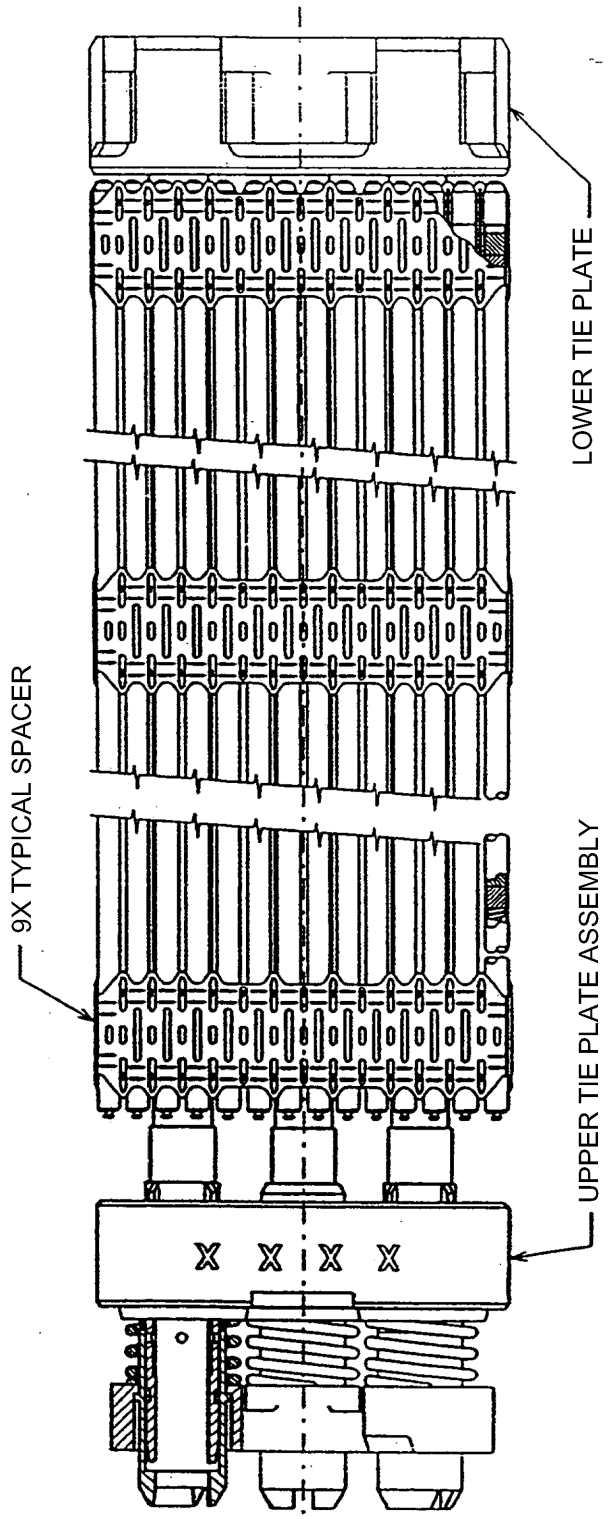

FIGURE 3.3–2A AREVA - RELOAD FUEL ASSEMBLY BATCH "S" AND PRIOR

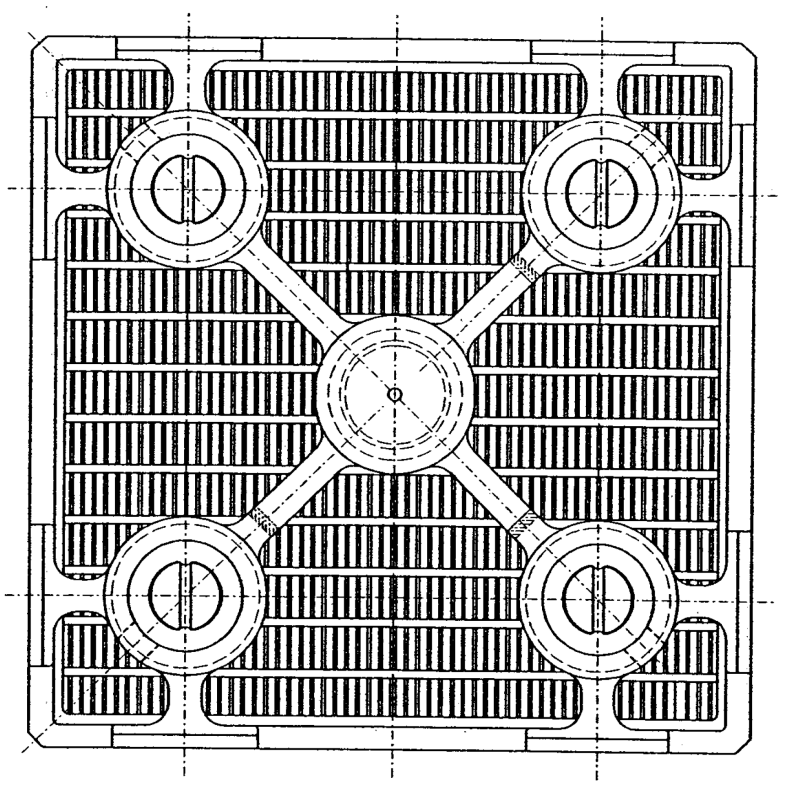

LOWER TIE PLATE

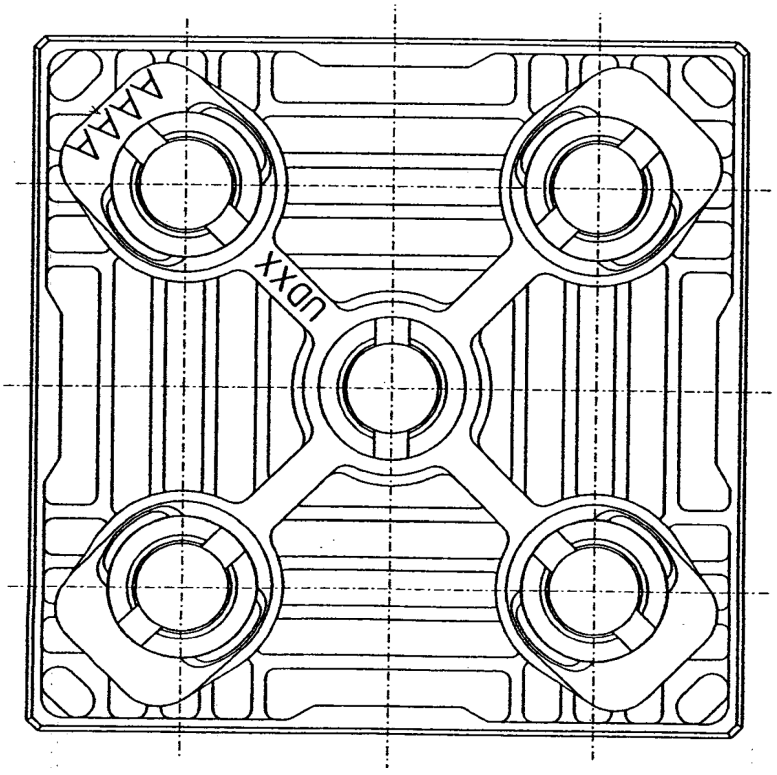

UPPER TIE PLATE

FIGURE 3.3–2B AREVA - RELOAD FUEL ASSEMBLY BATCH "T" AND LATER

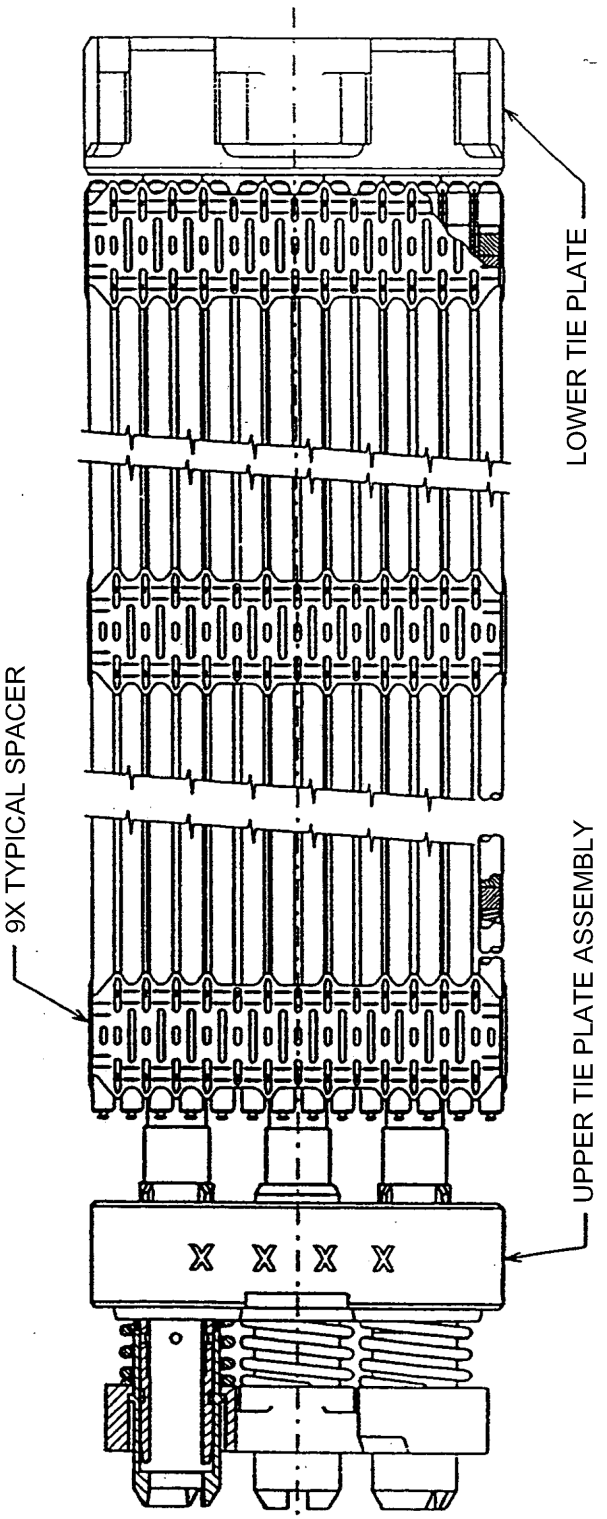

FIGURE 3.3–3A AREVA - RELOAD FUEL ASSEMBLY COMPONENTS BATCH "S" AND PRIOR

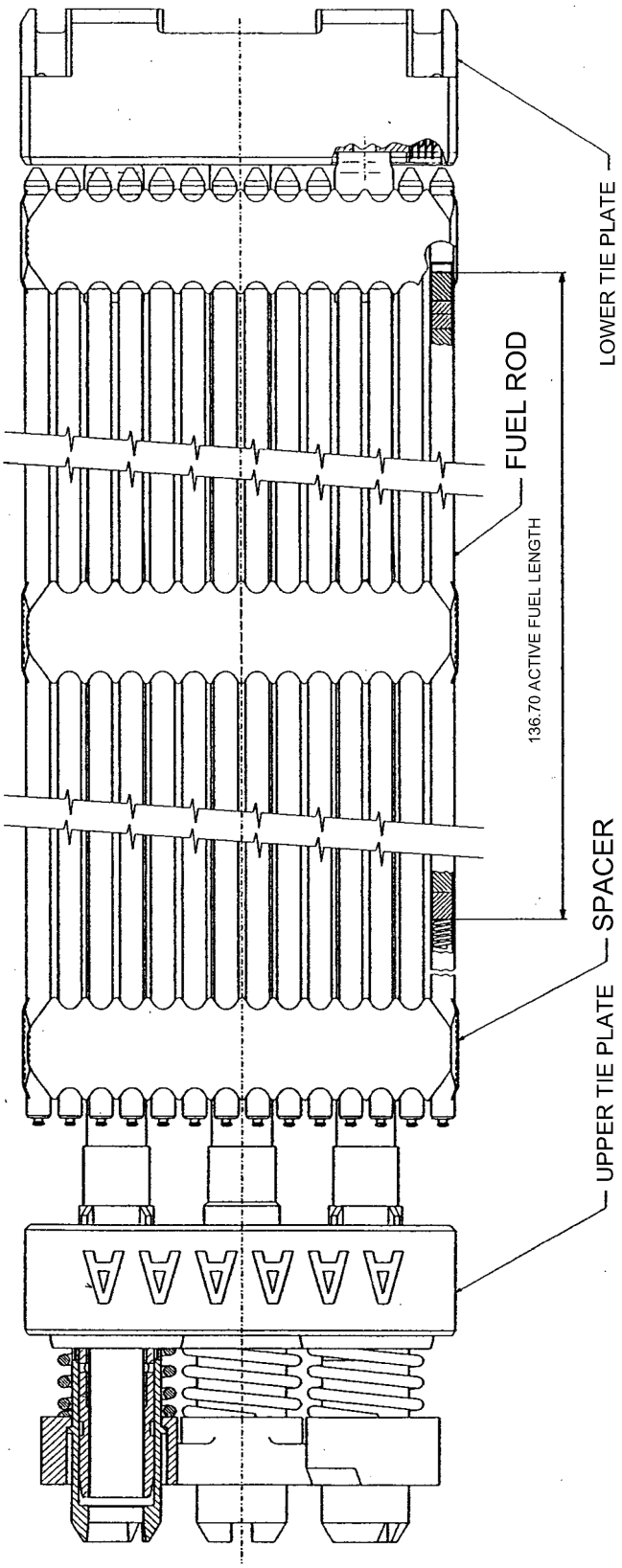

FIGURE 3.3–3B AREVA - RELOAD FUEL ASSEMBLY COMPONENTS BATCH "T" AND LATER

FIGURE 3.3–4A BI-METALLIC FUEL SPACER ASSEMBLY

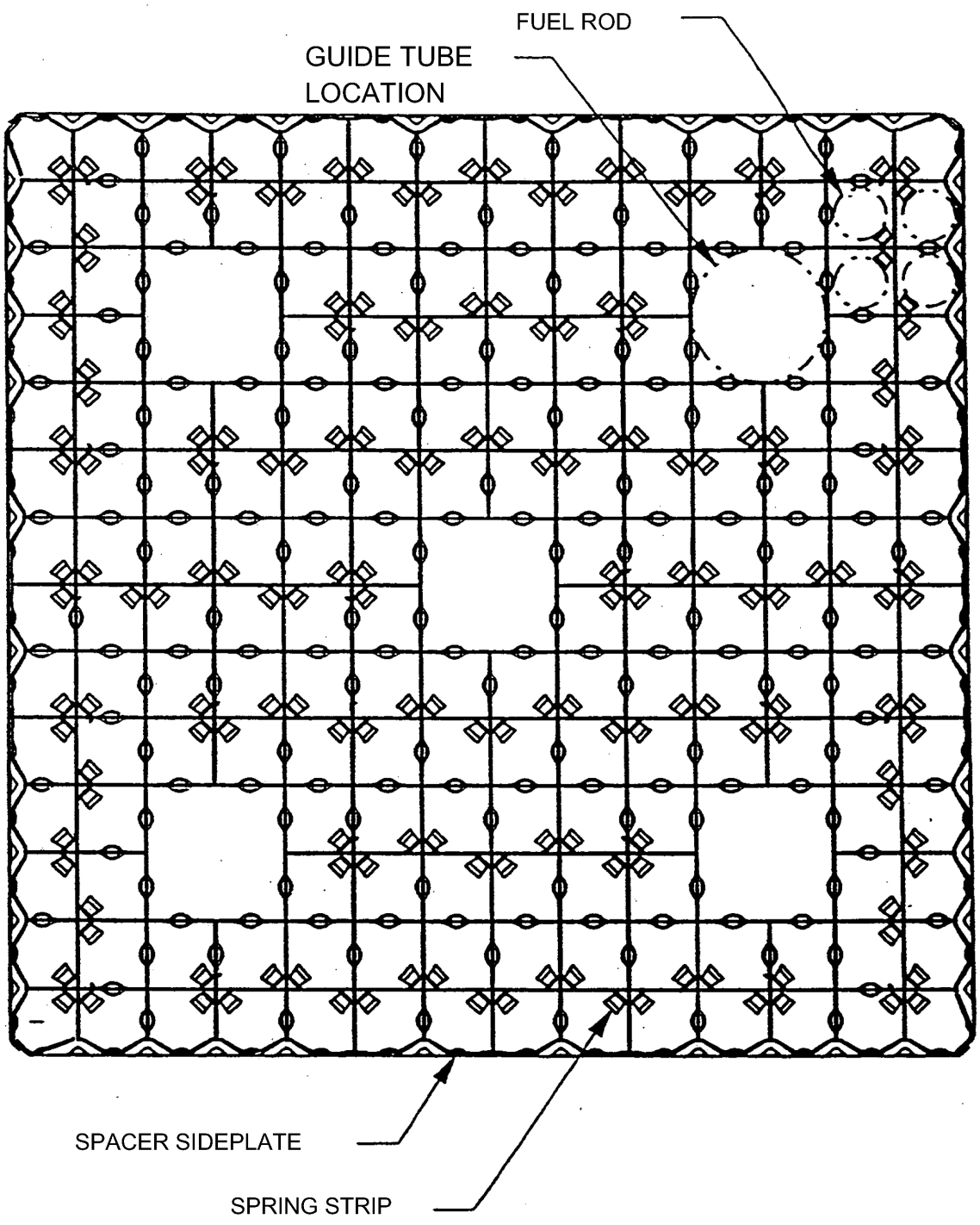

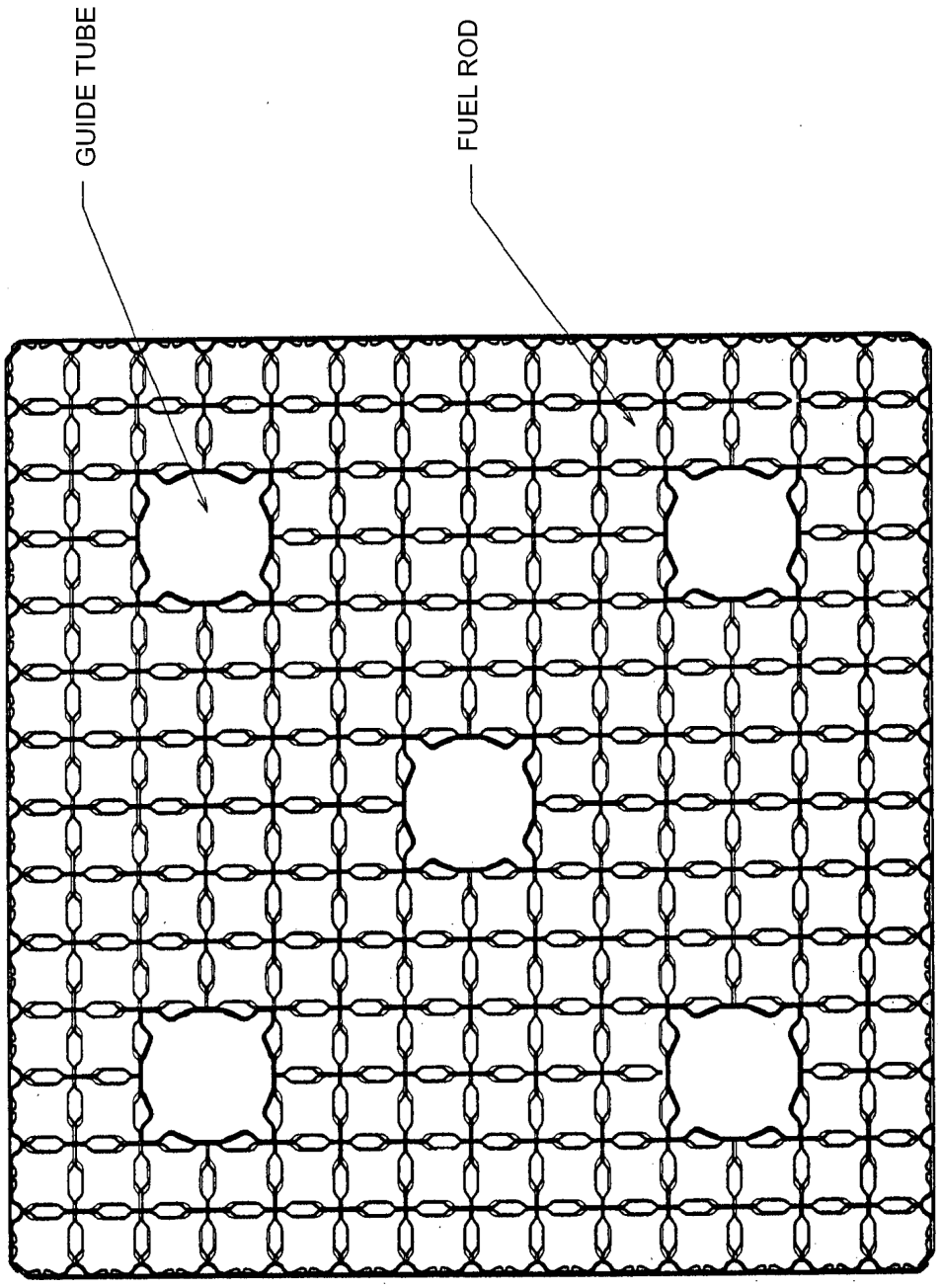

FIGURE 3.3–4B HTP FUEL SPACE ASSEMBLY

FIGURE 3.3–5 FUEL ASSEMBLY HOLD DOWN DEVICE

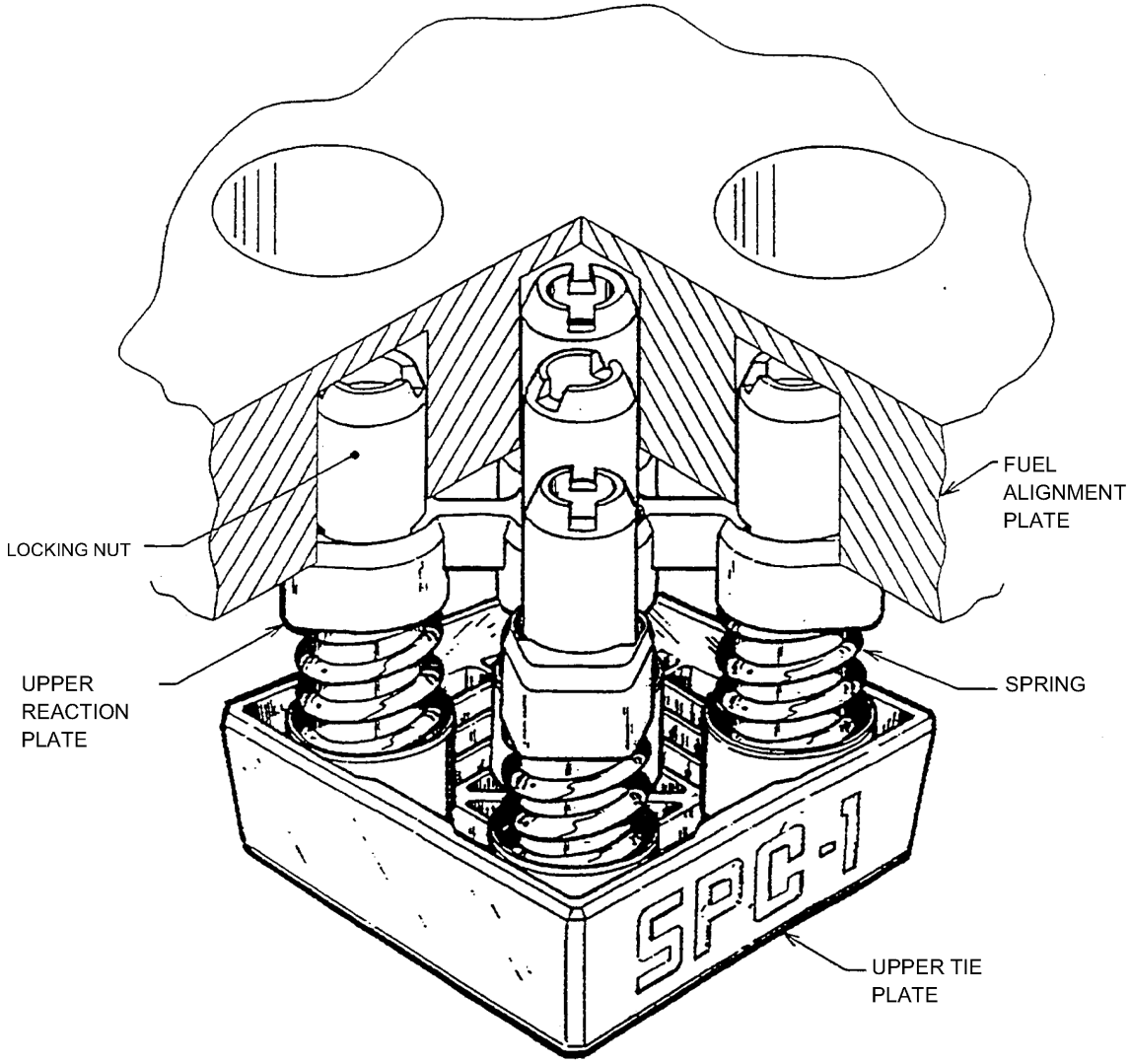

FIGURE 3.3–6 CONTROL ELEMENT ASSEMBLY

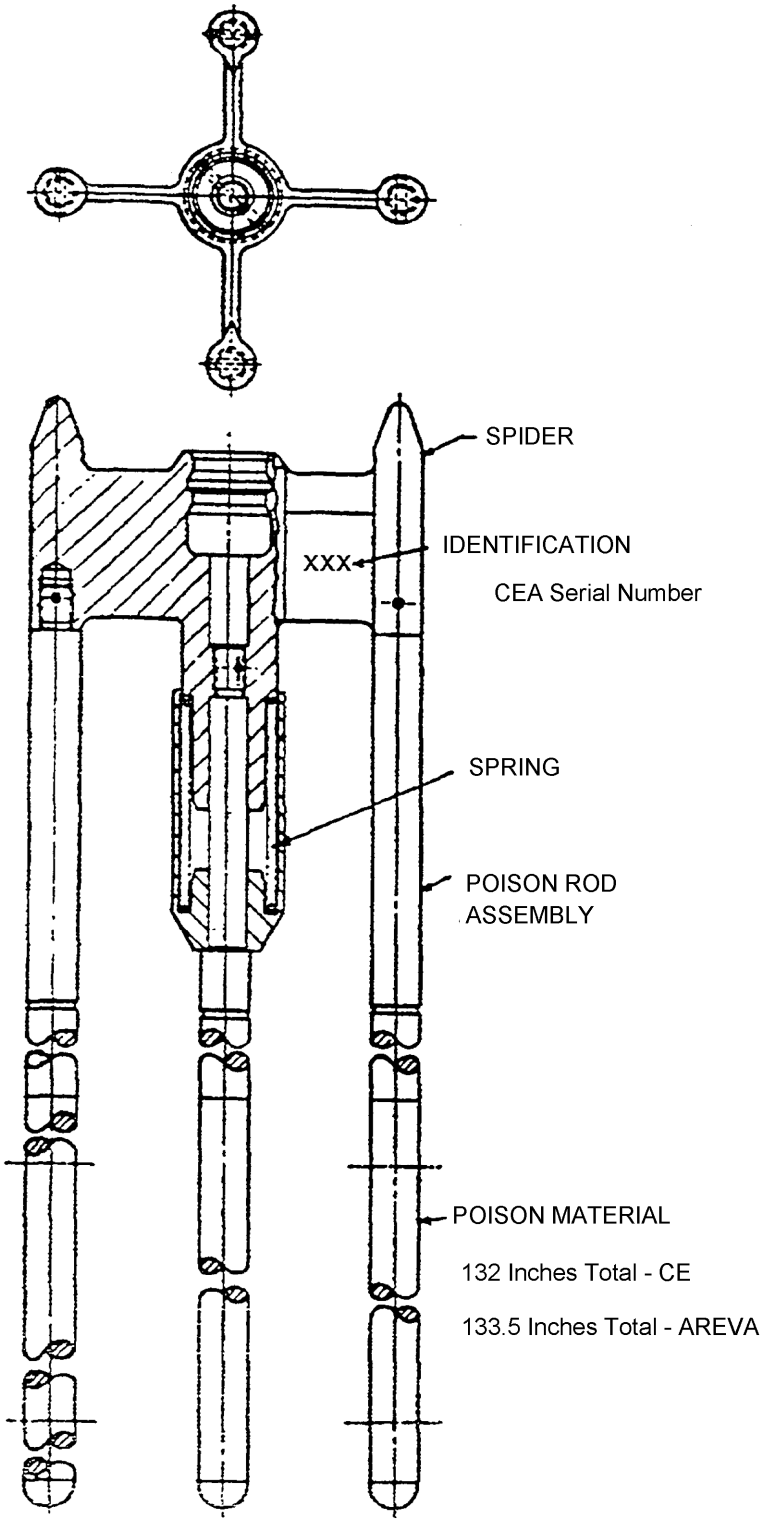

FIGURE 3.3–7 CONTROL ELEMENT ASSEMBLY MATERIALS

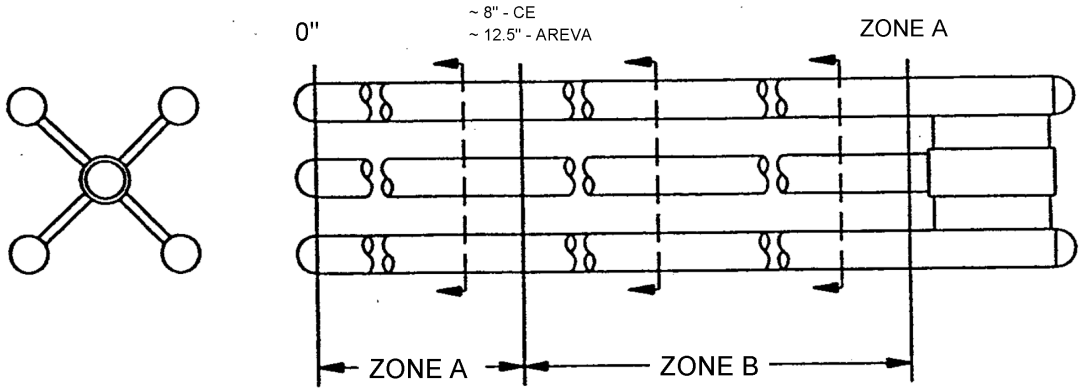

NUMBER	MATERIALS ZONE A	ZONE B
73	Ag Ag Ag Ag Ag	B B B B B

NOTES:

$B = B_4C$ $Ag = Ag - In - Cd$

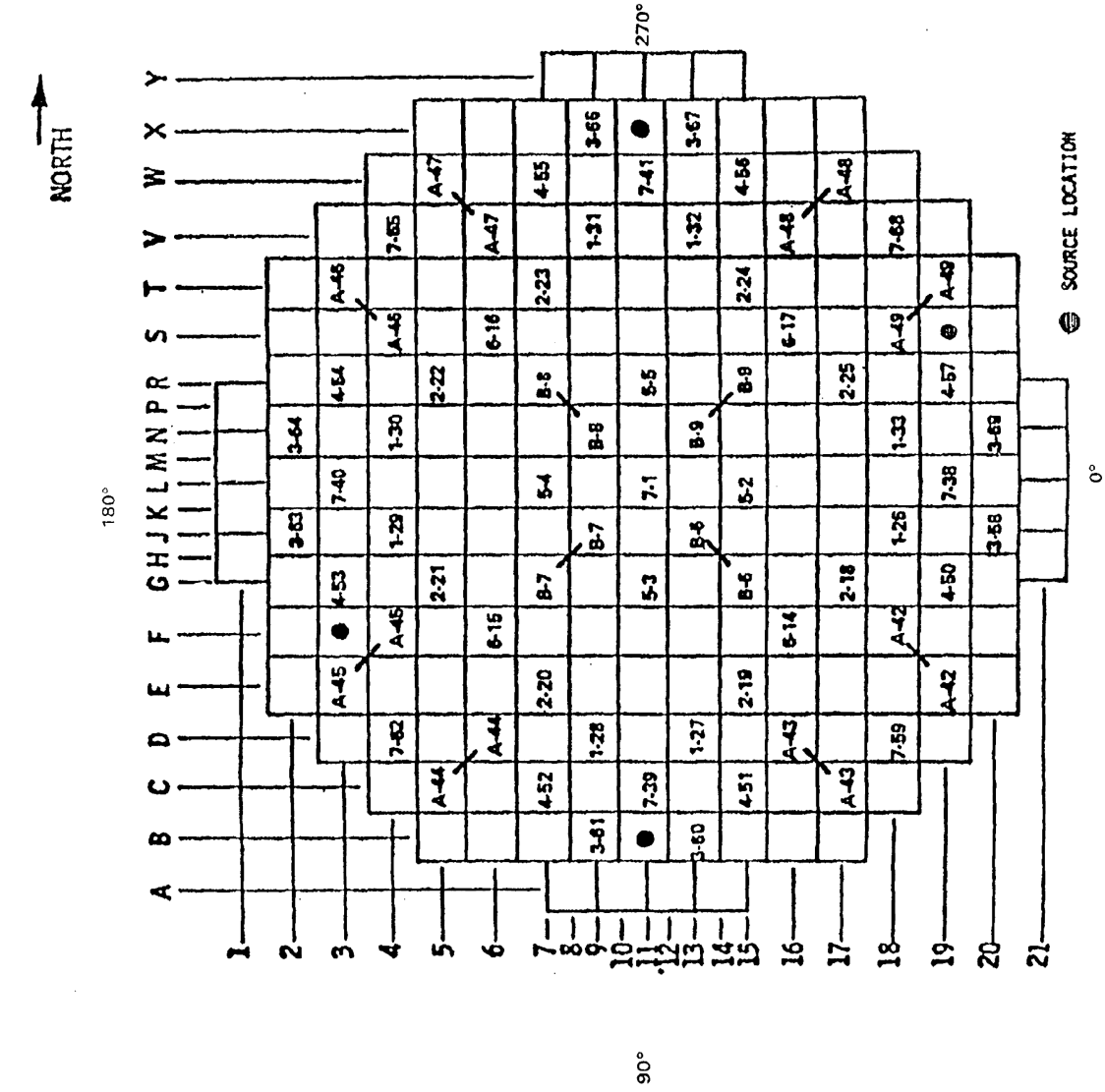

FIGURE 3.3–8 CONTROL ELEMENT ASSEMBLIES GROUP AND NUMBER DESIGNATION

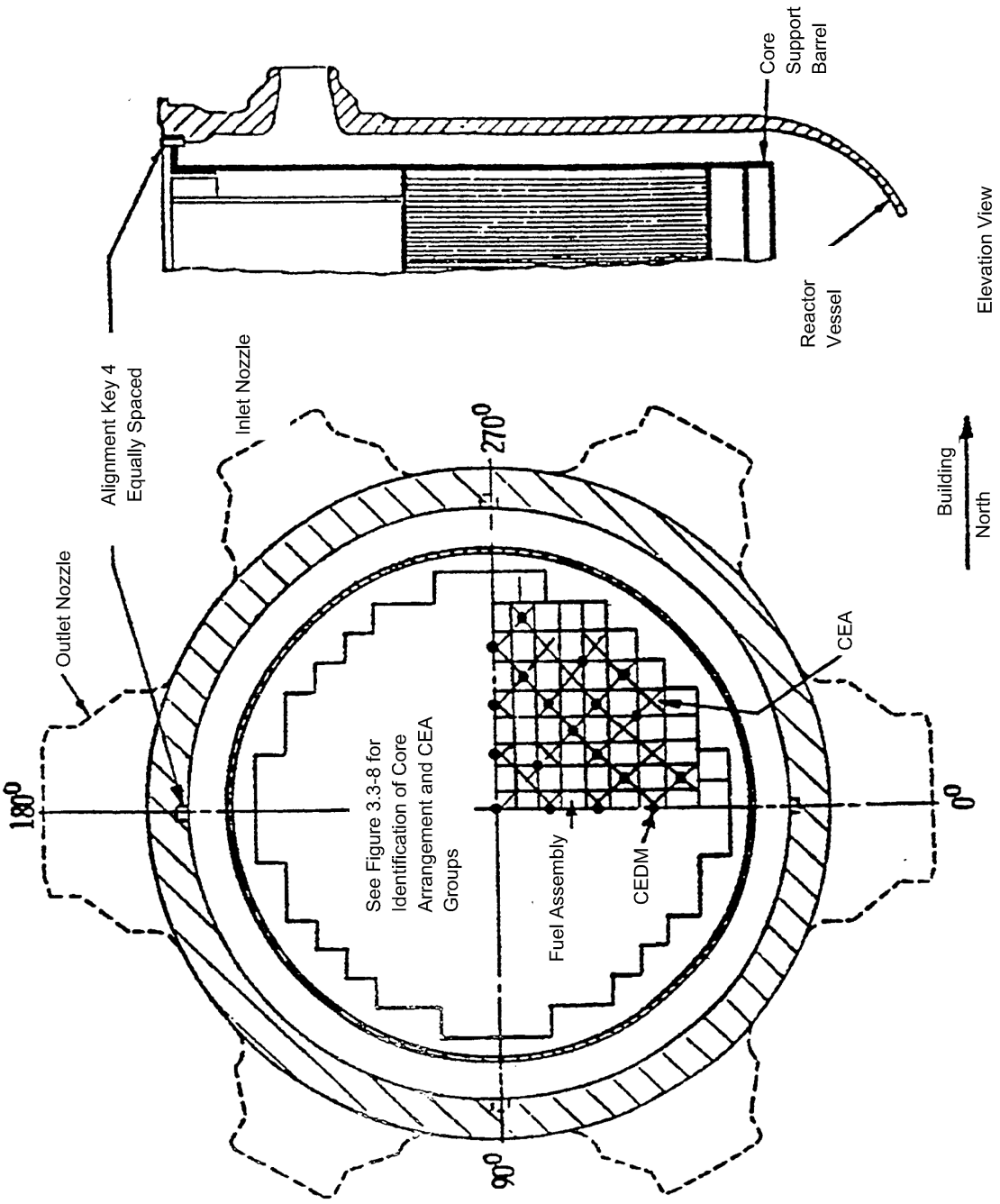

FIGURE 3.3–9 CORE ORIENTATION

FIGURE 3.3–10 IN-CORE INSTRUMENTATION ASSEMBLY

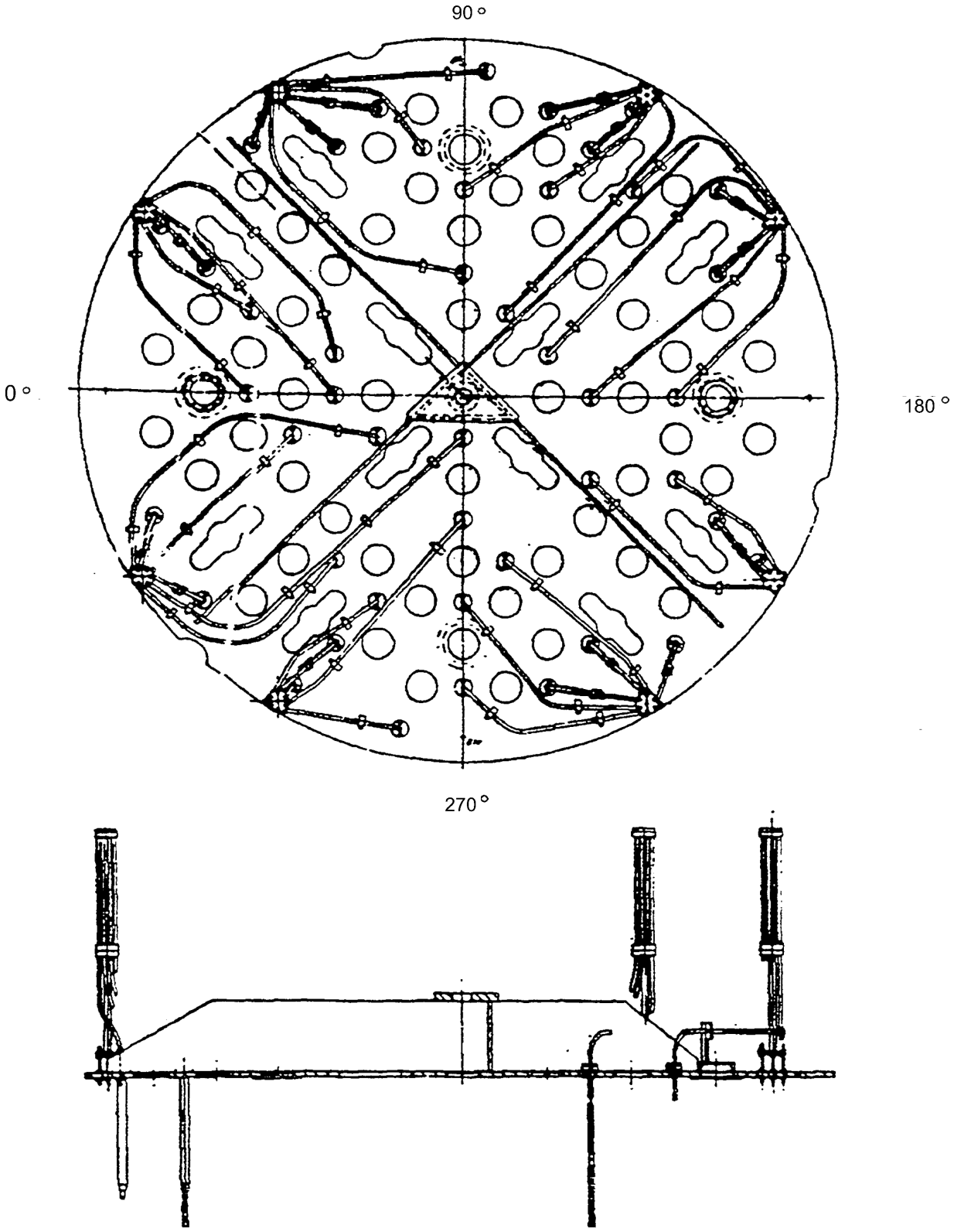

FIGURE 3.3–11 REACTOR INTERNALS ASSEMBLY

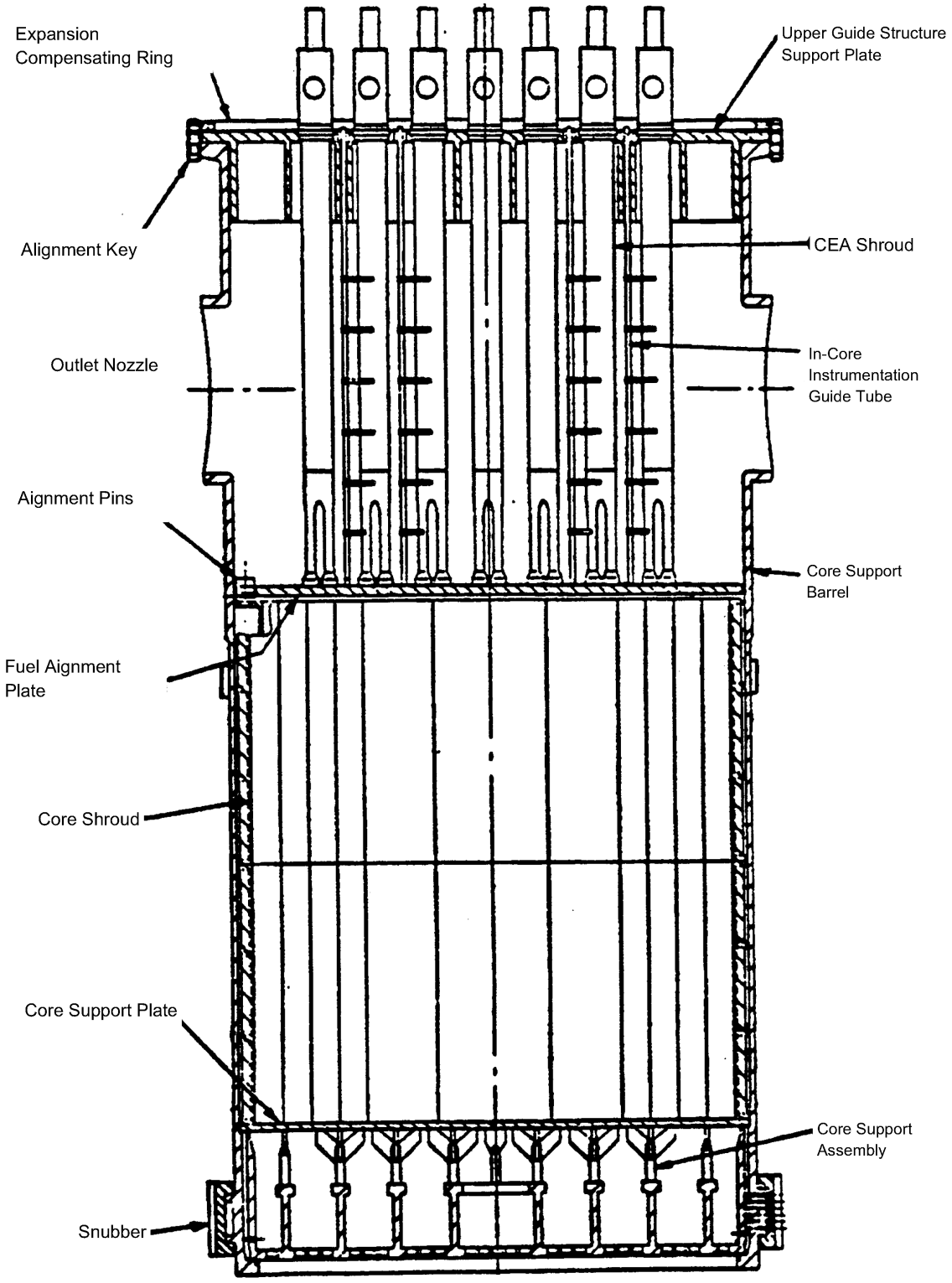

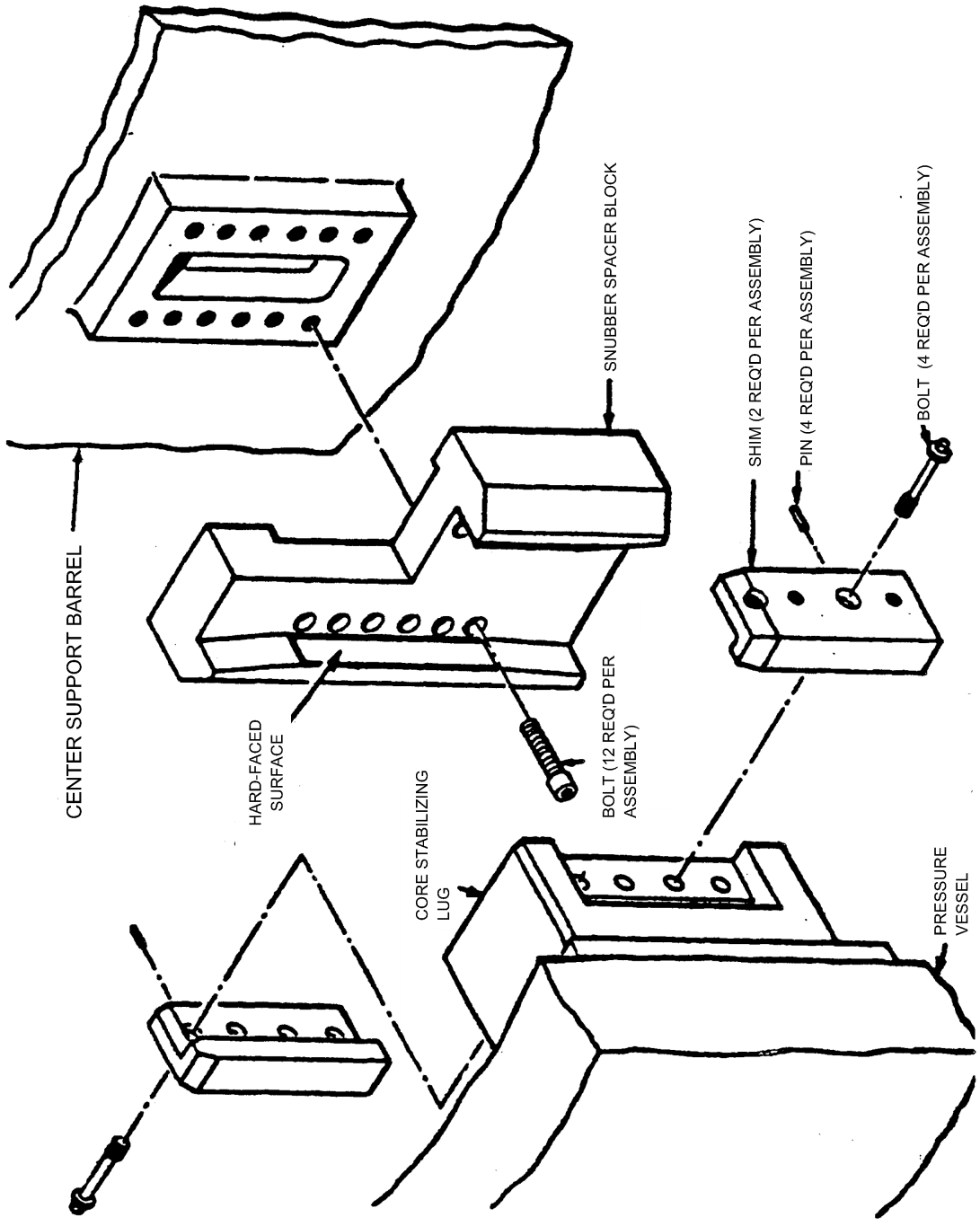

FIGURE 3.3–12 PRESSURE VESSEL-CORE SUPPORT BARREL SNUBBER ASSEMBLY

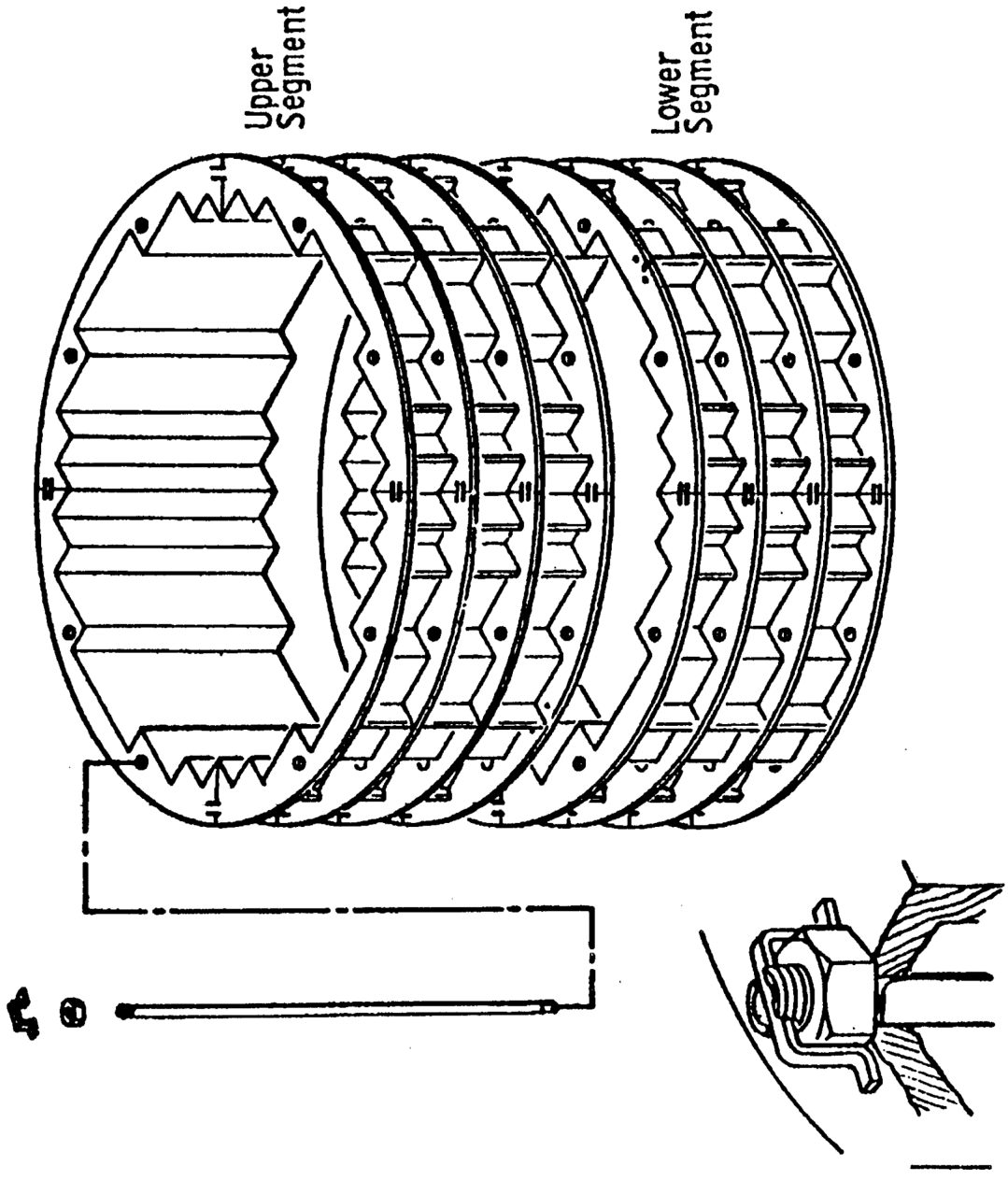

FIGURE 3.3–13 CORE SHROUD ASSEMBLY

FIGURE 3.3–14 UPPER GUIDE STRUCTURE ASSEMBLY

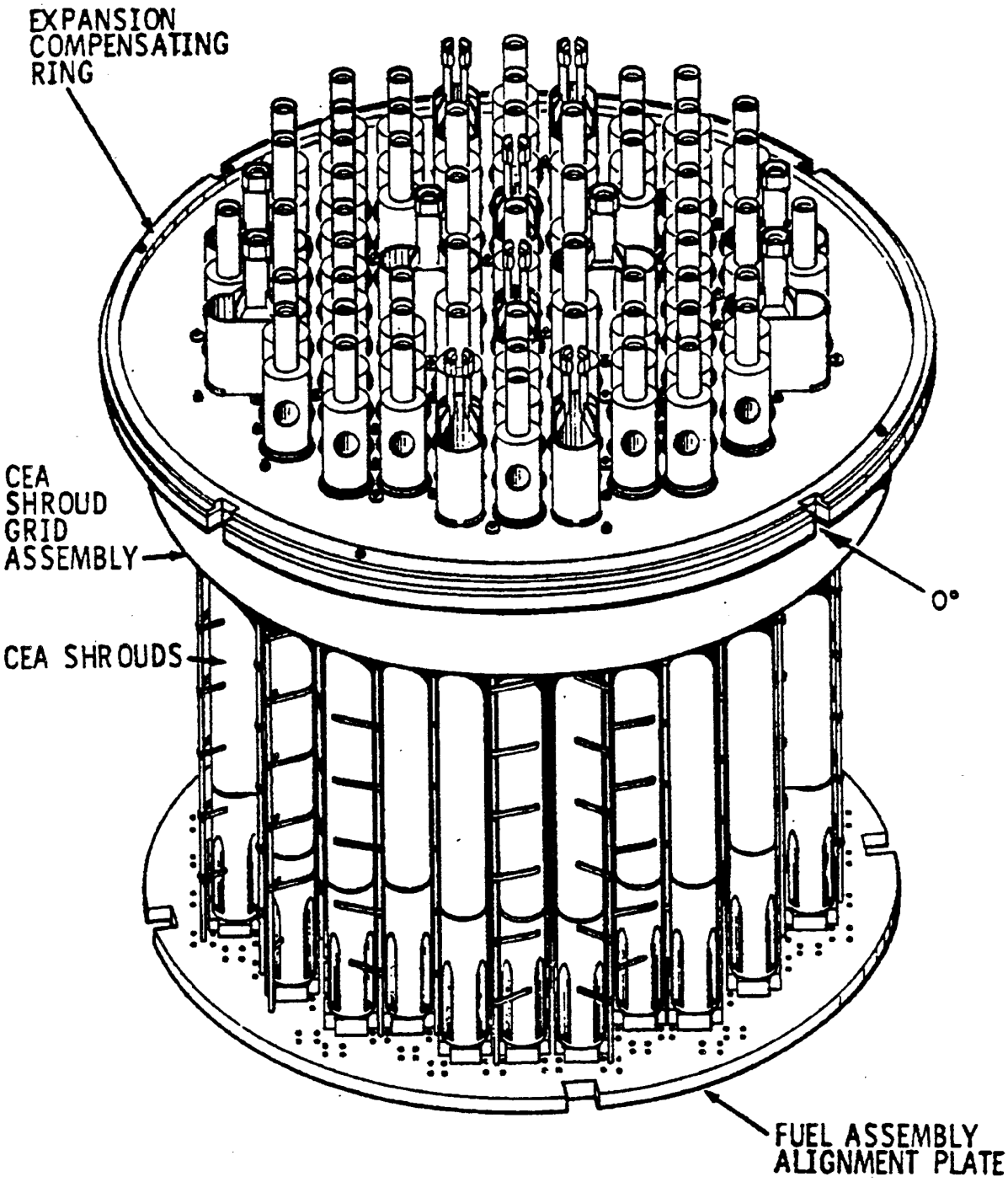

FIGURE 3.3–15 CONTROL ELEMENT DRIVE MECHANISM (MAGNETIC JACK)

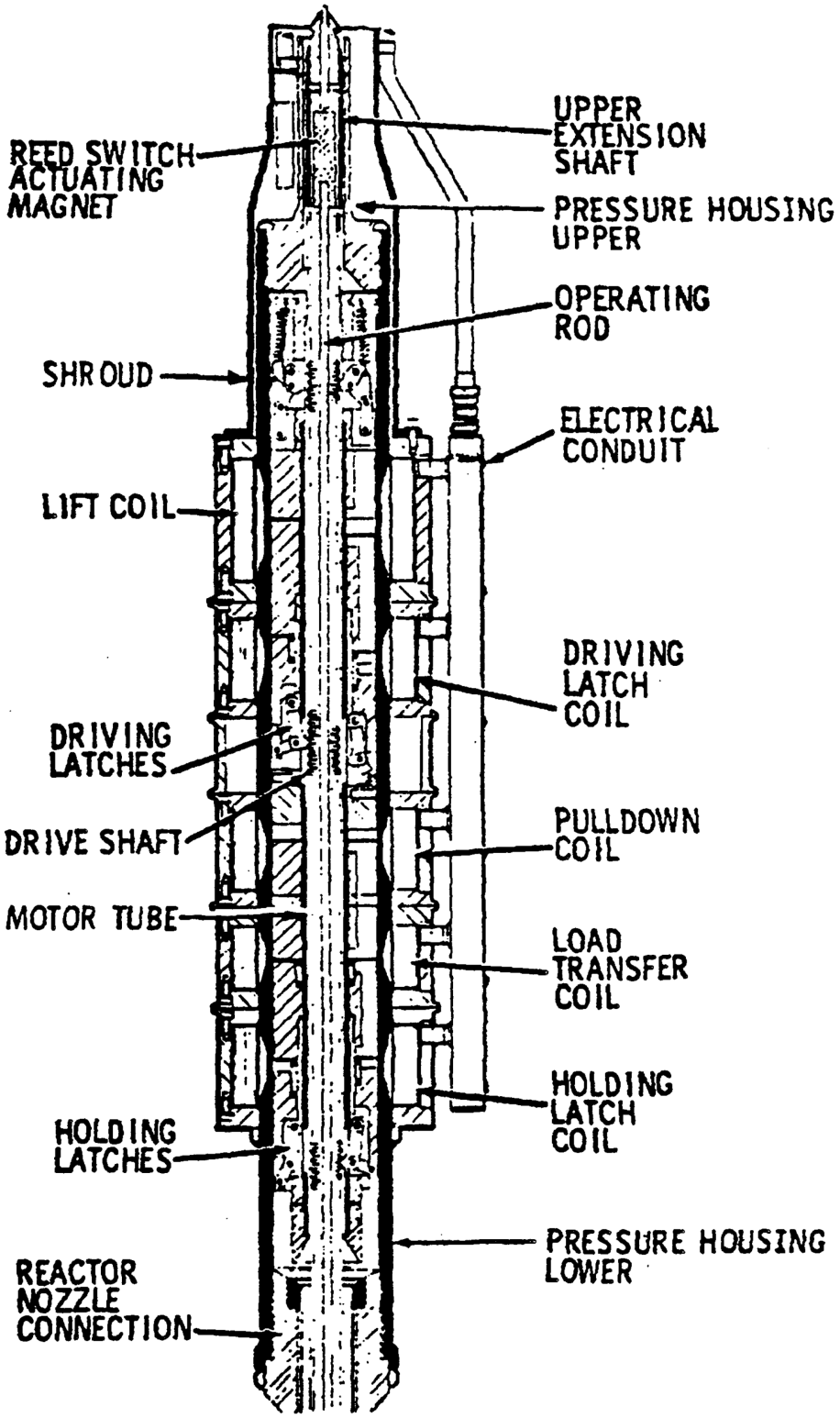

FIGURE 3.3–16 (LEFT BLANK INTENTIONALLY)

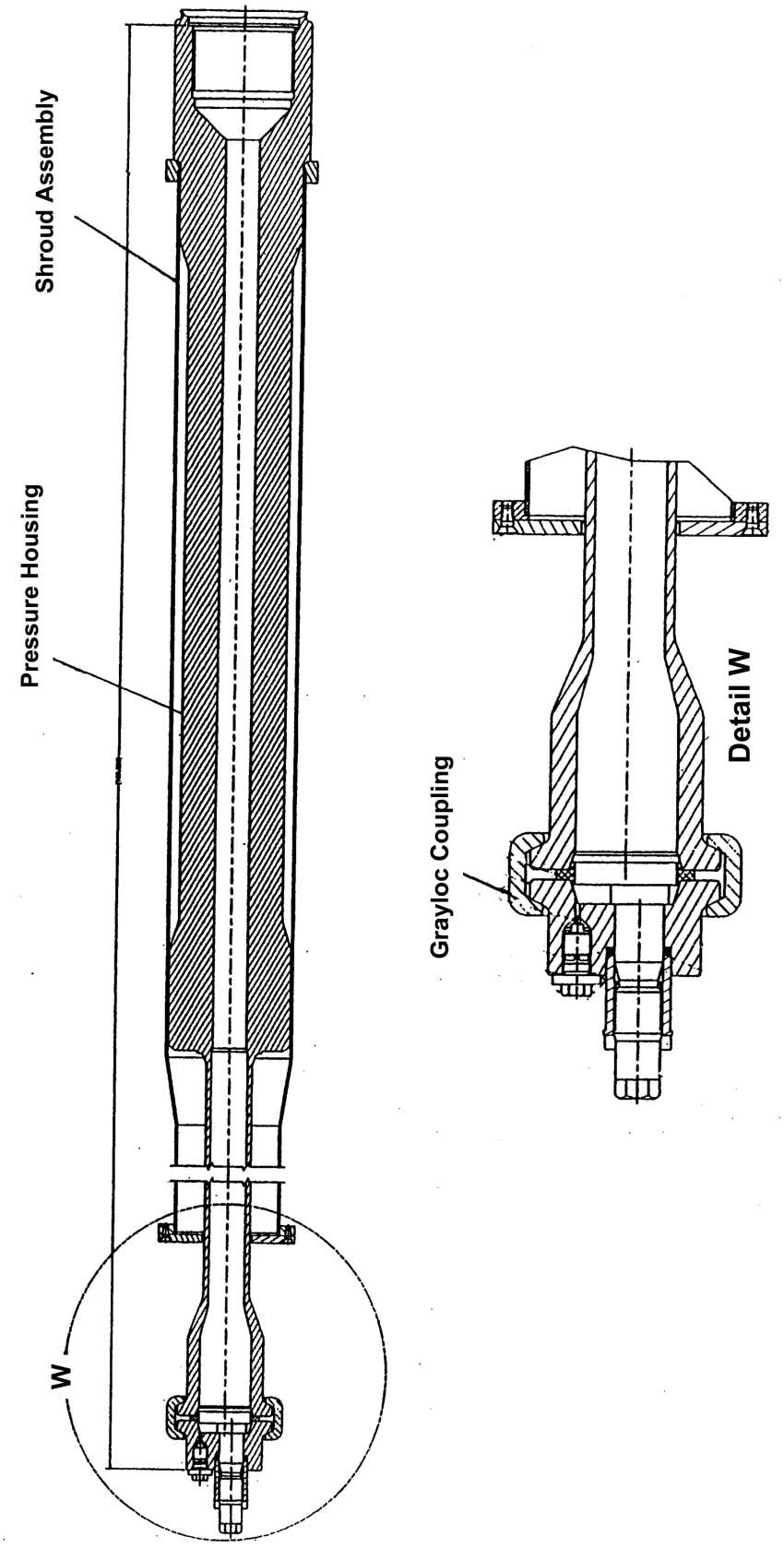

FIGURE 3.3–17 HEATED JUNCTION THERMOCOUPLE PROBE PRESSURE BOUNDARY INSTALLATION

FIGURE 3.3–18 TYPICAL HEATED JUNCTION THERMOCOUPLE PROBE ASSEMBLY INSTALLATION

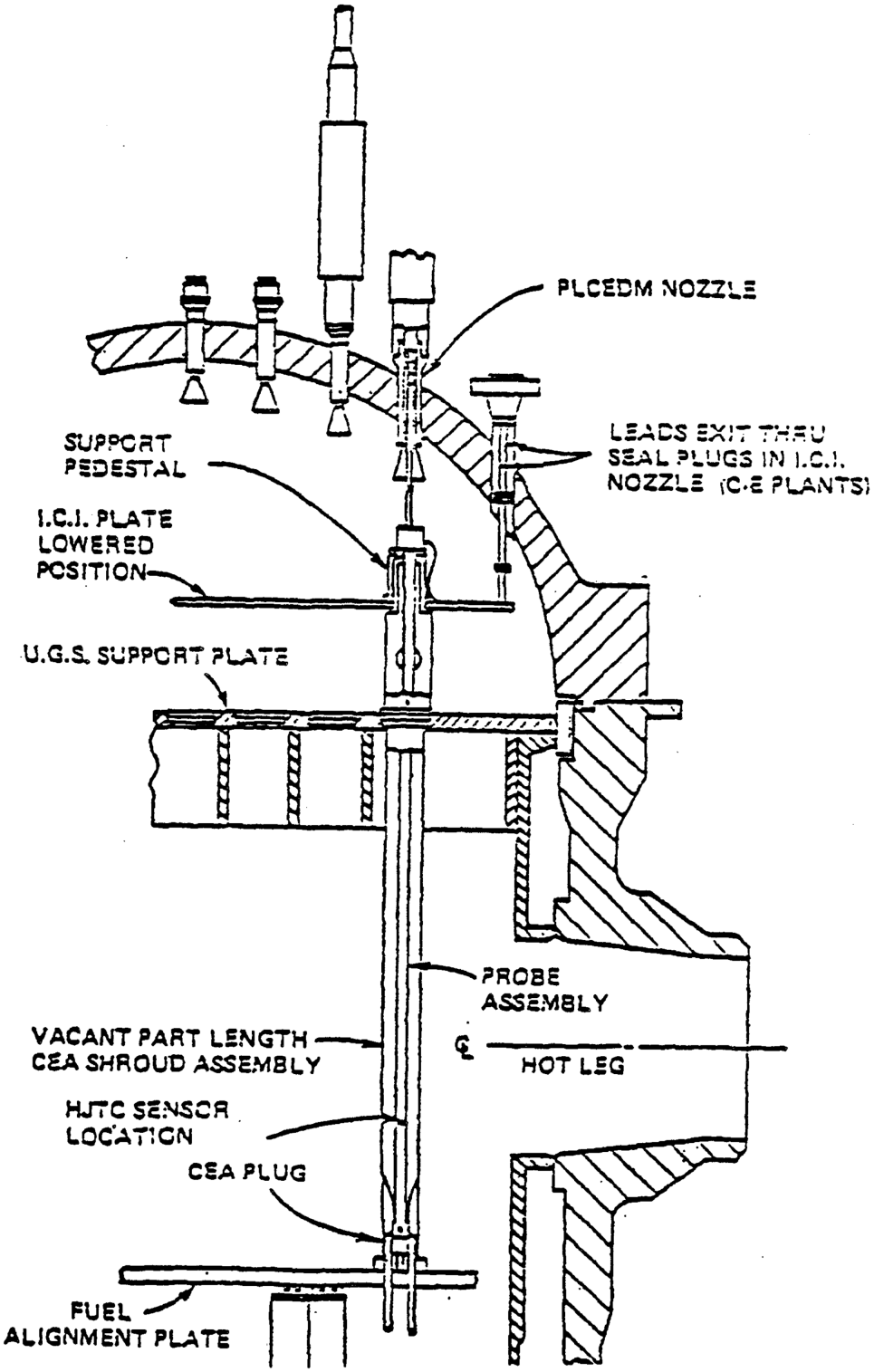

FIGURE 3.3–19 PLACEMENT OF NATURAL URANIUM REPLACEMENT FUEL RODS AND FUEL ASSEMBLY ORIENTATION RELATIVE TO THE CORE BAFFLE FOR CYCLE 19

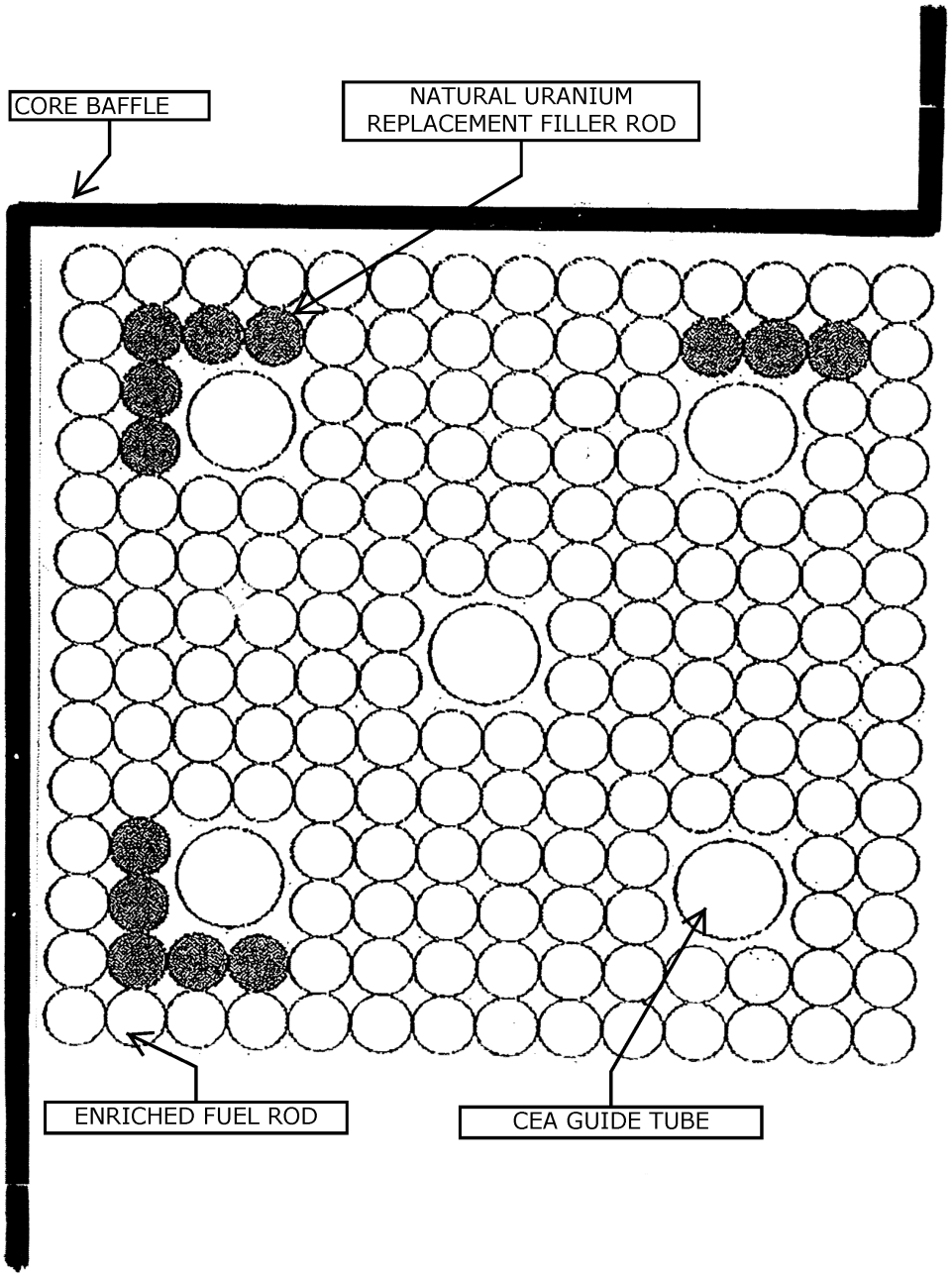

3.4 NUCLEAR DESIGN AND EVALUATION

3.4.1 GENERAL SUMMARY

This section summarizes the nuclear characteristics of the core and discusses the design parameters which are of significance to the performance of the core in normal transient and steady state operational conditions. A discussion of the nuclear design methods employed and comparisons with experiments which support the use of these methods is included.

The numerical values presented are based on a representative core design. Sufficient analyses are completed each cycle to ensure that actual reload batches keep operating parameters within design limits, accommodate essential reactivity requirements with the control system provided, and meet other requirements for safe operation.

3.4.2 CORE DESCRIPTION

The Millstone Unit 2 reactor consists of 217 assemblies, each having a 14 by 14 fuel rod array. The assemblies are composed of up to 176 fuel rods, four control rod guide tubes, and one center control rod guide tube/instrument tube. The fuel rods consist of slightly enriched UO_2 or UO_2-Gd_2O_3 pellets inserted into Zirconium Alloy tubes. The control rod guide and instrument tubes are made of Zircaloy-4. Each AREVA assembly contains nine spacers. A description of the AREVA supplied fuel design and design methods is contained in References 3.4-1, 3.4-2 and 3.4-3.

A representative loading pattern is shown in Figure 3.4–1 and is expressed in terms of previous cycle core locations and fuel assembly identifiers. A summary of fuel characteristics for a representative core design is presented in Table 3.4-1. Figure 3.4–2 presents representative quarter core assembly movements. Representative beginning of cycle (BOC) and end of cycle (EOC) assembly exposures are shown in a quarter core representation in Figure 3.4–3.

A representative low radial leakage fuel management plan results in scatter loading of the fresh fuel throughout the core. Some fresh assemblies loaded in the core interior contain gadolinia-bearing fuel in order to control power peaking and reduce the initial boron concentration to maintain the moderator temperature coefficient (MTC) within its Technical Specification limit. The exposed fuel is also scatter loaded in the center in a manner to control the power peaking.

3.4.3 NUCLEAR CORE DESIGN

The nuclear design bases for core design are as follows:

a. The design shall permit operation within the Technical Specifications for Millstone Unit 2 Nuclear Plant.

b. The design Cycle length (EFPD) shall be determined on the basis of an estimated Cycle energy and previous Cycle energy window.

c. The loading pattern shall be designed to achieve power distributions and control rod reactivity worths according to the following constraints:

1. The peak linear heat rate (LHR) and the peaking factor Fr shall not exceed Technical Specifications limits in any single fuel rod throughout the cycle under nominal full power operating conditions.

2. The SCRAM worth of all rods minus the most reactive rod shall exceed the shutdown requirement.

The neutronic design methods used to ensure the above requirements are consistent with those described in Reference 3.4-4.

3.4.3.1 Analytical Methodology

The neutronics methods used in the core analysis are described in Reference 3.4-4. The neutronic design analysis for each reload core is performed using the PRISM reactor simulator code. Full-core depletion calculations performed with PRISM are used to determine the core wide power distribution in three dimensions and to reconstruct the individual rod power and burnup distributions. Thermal-hydraulic feedback and axial exposure distribution effects are explicitly accounted for in the PRISM calculations. The CASMO/MICBURN assembly depletion model is used to generate the microscopic cross section input to the PRISM code.

3.4.3.2 Physics Characteristics

The neutronics characteristics of a representative reload core are presented in Table 3.4-2. The safety analysis for each cycle is applicable for a specified previous cycle energy window. A representative HFP letdown curve is shown in Figure 3.4–4.

3.4.3.2.1 Power Distribution Considerations

Representative calculated power maps are shown in Figures 3.4–5 and 3.4–6 for BOC (equilibrium xenon), and EOC conditions, respectively. The power distributions were obtained from a three-dimensional neutronics model with moderator density and Doppler feedback effects incorporated. The Technical Specification limits on Fr and LHR are 1.69 and 15.1 kW/ft, respectively.

3.4.3.2.2 Control Rod Reactivity Requirements

A representative shutdown margin evaluation is given in Table 3.4-3. The Millstone Unit 2 Technical Specifications require a minimum shutdown margin of 3,600 pcm.

3.4.3.2.3 Moderator Temperature Coefficient Considerations

The Technical Specifications require that the MTC be less than +7 pcm/°F at or below 70 percent of rated thermal power, less than +4 pcm/°F above 70 percent power and greater than -30 pcm/°F at 100 percent of rated thermal power. Representative MTC calculation results are presented in Table 3.4-2.

3.4.4 POST-RELOAD STARTUP TESTING

Startup tests will be performed at the beginning of each reload cycle to obtain the as-built core characteristics and to verify Technical Specification and core physics design parameters. The reload startup physics test program is based on ANSI-19.6-1 (Reference 3.4-9). The Startup Test Activity Reduction (STAR) Program (Reference 3.4-10) provides an alternative to the ANSI-19.6-1 test program provided that specific criteria for the reload core design and construction are satisfied. The STAR Program criteria are established in station procedures and include additional applicability requirements for core design, fuel and control element assembly (CEA) fabrication, CEA lifetime monitoring, refueling and startup testing.

The reload startup physics test program shall consist of the following:

a. Critical Boron Concentration - HZP, Control Rods Withdrawn.

b. Critical Boron Concentration - HZP, Control Rod Group(s) of at least 1% reactivity are fully inserted in the core. [1]

c. Control Rod Group Worths - HZP, two or more control rod groups shall be measured which are well distributed radially and represent a predicted total worth of at least 3% reactivity. [1]

d. Isothermal Temperature Coefficient - HZP.

e. Flux Symmetry - between 0 and 30% of full power.

f. Power Distribution - between 40 and 75% of full power.

g. Isothermal Temperature Coefficient - greater than 70% of full power.

h. Power Distribution - greater than 90% of full power.

i. Critical Boron Concentration - greater than 90% of full power.

j. HZP to full power reactivity difference.

1.This test may be eliminated if performing the STAR Program per Reference 3.4-10.

3.4.5 REACTOR STABILITY

3.4.5.1 General

Xenon induced spatial oscillations on the Millstone Unit 2 core fall into three classes or modes. These are referred to as axial oscillations, azimuthal oscillations, and radial oscillations. An axial oscillation is one in which the axial power distribution periodically shifts to the top and bottom of the core. An azimuthal oscillation is one in which the X-Y power distribution periodically shifts from one side of the core to the other. A radial oscillation is one in which the X-Y power distribution periodically shifts inward and outward from the center of the core to the periphery.

Xenon stability analyses indicate that a number of general statements can be made:

a. The time scale on which the oscillations occur is long, and any induced oscillations typically exhibit a period of 25 to 30 hours.

b. As long as the initial power peaking associated with the perturbation initiating the oscillation is within the limiting conditions for operation, specified acceptable fuel design limits will not be approached for a period of hours allowing an operator time to decide upon and take appropriate remedial action prior to the time when allowable peaking factors would be exceeded.

c. The core will be stable to radial mode oscillations at all times in the burnup cycle.

d. The core will be stable to azimuthal mode oscillations at all times in the burnup cycle.

e. All possible modes of undamped oscillations can be detected by both exactor and in-core instrumentation as discussed below.

3.4.5.2 Detection of Oscillations

Primary reliance for the detection of any xenon oscillations is placed on the exactor flux monitoring instrumentation. The power range excore neutron detectors (one axial pair per quadrant) are used to monitor the symmetry of power distributions and are located at distinct azimuthal and axial positions. These detectors are sensitive primarily to the power density variations produced by peripheral fuel assemblies in the vicinity of the detectors. All possible xenon induced spatial oscillations will affect the power densities of the peripheral fuel assemblies in the core.

In addition, the in-core instrumentation provides information which will be used in the early stages of cycle operation to confirm predicted correlations between indications from the excore detectors and the space-dependent flux distribution within the core. Later on, during normal operation, the in-core detector system provides information which may be used to supplement that available from the excore detectors.

3.4.5.3 Control of Oscillations

Since the reactor will not be operated under conditions that imply instability with respect to azimuthal xenon oscillation, no special protective system features are needed to accommodate asimuthal mode oscillations. Regardless, a maximum azimuthal power tilt is prescribed in the Technical Specifications along with prescribed operating restrictions in the event that the azimuthal power tilt limit is exceeded.

As described earlier, the power range excore neutron detectors are used to monitor the azimuthal symmetry of the power distributions since they are located at distinct locations in the X-Y plane. Should the excore detectors indicate different readings in the azimuthal direction, a tilt in the core power distribution would be indicated. When the tilt exceeds a preset magnitude an alarm will occur. In the event of an alarm, the orientation of the tilt will be determined and, on the basis of orientation, the proper CEA's will be manually adjusted to reduce the magnitude of the tilt.

The features provided for azimuthal xenon oscillation control are:

a. instrumentation for monitoring azimuthal power tilt.

b. administrative limits on azimuthal power tilt.

The excore detectors are used to monitor the axial power distribution and to detect deviations from the equilibrium distribution such as those which would occur during an axial xenon oscillation. This is done by monitoring variations in the external axial shape index, a parameter derived from the excore detector readings which is related to the axial power distribution. Control of axial xenon oscillation is accomplished utilizing Regulating Bank 7. When it is determined that the axial shape index may exceed the boundaries of a specified control band about the equilibrium value, this bank is slowly inserted and eventually withdrawn over a period of several hours. The core is then stabilized until a new oscillation develops.

The features provided for axial xenon control and protection are:

a. equipment for monitoring axial shape index.

b. administrative limits on axial power distribution, external axial shape index.

c. an axial shape index reactor trip (local power density - high).

d. use of Regulating Bank 7 for control of axial power distribution.

3.4.5.4 Operating Experience

Recent core designs for Millstone Unit 2 (Cycles 10 and beyond) have been developed to include longer fuel cycles along with low radial leakage fuel management. These current designs scatter load fresh fuel assemblies throughout the interior of the core with the highest burnup fuel assemblies being loaded along the core periphery. Core designs prior to Cycle 10 operation were not of a low radial leakage design due to the loading of fresh fuel assemblies along the core periphery.

With respect to xenon oscillations in the radial and azimuthal directions, studies indicate that core designs of a low radial leakage design (i.e., highest burnup assemblies loaded on the core periphery with fresh fuel assemblies scatter loaded about the core interior) are more stable than those designs which load fresh fuel assemblies along the core periphery. Therefore, the conclusions regarding xenon oscillations in the radial and azimuthal directions, which are presented in Section 3.4.5.5, remain applicable to current plant operations.

With regard to axial xenon oscillations, the core near end-of-cycle may be naturally unstable in the absence of any control rod action even if low leakage core designs are utilized. But axial xenon oscillations are sufficiently slow (the period of oscillation being 25 to 30 hours) so that there would be sufficient time to control the oscillations. In addition, automatic protection is provided if operator action is not taken to remedy the situation. Regulating Bank 7 CEA's are utilized for controlling axial xenon oscillations.

3.4.5.5 Method of Analysis

The classic method for assessing spatial xenon oscillations is that developed by Randall and St. John (Reference 3.4-5) which consists of expanding small perturbations of the flux and xenon concentrations about equilibrium values in eigenfunctions of the system with equilibrium xenon present. However, it is necessary to extend this simple linear analysis to treat cores which are nonuniform because of fuel zoning, depletion, and CEA patterns, for example. Such extensions have been worked out and are reported in References 3.4-6 and 3.4-8. In this extension, the eigenvalue separations between the excited state of interest and the fundamental are computed numerically for symmetrical flux shapes. For nonsymmetrical flux shapes, the eigenvalue separation can usually be obtained indirectly from the dominance ratio λ_1/λ_0, computed during the iteration cycle of the spatial calculation.

Numerical space time calculations are performed in the required number of spatial dimensions for the various modes as checkpoints for the predictions for the extended Randall-St. John treatment described above.

3.4.5.5.1 Radial Xenon Oscillations

To confirm that the radial oscillation mode is extremely stable, a space-time calculation was run for a reflected, zoned core 11 feet in diameter without including the damping effects of the negative power coefficient. The initial perturbation was a poison worth of 0.4 percent in reactivity placed in the central 20 percent in the core for 1 hour. Following removal of the perturbation, the resulting oscillation was followed in 4-hour time steps for a period of 80 hours. Results show that the oscillation died out very rapidly with a damping factor of about minus 0.06 per hour. When this damping coefficient is corrected for a finite time mesh by the formula in Reference 3.4-7, it is more strongly convergent. On this basis, it is concluded that radial oscillation instability will not occur.

This conclusion is of particular significance because it means that there is no type of oscillation where the inner portions of the core act independently of the peripheral portions of the core whose behavior is most closely followed by the excore flux detectors. Radial mode oscillations, even though highly damped, would be manifested as periodic variation in the excore flux power signal while the delta-T power signals remained constant. Primary reliance is placed on the excore flux detectors for the detection of any xenon oscillations.

3.4.5.5.2 Azimuthal Xenon Oscillations

Analyses indicate that the eigenvalue separation between the first asimuthal harmonic and the fundamental is about 0.86 percent in λ. The calculated damping coefficient for the first azimuthal mode is minus 0.016 per hour, and the higher modes will be even more strongly damped. Furthermore, the Doppler coefficient applicable to the Millstone Unit 2 reactor is calculated to be approximately minus 1.36×10^{-3} $\delta\rho/(kW/ft)$ which is sufficiently negative to ensure stability of all the azimuthal modes.

3.4.5.5.3 Axial Xenon Oscillations

As checkpoints for the predictions for the modified Randall-St. John approach, numerical spatial time calculations have been performed for the axial case at both beginning and end-of-cycle. The fuel and poison burnup distributions were obtained by depletion with soluble boron control so that the power distribution was strongly flattened. Spatial Doppler feedback was included in these calculations. The initial perturbation used to excite the oscillations was a 50 percent insertion into the top of the core of a 1.5 percent reactivity CEA bank for 1 hour. The damping factor for this case was calculated to be about +0.02 per hour; however, when corrected for finite time mesh intervals by the methods of Reference 3.4-7, the damping factor is increased to approximately +0.04. When this damping factor is plotted at the appropriate eigenvalue separation for this mode at end-of-cycle, it is apparent that good agreement is obtained with the modified Randall-St. John prediction.

Calculations performed with both Doppler and moderator reactivity feedback have resulted in damping factors which are essentially the same as those obtained with Doppler feedback alone. This result suggests that the constant power condition which applies to the axial oscillations results in a very weak moderator feedback since the moderator density distribution is fixed at the top and bottom of the core and only the density distribution in between can change.

For the calculated Doppler coefficient of minus 1.36 x 10^{-3} $\delta\rho$/(kW/ft), the damping factor toward the end of the burnup cycle is positive. Thus, within the uncertainties in predicting power coefficients and uncertainties in the analyses, there is a prediction of unstable axial xenon oscillations in the absence of any control action. These oscillations are sufficiently slow (the period of oscillation being 25 to 30 hours) so that there would be sufficient time to control the oscillations. In addition, automatic protection is provided if operator action is not taken to remedy the situation. Regulating Bank 7 CEA's are utilized for controlling axial xenon oscillations.

3.4.6 REFERENCES

3.4-1 "Generic Mechanical Design Report Exxon Nuclear 14 x 14 Fuel Assemblies for Combustion Engineering Reactors," XN-NF-82-09(A), Exxon Nuclear Company, Richland, WA 99352, November 1982.

3.4-2 "Design Report for Millstone Point Unit 2 Reload ANF-1," ANF-88-088(P), Rev. 1, Advanced Nuclear Fuels Corporation, Richland, WA 99352, August 1988.

3.4-3 "Millstone Unit 2 Mechanical Design Report for Increased Peaking" EMF-91-245(P), Siemens Nuclear Power Corporation, January 1992.

3.4-4 EMF-96-029(P)(A) Volumes 1 and 2, "Reactor Analysis System for PWRs Volume 1 - Mehodology Description, Volume 2 - Benchmarking Results", Siemens Power Corporation, January 1997.

3.4-5 Randall, D., "Xenon Spatial Oscillations," Nucleonics, 16, 3, pages 82-86 (1958).

3.4-6 Stacey, Jr., W. M., "Linear Analysis of Xenon Spatial Oscillations," Nuclear Sci. Eng., 30, pages 453-455 (1967).

3.4-7 Poncelet, C. G., "The Effect of a Finite Time Step Length on Calculated Spatial Xenon Stability Characteristics in Large PWR's" Trans. ANS, 10, 2, page 571 (1967).

3.4-8 CEND-TP-26., Diatch, P.B.

3.4-9 ANSI/ANS-19.6-1 "Reload Startup Physics Tests for Pressurized Water Reactors," 2005.

3.4-10 WCAP-16011-P-A, Revision 0, "Startup Test Activity Reduction Program," February 2005.

TABLE 3.4-1 FUEL CHARACTERISTICS FOR A REPRESENTATIVE RELOAD CORE

Fuel Types	N1	N2	N3	N4	P1	P2	P3	P4	P5	R1	R2	R3	R4	R5	R6
Central Zone Assembly Average Enrichment (w/o)	3.94	3.90	3.87	3.82	3.87	3.86	3.84	3.81	3.76	4.49	4.49	4.47	4.39	4.33	4.42
Number Gadolinia Bearing Rods	0	6	12	16	0	4	8	12	16	0	4	8	12	16	12
Nominal Density (% TD)	94	94	94	94	94	94	94	94	94	95	95	95	95	95	95
Pellet OD (inches)	0.370	0.370	0.370	0.370	0.370	0.370	0.370	0.370	0.370	0.377	0.377	0.377	0.377	0.377	0.377
Clad OD (inches)	0.440	0.440	0.440	0.440	0.440	0.440	0.440	0.440	0.440	0.440	0.440	0.440	0.440	0.440	0.440
Diametral Gap (inches)	0.0080	0.0080	0.0080	0.0080	0.0080	0.0080	0.0080	0.0080	0.0080	0.007	0.007	0.007	0.007	0.007	0.007
Clad Thickness (inches)	0.031	0.031	0.031	0.031	0.031	0.031	0.031	0.031	0.031	0.028	0.028	0.028	0.028	0.028	0.028
Rod Pitch (inches)	0.580	0.580	0.580	0.580	0.580	0.580	0.580	0.580	0.580	0.580	0.580	0.580	0.580	0.580	0.580
Spacer Material	Bimetallic	Bimetallic	Bimetallic	Bimetallic	Bimetallic	Bimetallic	Bimetallic	Bimetallic	Bimetallic	Bimetallic	Bimetallic	Bimetallic	Bimetallic	Bimetallic	Bimetallic
Fuel Supplier	AREVA	AREVA	AREVA	AREVA	AREVA	AREVA	AREVA	AREVA	AREVA	AREVA	AREVA	AREVA	AREVA	AREVA	AREVA
Fuel Stack Height Nominal (inches)	136.7	136.7	136.7	136.7	136.7	136.7	136.7	136.7	136.7	136.7	136.7	136.7	136.7	136.7	136.7
Number of Assemblies	8	20	8	25	8	8	12	8	36	8	8	8	8	48	4
Regionwise Loading (MTU)	3.04	7.60	3.03	9.43	3.04	3.04	4.55	3.03	13.58	3.19	3.19	3.19	3.17	18.98	1.59

TABLE 3.4-2 NEUTRONICS CHARACTERISTICS FOR A REPRESENTATIVE RELOAD CORE

<characteristic>	BOC	EOC
Critical Boron (ppm): HZP, ARO, No Xenon	1453	---
Critical Boron (ppm): HFP, ARO, Equilibrium Xenon	1024	0
Moderator Temperature Coefficient (pcm/°F): HZP	+2.0	-10.4
Moderator Temperature Coefficient (pcm/°F): HFP	-6.0	-23.3
Doppler Coefficient (pcm/°F)	-1.17	-1.33
Boron Worth (pcm/ppm): HZP	-8.8	-10.8
Boron Worth (pcm/ppm): HFP	-8.4	-10.4
LHR (kW/ft) HFP [(a)]	12.8	11.6
Delayed Neutron Fraction	0.0064	0.0054
HFP, PDIL Worth (pcm)	157	241
N-1 Rod Worth, HZP (pcm)	6271	7696
Excess Shutdown Margin (pcm): HFP	124	323
Excess Shutdown Margin (pcm): HZP	140	751

(a) Including uncertainties.

TABLE 3.4-3 REPRESENTATIVE SHUTDOWN MARGIN REQUIREMENTS

Control Rod Worth (pcm)

<parameter>	**BOC: HZP**	**BOC: HFP**	**EOC: HZP**	**EOC: HFP**
ARI	9315	9315	10450	10450
N-1	6271	6271	7696	7696
PDIL	2116	157	2862	241
[(N-1) - PDIL] * 0.9	3740	5503	4351	6710

Reactivity Insertion (pcm)

<parameter>	**BOC: HZP**	**BOC: HFP**	**EOC: HZP**	**EOC: HFP**
Power Defect	0	1507	0	2515
Void	0	50	0	50
Flux Redistribution	0	222	0	222
Total Requirements	0	1779	0	2787

Shutdown Margin (pcm)

<parameter>	**BOC: HZP**	**BOC: HFP**	**EOC: HZP**	**EOC: HFP**
[(N-1) * PDIL] * 0.9 - Total	3740	3724	4351	3923
Required Shutdown	3600	3600	3600	3600
Excess Shutdown Margin	140	124	751	323

FIGURE 3.4–1 REPRESENTATIVE FULL CORE LOADING PATTERN

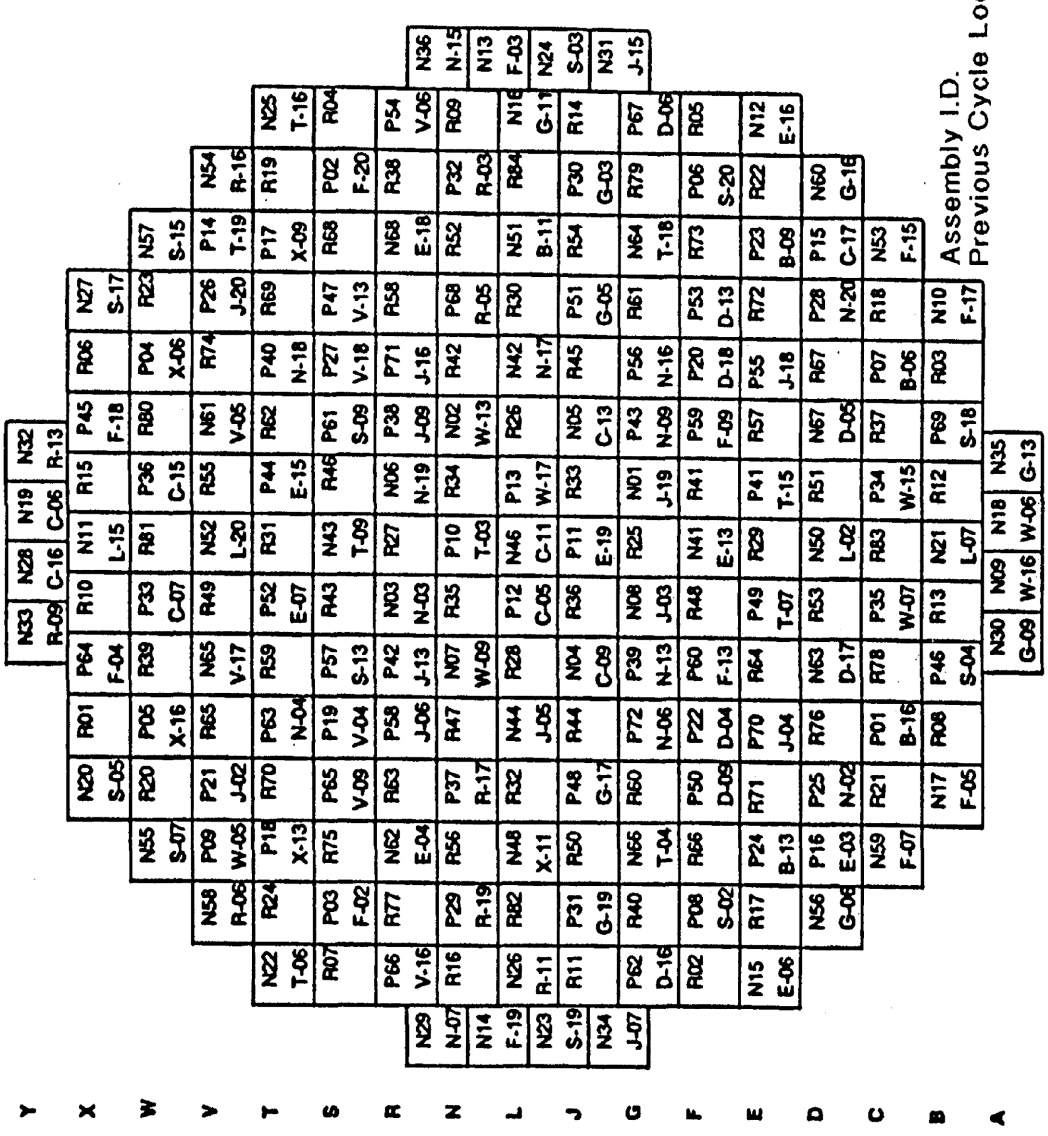

FIGURE 3.4–2 REPRESENTATIVE QUARTER CORE LOADING PATTERN

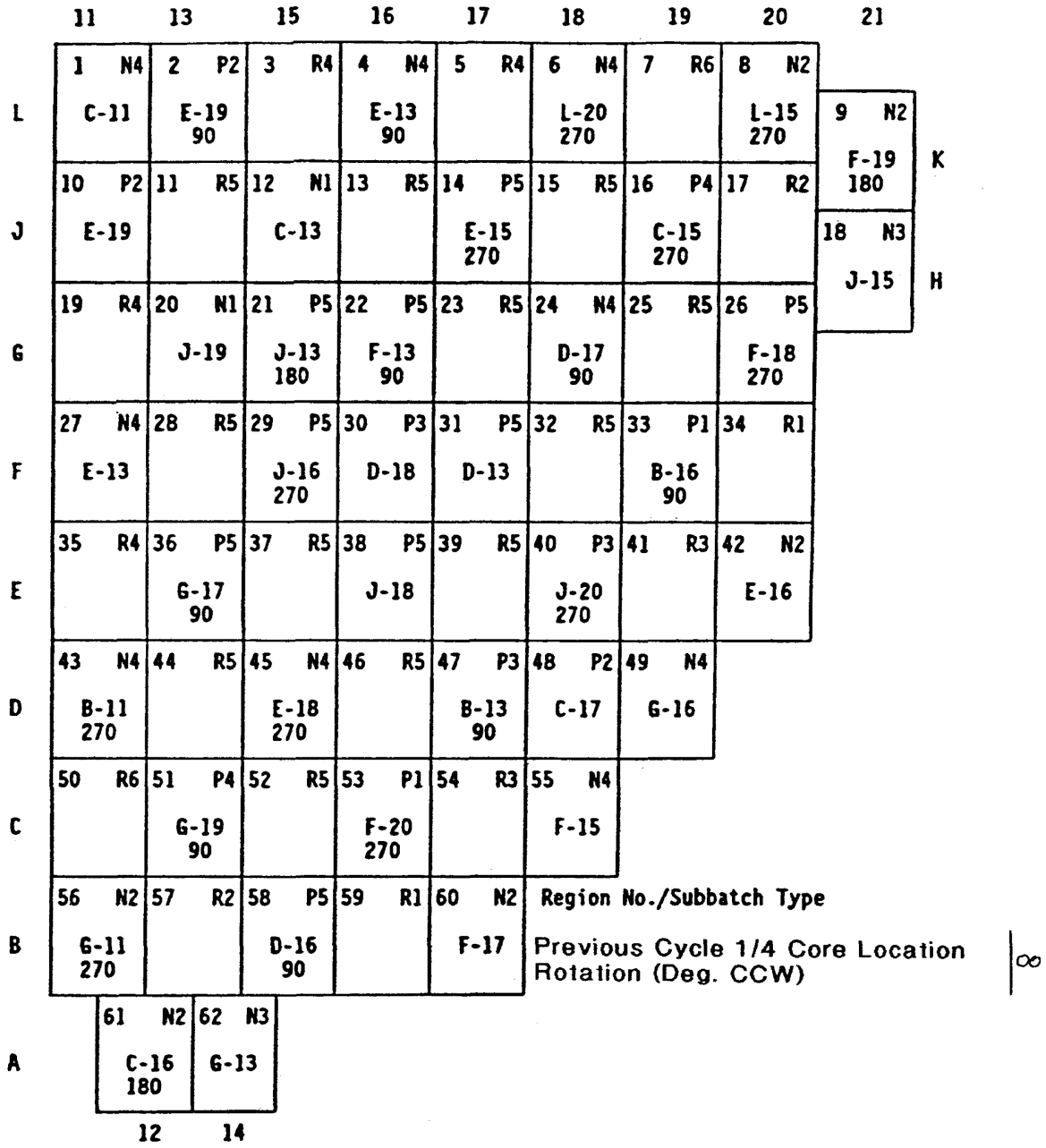

FIGURE 3.4–3 REPRESENTATIVE BOC AND EOC EXPOSURE DISTRIBUTION

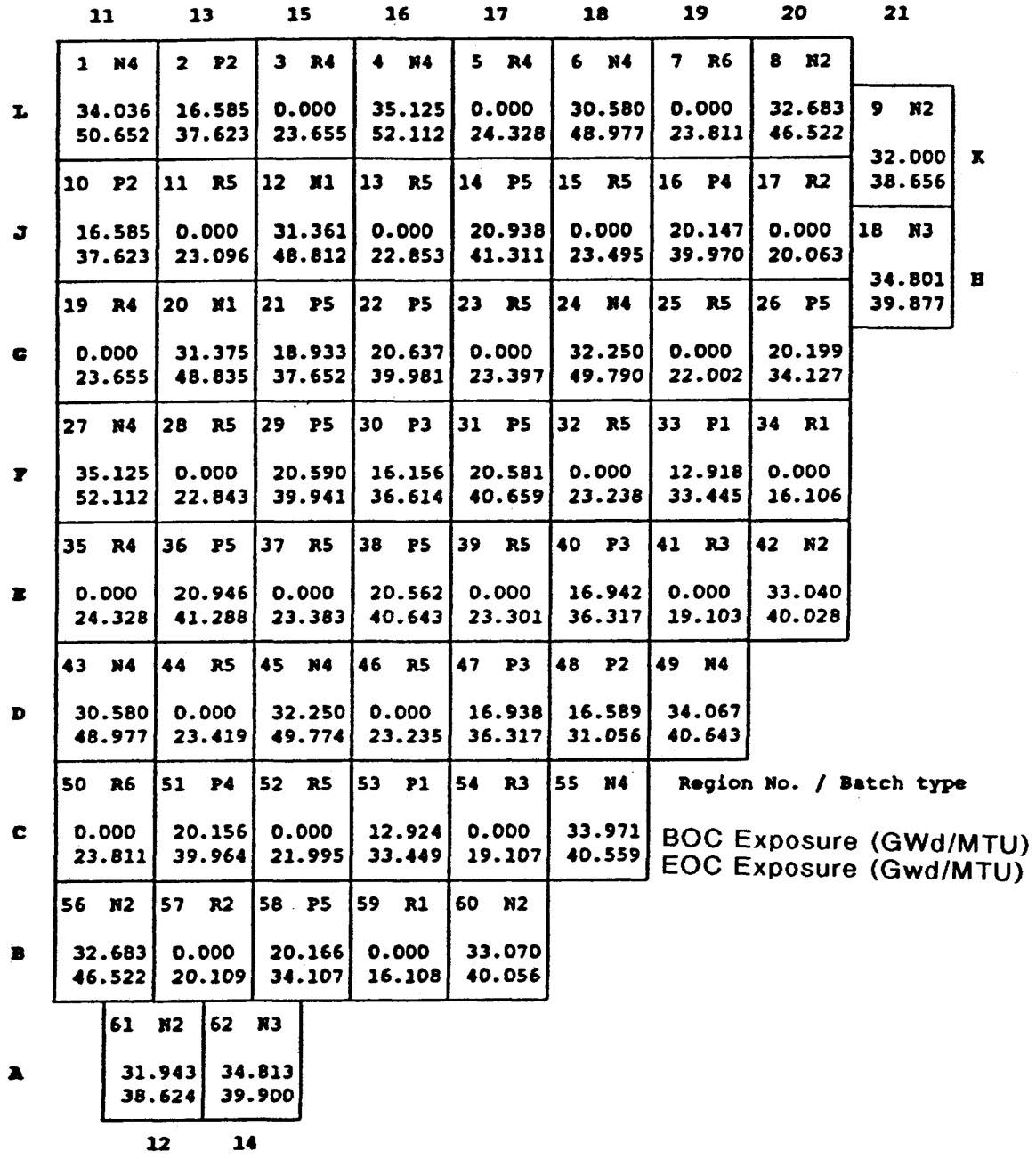

FIGURE 3.4–4 REPRESENTATIVE BORON LETDOWN, HFP, ARO

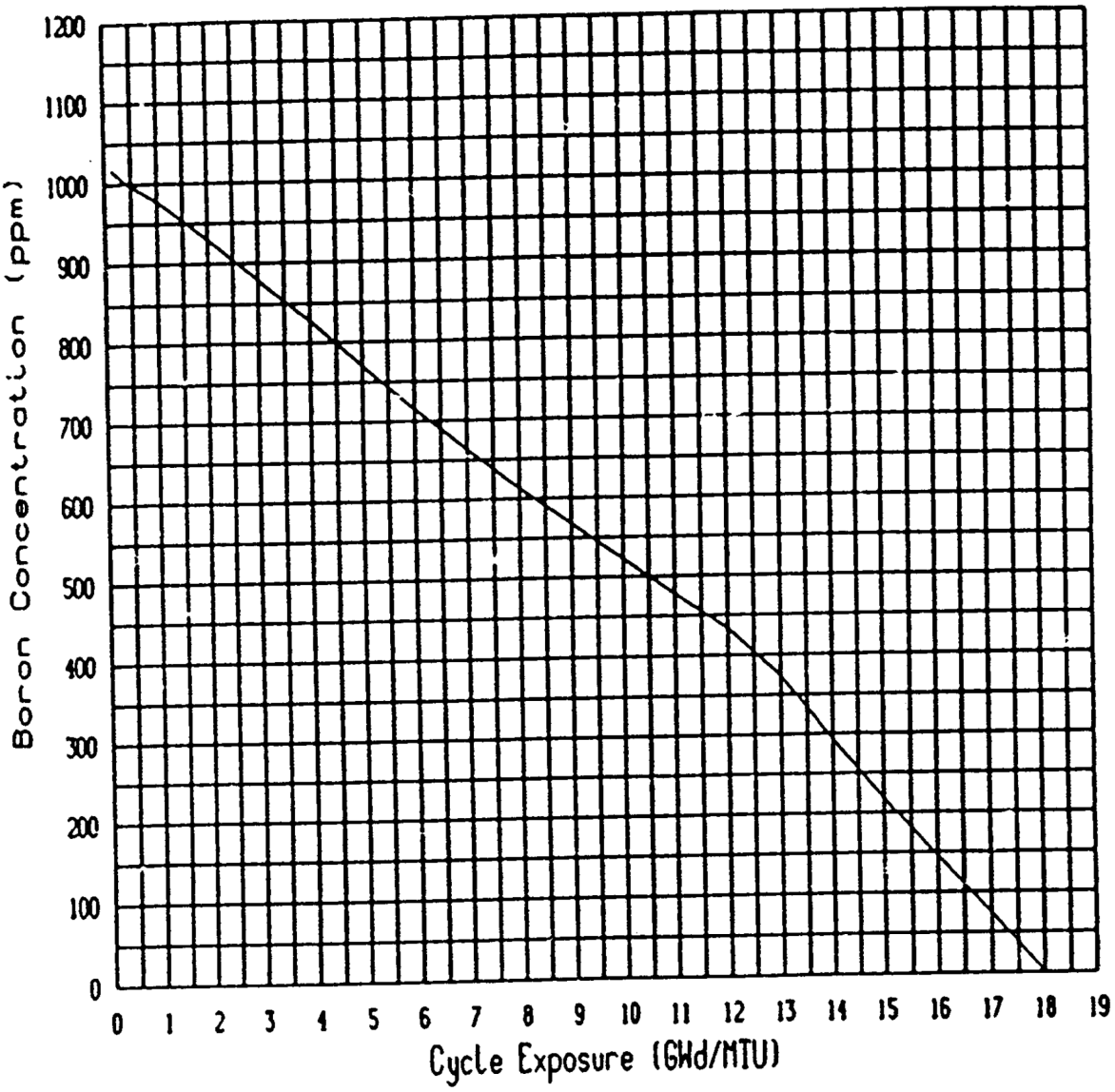

FIGURE 3.4–5 REPRESENTATIVE NORMALIZED POWER DISTRIBUTIONS, HOT FULL POWER, EQUILIBRIUM XENON, 150 MWD/MTU

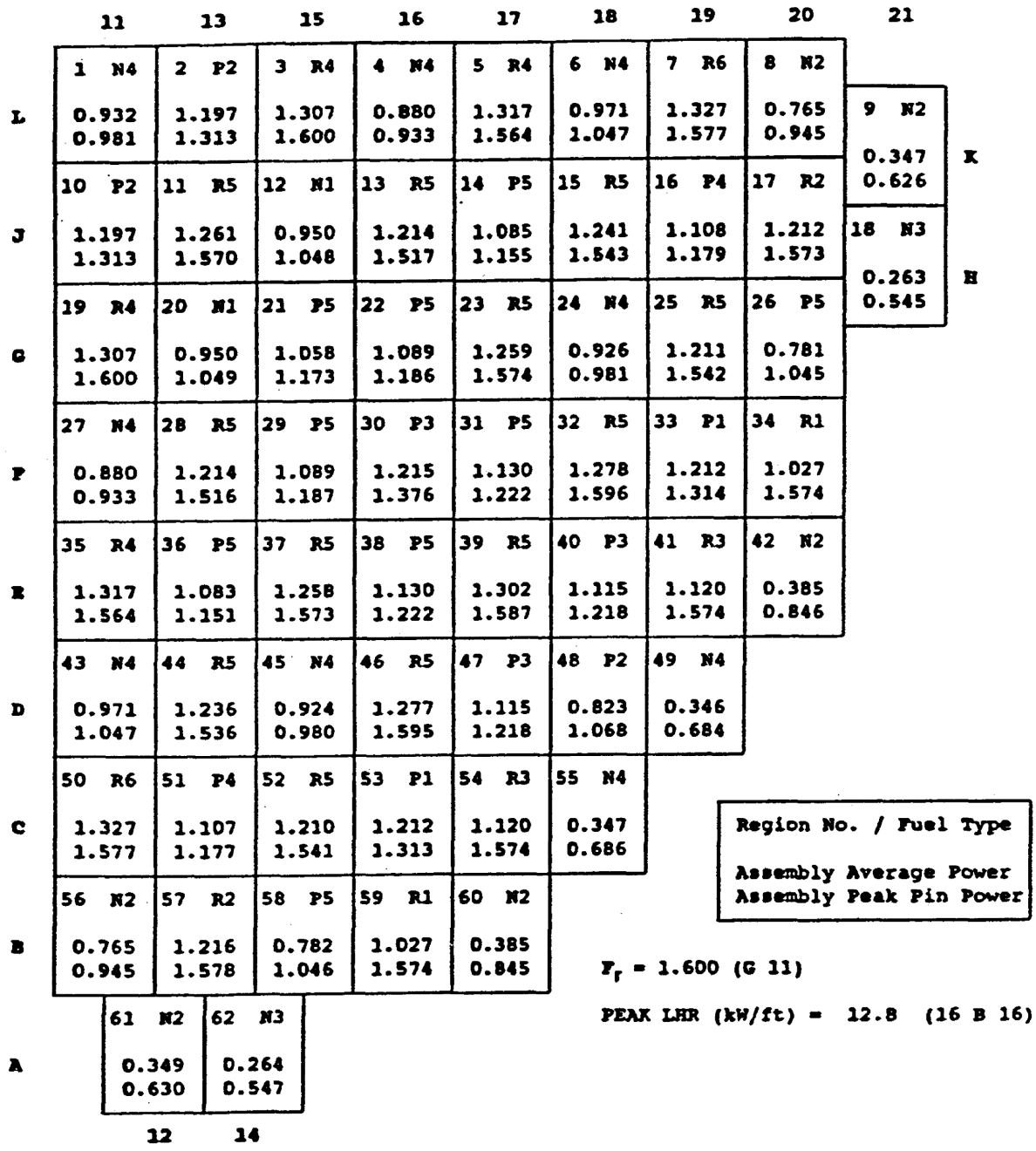

FIGURE 3.4–6 REPRESENTATIVE NORMALIZED POWER DISTRIBUTION, HOT FULL POWER, EQUILIBRIUM XENON, 18,020 MWD/MTU

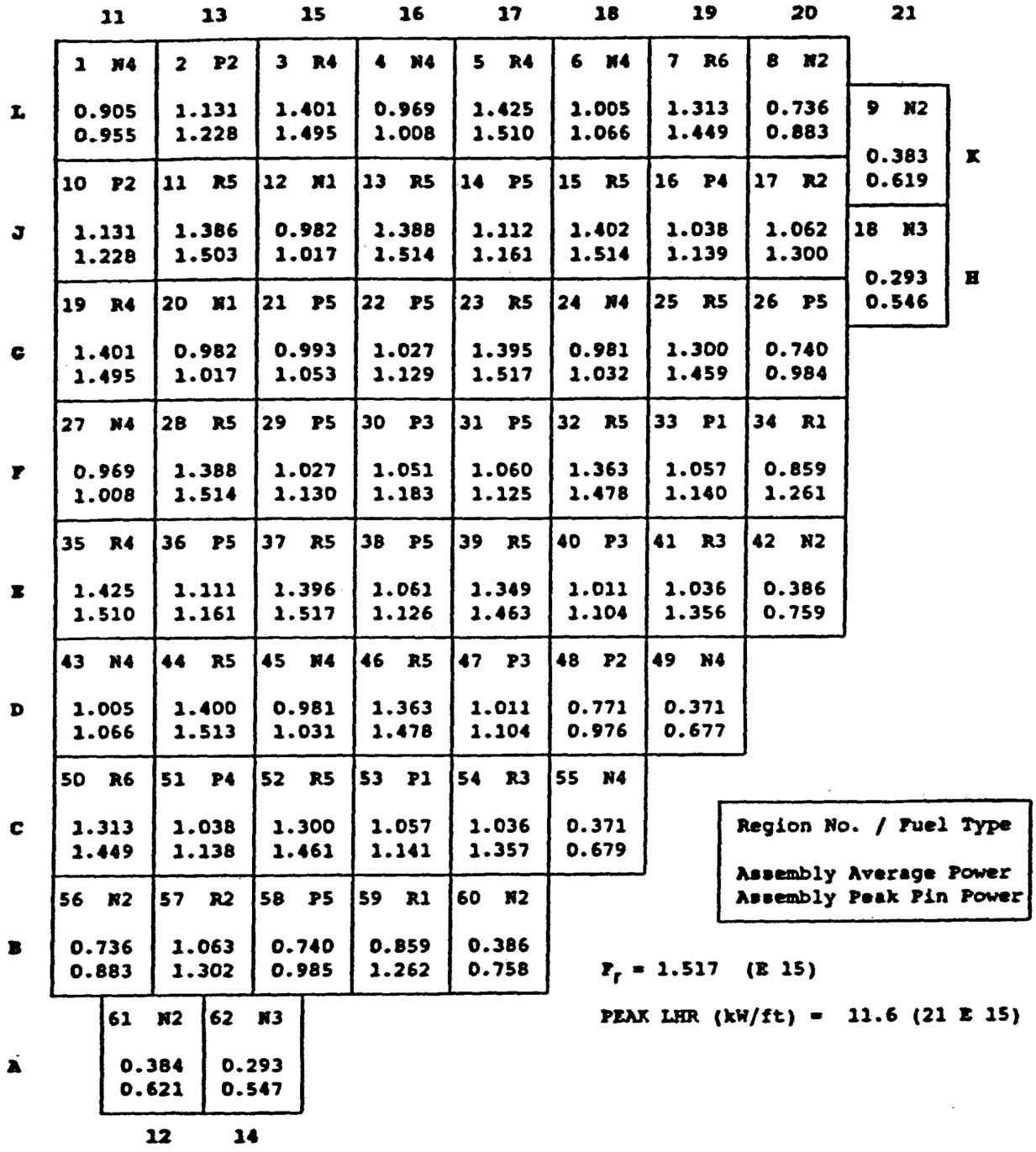

3.5 THERMAL-HYDRAULIC DESIGN

This section presents thermal and hydraulic analysis of the reactor core, analytical methods utilized, and experimental work supporting the analytical techniques. The prime objective of the thermal and hydraulic design of the reactor is the assurance that the core can meet normal steady state and anticipated transient performance requirements without exceeding the design bases. A summary of the significant reactor and fuel parameters used in the thermal and hydraulic design and analysis is presented in Table 3.5-1.

3.5.1 DESIGN BASES

3.5.1.1 Thermal Design

Avoidance of thermally induced fuel damage during any normal steady state and anticipated transient operation is the principal thermal and hydraulic design basis. The following limits are established, but violation of them will not necessarily result in fuel damage. The Reactor Protection System will provide for automatic reactor trip or other corrective action before these design limits are exceeded.

a. Avoidance of departure from nucleate boiling (DNB) for the limiting rod in the core with 95 percent probability at a 95 percent confidence level.

b. Limitation of the peak temperature of the fuel to less than the melting point during normal operation and anticipated transients.

Since the departure from nucleate boiling ratio (DNBR) criterion ensures that the cladding temperature remains close to the coolant temperature, no additional criteria for cladding temperature are required for normal operation and anticipated transients. For design basis accident conditions (loss of coolant accidents (LOCA)), under which the DNBR criterion does not apply, cladding temperatures are calculated to ensure that they remain below 2200°F, which is the peak clad temperature criterion of 10 CFR 50.46. For other postulated accidents, fuel failure is assumed to occur if the calculated DNBR is below the DNB correlation 95/95 limit.

3.5.1.2 Hydraulic Stability

Operating conditions shall not lead to flow instability during normal steady state and anticipated transient operation.

3.5.1.3 Coolant Flow Rate, Distribution and Void Fraction

A lower limit on the total primary coolant flow rate, called “design” flow, is set to assure that the core is adequately cooled when uncertainties in system resistance, pump head, and core bypass flow are taken in the adverse direction. By design of the reactor internal flow passages, this flow is distributed to the core such that the core is adequately cooled with all permissible core power distributions. The hydraulic loads for the design of the internals are based on the upper limit of the

flow. The upper limit is obtained in a similar manner as the design flow but with the uncertainties taken in the opposite direction.

To ensure that sufficient coolant flow reaches the fuel, the amount of coolant flow which bypasses the core through the guide tubes must not excessively reduce the active core flow. The guide tube coolant flow must, however, be sufficient to ensure that coolant in the guide tubes will not boil and ensure adequate cooling of the CEA fingers. The CEA drop time in the guide tubes must also meet the criterion of 90 percent insertion within 2.75 seconds to ensure that scram performance is in accordance with plant Technical Specifications.

Although the coolant velocity, its distribution, and the coolant voids affect the thermal margin, design limits need not be applied to these parameters because they are not themselves limiting with respect to thermal margin. These parameters are included in the thermal margin analyses and thus affect the thermal margin to the design limits.

3.5.2 THERMAL AND HYDRAULIC CHARACTERISTICS OF THE DESIGN

3.5.2.1 Fuel Temperatures

The RODEX2 code (Reference 3.5-1) incorporates models to describe the thermal and mechanical behavior of the fuel rod in a flow channel including the gas release, swelling, densification, and cracking in the pellet; the gap conductance; the radial thermal conduction; the free volume and gas pressure internal to the fuel rod; the fuel and cladding deformations; and the cladding corrosion as a function of burnup. The calculations are performed on a time-incremental basis with conditions being updated at each calculated increment.

3.5.2.1.1 Fuel Cladding Temperatures

The RODEX2 thermal-hydraulic model (Reference 3.5-1) calculates the lowest cladding surface temperature based on one of two heat transfer regimes; i.e., forced convection and fully developed nucleate boiling. The forced convection and fully developed nucleate boiling heat transfer correlations in RODEX2 were developed by Kays and Thom et al., respectively.

3.5.2.1.2 Fuel Pellet Temperatures

The RODEX2 radial temperature distribution model begins with the standard differential equation of heat conduction (Poisson Equation) for an isotropic solid with internal heat generation. The equation is written in cylindrical coordinates assuming that the thermal conductivity of the fuel is a function of fuel temperature, but is independent of position. With additional assumptions of axial symmetry, negligible heat conduction in the axial direction, and steady state conditions, a one-dimensional (i.e., radial) steady state form of the equation is derived and employed.

The minimum power level required to produce centerline melt in zirconium alloy clad uranium fuel rods is defined as the Fuel Centerline Melt Linear Heat Rate (FCMLHR) limit and is expressed in kW/ft. This FCMLHR is determined using the methodology of Reference 3.5-22. A conservative cycle specific FCMLHR limit is used for Millstone Unit 2. The maximum LHR for

normal operation and anticipated transients is typically well below the conservative FCMLHR limit. It should be noted that a gadolinia-bearing fuel rod will, for a given LHGR, operate with a higher fuel temperature than an all-uranium-bearing fuel rod. Gadolinia rods are specifically analyzed to centerline melt criteria.

3.5.2.1.3 UO_2 Thermal Conductivity

Lyon's expression for thermal conductivity of the fuel is used in RODEX2. Three corrections are applied: one for density, one to account for burnup-dependent degradation, and one to account for the gadolinia content in the fuel.

3.5.2.1.4 Gap Conductance

The RODEX2 gap conductance model is based on that proposed by Kjaerheim and Rolstad. The total gap conductance has three components: (1) gas conductance, (2) radiation, and (3) fuel/cladding solid-to-solid contact.

3.5.2.2 Departure from Nucleate Boiling Ratio

DNBRs are calculated using approved correlations. An approved core thermal-hydraulic computer code is used to determine the flow and enthalpy distribution in the core and the local conditions in the hot channel for use in the DNB correlation.

3.5.2.2.1 Departure from Nucleate Boiling

The XCOBRA-IIIC (Reference 3.5-2) computer code is employed to evaluate the thermal-hydraulic conditions in the various assemblies and in the subchannels of the limiting assembly. Heat, mass, and momentum fluxes between the inter-rod flow channels are explicitly calculated. Fuel and reactor design conditions employed in these calculations are given in Table 3.5-1.

The calculations include a statistically determined engineering factor to account for manufacturing tolerances, thermal expansion and densification effects. The engineering factor is applied to the local heat flux in the calculation of DNBR.

In-reactor densification results in a shortening of the fuel column. At power levels typical of DNBR-limiting rods, thermal expansion tends to offset the densification effect. The XCOBRA-IIIC model does not specifically model changes in stack length due to thermal expansion and densification.

The HTP DNB correlation, demonstrated to be applicable to the Framatome 14 by 14 reload fuel assemblies for CE reactors, is described in Reference 3.5-3. A minimum allowable limit corresponding to 95% probability with 95% confidence is set on the DNBR during normal operation and any anticipated transients. The XNB CHF correlation, applicable for use in the non-mixing grid region, is described in Reference 3.5-24.

3.5.2.2.2 Hot Channel Factors

Hot channel factors for heat flux and enthalpy rise, F_q and F_r:

The total hot channel factors for heat flux and enthalpy rise are defined as the maximum-to-core average ratios of these quantities. The heat flux hot channel factor (F_q) considers the local maximum linear heat generation rate at a point (the hot spot), and the enthalpy rise hot channel factor (F_r) involves the maximum integrated linear heat generation rate along a channel (the hot channel).

Engineering hot channel factor, F_E:

The engineering hot channel factor is used to evaluate the maximum linear heat generation rate in the core. This subfactor is determined by statistically combining the fabrication uncertainties for fuel pellet diameter, density, and enrichment, as well as the effect of densification. A conservative value of 1.03 is used. The effect of variations in fabrication tolerances is considered in the analysis. To account for manufacturing uncertainties and densification, the peak rod heat flux is increased by 3% in the calculation of DNBR.

3.5.2.2.2.1 Nuclear Peaking Factors

Assembly and rod peaking factors and axial power distributions are input into the XCOBRA-IIIC code. Departure from nucleate boiling is dependent on the local rod heat flux and the local fluid conditions within the channel.

The effect of asymmetries in core power distribution (specifically azimuthal power tilt) is not directly taken into account in the XCOBRA-IIIC thermal-hydraulic calculations. The effects of azimuthal power tilt are accounted for in the generation (verification) of the TM/LP trip and LPD trip monitoring setpoints through the measurement of radial peaking factors.

3.5.2.2.2.2 Rod Bowing Factor

As the fuel assembly burnup increases, the gaps between fuel rods change. Decreased rod-to-rod gaps can occur, which can reduce the DNB ratio. Penalties are calculated as a function of burnup and applied to the DNBR or peak linear power as appropriate.

3.5.2.2.2.3 Inlet Flow Distribution Factor

Inlet flow maldistribution is treated in the XCOBRA-IIIC model by applying a generic inlet flow penalty to the limiting assembly and its crossflow neighbors.

3.5.2.2.2.4 Flow Mixing Factor

The effects of both pressure-driven and turbulent flow mixing between channels on the hot channel enthalpy rise are calculated by the XCOBRA-IIIC computer code. The turbulent flow

mixing is modeled empirically and is based on the reduction of the data from hot mixing tests using XCOBRA-IIIC.

The geometry of the channels surrounding the hot channel and the radial power distribution affect the lateral enthalpy transport for both the pressure-driven and turbulent flow mixing.

3.5.2.2.3 Effects of Rod Bow on DNBR

In accordance with AREVA rod bow methodology (Reference 3.5-4), the magnitude of rod bow for assemblies of the type used in Millstone Unit 2 has been estimated. Significant impact on the DNBR due to rod bow does not occur until the gap closures exceed 50 percent. The maximum design exposure for AREVA reload fuel in Millstone Unit 2 is significantly less than that at which 50 percent closure occurs; therefore, rod bow does not significantly impact the minimum DNBR (MDNBR). A further consequence of the small amount of rod bow for AREVA fuel is that total power peaking is not significantly impacted.

3.5.2.3 Void Fraction and Distribution

The XCOBRA-IIIC model calculates the local thermal and hydraulic conditions for input to the DNB correlation. While local conditions of enthalpy, quality, flow rate and pressure are associated with a code-calculated local void fraction, the void fraction is not input to the DNB correlation. The DNB correlation is approved over a local quality range, but it is not a direct function of void fraction. Therefore, there is no explicit limit set on average or local void fraction beyond that implied in the test conditions used to develop the DNB correlation.

3.5.2.4 Coolant Flow Distribution

3.5.2.4.1 Coolant Flow Distribution and Bypass Flow

The minimum primary coolant flow rate at full power conditions is given in Table 3.5-1.

Tracing the coolant flow path in Figure 3.1–1, the coolant enters the four inlet nozzles and flows into the annular plenum between the reactor vessel and core support barrel. It then flows down the annulus between the reactor vessel and core barrel and up through the flow skirt to the plenum below the core lower support structure. The skirt and lower support structure help to even out the inlet flow distribution to the core. The coolant passes through the openings in the lower core plate and flows axially through the fuel assemblies. A portion of the coolant passes through the lower core plate and into the guide tubes in the fuel assemblies. The fuel assembly alignment plate is not drilled through in guide tube locations without CEAs; therefore, core bypass flow is limited in these guide tubes. After passing through the core, the coolant flows into the region outside the control element assembly shrouds. From this region, the coolant flows across the control element assembly shrouds and passes out through the outlet sleeves on the core barrel to the outlet nozzles.

The coolant which does not contact any fuel rods is termed core bypass coolant. The following are the principal core bypass routes:

a. Direct inlet to outlet coolant flow at the joint between the core support barrel sleeve and reactor vessel nozzle.

b. Coolant flow into the guide tubes in the fuel assemblies.

c. Coolant flow in the region between the core support barrel and core shroud.

d. Coolant flow from the inlet nozzle region through the alignment keyways to the vessel head region.

Table 3.5-1 gives the “best estimate” value for the core bypass flow rate as a fraction of the total primary flow rate. Taking into account the core bypass flow rate, the core flow rate, which is the effective flow rate for heat transfer, can be calculated from the total primary coolant flow rate.

3.5.2.4.2 Core Flow Distribution

The core flow distribution (CFD) analysis is performed to assess cross flow between assemblies in the core for use in subsequent MDNBR subchannel analyses. A full core model provides cross-flow boundary conditions to a full assembly model at the assembly boundaries. MDNBRs are computed from a full assembly simulation.

In the analysis, each fuel assembly in the Millstone Unit 2 core is modeled as a hydraulic channel. The calculations are performed with the XCOBRA-IIIC computer code (Reference 3.5-2). Cross flow between adjacent assemblies in the open lattice core is directly modeled. The single-phase loss coefficients are used in the CFD analyses to hydraulically characterize the assemblies in the core.

This computational procedure is designed to evaluate thermal-hydraulic conditions during boiling and non-boiling conditions. One-dimensional, two phase separated, slip flow is assumed in the XCOBRA-IIIC calculation. These assumptions are valid only if the cross flow between connecting channels is small compared to the axial velocities in the individual channels. Because small cross flow does exist, mathematical models have to be postulated for both turbulent and diversion cross-flow mixing. Models of the two-phase state are also defined in terms of void fraction, which is a function of enthalpy, flow rate, heat flux, pressure, and axial position. This computational procedure is not applicable when large blockages exist in the fuel bundles since this leads to considerable cross flow which cannot be adequately represented by the one-dimensional analysis.

Table 3.5-1 summarizes the reactor and fuel design parameters used in these CFD calculations and subsequent MDNBR analyses.

3.5.2.5 Pressure Losses and Hydraulic Loads

3.5.2.5.1 Pressure Losses

The fuel assembly irrecoverable pressure losses have been calculated using standard loss coefficient methods and results from model tests. The pressure loss across the AREVA fuel assembly was determined based on the results of Reference 3.5-5 and analyses.

3.5.2.5.2 Hydraulic Loads

3.5.2.5.2.1 Hydraulic Loads on Vessel Internal Components

The design hydraulic loads for the internal components for steady state operating conditions are listed in Table 3.5-2. These loads were derived from analysis and from reactor flow model and component test results. All hydraulic loads in Table 3.5-2 are based on the maximum expected system flow rate and a coolant temperature of 500°F. When these hydraulic loads are used in the structural analysis, they are adjusted for coolant temperature. The worst condition (i.e., coolant temperature) is not necessarily the same for each internal component; therefore, the loads are adjusted to reflect the difference in coolant temperature. This is done to ensure the design hydraulic stresses are acceptable during start-up and during power operation.

The types of loads considered in the analysis are: (1) steady-state drag and impingement loads, and (2) fluctuating loads induced by pump pressure pulsations, turbulence, and vortex shedding. All of these loads are not exerted on each internal component, but each component sees at least one of the loads. Table 3.5-2 lists the components and type of loads that are exerted on them.

3.5.2.5.2.2 Core Hydraulic Loads/Fuel Assembly Liftoff

The holddown spring force and the assembly weight force prevent the fuel assembly from lifting off the core support plate during reactor steady-state operation, based on the most adverse combination of component dimensional and material property tolerances. In addition, the holddown springs are designed to accommodate the additional load associated with a pump overspeed transient (resulting in possible temporary liftoff of the fuel assemblies), and to continue to ensure fuel assembly holddown following such occurrences. The limiting reactor steady-state conditions are the 4^{th} pump startup conditions. These correspond to the minimum temperature and maximum pressure and coolant flow for reactor startup. Thermal expansion of the reactor vessel and fuel assembly is also considered.

3.5.2.6 Correlation and Physical Data

Reference 3.5-1 describes the correlations and physical data employed in heat transfer calculations performed by RODEX2. Reference 3.5-7 describes the correlations and physical data employed in the hydraulic calculations performed by XCOBRA-IIIC. Reference 3.5-3 describes the correlations and physical data employed in the DNB correlation.

3.5.2.7 Plant Parameters for Thermal-Hydraulic Design

The plant parameters considered include total primary coolant flow rate, vessel inlet temperature, primary pressure, and core thermal power. Two sets of thermal-hydraulic conditions are defined: nominal conditions and design conditions. Nominal plant conditions represent the best estimate for the primary coolant flow rate, pressure, and vessel inlet temperature and do not include allowances for instrument errors. Design plant conditions represent the lower limit on primary flow rate when uncertainties in system resistance and pump head are included, and represent the upper limit on vessel inlet temperature when design margins on steam generator performance are included. Furthermore, the variations which occur during steady state operation in the power, pressure, and inlet temperature due to controller deadband and instrument error are considered with the design plant parameters. During steady state operation, the possible variations in these parameters define an operating envelope. One combination of these parameters gives the MDNBR, and this combination is utilized in Chapter 14 as the initial conditions in transient and accident analysis. Table 3.5-1 lists the nominal plant parameters.

3.5.2.8 Summary of Thermal and Hydraulic Parameters

The thermal and hydraulic parameters for the reactor are listed in Table 3.5-1.

3.5.3 THERMAL AND HYDRAULIC EVALUATION

3.5.3.1 Analytical Techniques and Uncertainties

3.5.3.1.1 XCOBRA-IIIC DNBR Analyses

The thermal-hydraulic simulations employed to evaluate the MDNBR were performed in accordance with AREVA’s Nuclear Regulatory Commission (NRC) approved thermal-hydraulic methodology for mixed cores (Reference 3.5-8).

The MDNBR performance of the core during anticipated transients will be demonstrated to meet the thermal-hydraulic design criterion on DNBR through the performance of transient analysis of the limiting events. The results of this analysis are included in Chapter 14.

3.5.3.1.2 Parameter Uncertainties

Tables 14.0.7-2 through 14.0.7-5 identify parameter uncertainties included in the AREVA thermal and hydraulic and DNB methodology. Plant instrument calibration procedures and related specification requirements are designed so that these uncertainties do not increase.

3.5.3.2 Hydraulic Instability Analysis

Boiling flows may be susceptible to thermohydrodynamic instabilities. These instabilities are undesirable in reactors since they may cause a change in thermohydraulic conditions that may lead to a reduction in the DNB heat flux or to undesired forced vibrations of core components. However, unlike in Boiling Water Reactors (BWRs), hydraulic stability is not a concern in PWR

cores. This statement, which is discussed below, is supported by the literature and the state of the art on instabilities occurring in two-phase flow systems.

Instabilities in vertical up-flow of a two-phase mixture in a heated channel can be broadly classified into several categories. Of these, the following relevant instabilities are discussed.

1. Flow Excursion

   Also called Ledinegg Instability, this is well described in Ref. 3.5-10. This instability occurs when the slope of the boiling channel pressure drop-flow rate curve (internal characteristic) becomes smaller than the slope of the loop supply pressure drop-flow rate curve (external characteristic), i.e.,

$$\frac{d(\Delta P)}{dG}\Big|_{internal} < \frac{d(\Delta P)}{dG}\Big|_{external}$$

   where ΔP is the pressure drop and G is the mass flow rate.

   In this manner, a negative flow perturbation will be amplified as the internal pressure drop becomes larger than the external at the perturbed flow and the flow decelerates further until a stable point is reached.

   If the core is considered as a single average channel, the external pressure and flow characteristics as seen by the core exhibit

$$\frac{d(\Delta P)}{dG}\Big|_{external} < 0$$

   due to the pump characteristics. This negative slope is stabilizing.

   On the other hand, considering flow in a single limiting bundle, the other parallel flow paths impose a flat pressure drop versus flow relation where $d(\Delta P)/dG = 0$. While this situation is less stable than the average core assumption, it is mitigated by the cross flow and mixing between this limiting bundle and the neighboring bundles. Ref. 3.5-11 shows experimentally a definite stabilizing influence of cross flow mixing.

   The internal pressure drop versus flow characteristics were shown to satisfy the Ledinegg stability criterion

$$\frac{d(\Delta P)}{dG}\Big|_{internal} > 0$$

for a wide range of conditions in the LOFT reactor (Ref. 3.5-12) which closely approximates a PWR core during nominal and worst case operating conditions.

Therefore, in conclusion, Ledinegg Instability is not a concern in PWR cores.

2. Density Wave Instability

Dynamic instabilities may occur even when the static stability criterion is satisfied (pressure drop increases when flow increases). For a density wave dynamic instability, consider an inlet flow increase perturbing the initial value. The rate of enthalpy rise and density effects will travel up the channel, and the pressure drop increase is delayed. In the case of a sinusoidal inlet flow perturbation of particular frequency, the lagging pressure drop response is such that its instantaneous value supports the growth of the initial perturbation (Ref. 3.5-13). Such unstable behavior requires the delayed portion of the total pressure drop (in the two-phase region) to be large compared with the single-phase pressure drop. The onset of this instability depends on the operating conditions and the distribution of pressure drop along the channel, as well as the external loop characteristics. A vast body of literature and several computer programs for the analysis of density waves exists mainly for BWR concerns (see for example the collection of papers in Ref. 3.5-14). Inferences from BWR experience are drawn to dismiss the possibility of density wave instabilities in a PWR core:

- Unlike a BWR, there is no riser section contributing significantly to the 2-phase pressure drop.

- For a single limiting channel with a constant pressure drop boundary condition, the cross flow in a PWR core has a stabilizing effect.

- Density wave oscillations are known to be stabilized with increasing pressure (decreasing enthalpy and density difference between the two phases). No unstable density wave oscillations could be obtained for pressures higher than 1200 psia (Ref. 3.5-15).

- BWR oscillations occur when the saturated boiling boundary is low (elevation <<4 feet). For a PWR, such boiling boundary can be achieved at nominal flow rates by more than doubling the power, which leaves a considerable stability margin even for the worst case transient.

- Considering the nuclear coupling, the void-reactivity coefficient in a PWR is reduced when the coolant is borated. Such reduction in the void-reactivity coefficient is stabilizing to this mode of oscillation.

- For a density wave coupled with an out-of-phase neutron flux oscillation mode, the large subcritical reactivity of the first flux harmonic stabilizes this mode of hydraulic-neutronic oscillation. This is due to the PWR core being small compared with typical BWR cores.

The LOFT reactor stability study also addressed the density wave oscillations and concluded that these are not likely (Ref. 3.5-12).

In conclusion, Density Wave Instability is not a concern in PWR cores.

3. Flow Pattern Transition Instability

The term “Flow Pattern Instability” is used in the literature in two connotations. The first refers to the slug flow pattern where a particular elevation in a heated channel experiences a succession of high void and low void flows as a vapor slug passes through (Ref. 3.5-12). As a vapor slug clears the channel exit, the average void content in the channel is temporarily reduced and vice versa resulting in pressure drop and flow rate oscillations. In a worst case condition in a PWR, slug flow may occur in a small number of channels near the exit. No significant oscillatory response is expected, particularly since the slug formation is limited to a short segment near the exit of the hot channels.

The more common meaning of the “Flow Pattern Transition Instability” refers to unstable transitions between bubbly and annular flow (Ref. 3.5-10). A flow rate perturbation decreasing the flow rate and increasing the void fraction will result in flow transition from bubbly-slug to annular pattern. The annular flow is characterized with lower pressure drop, which results in accelerating the flow. The increase in flow rate brings the void fraction back below the value required to support annular flow. Thus the transition back to bubbly-slug regime takes place.

Extensive work has been done on flow pattern transition (see for example Ref. 3.5-16). Most work was limited to pressures of 1000 psia and below where these transitions are more distinct. At higher pressures, Hosler (Ref. 3.5-17) notes for 1400 and 2000 psia, that the flow appears more homogeneous with no reliable observation of pattern transition.

Weisman et. al. (Ref. 3.5-18) observed no premature DNB due to bubbly-to-slug flow transition which they expected as the range of tested void fractions covers the transition range. Hosler (Ref. 3.5-17), on the other hand, noted that CHF occurred via a film dryout mechanism in established annular flow, which is far from the transition boundary to bubbly-slug pattern.

In conclusion, Flow Pattern Transition Instability is not a concern in PWR cores.

3.5.3.3 Core Hydraulics

3.5.3.3.1 Fuel Assembly Pressure Drop Coefficients

Pressure drop coefficients for the AREVA reload fuel presented are derived from pressure drop tests performed in AREVA's portable hydraulic test facility (Reference 3.5-5). The pressure drop coefficients are for the liquid phase and are referenced to the bare rod flow area.

The introduction of the AREVA Standard CE14 HTP fuel with M5 cladding in Reload Batch EE has a negligible effect on core hydraulics. The AREVA Standard CE14 HTP fuel with M5 cladding is hydraulically equivalent to the HTP fuel with Zircaloy-4 cladding (Reload Batches Y through DD fuel).

3.5.3.3.2 Guide Tube Bypass Flow and Heating Analysis

The guide tube thermal-hydraulic design calculations are performed to demonstrate adequate cooling of the CEA fingers and to ensure that bypass flow through the guide tubes does not unduly reduce core flow.

Flow enters the guide tube through the weep holes and cap screw and exits through the top of the guide tube. In the Millstone Unit 2 core, there are 81 assemblies under CEA positions. Of these, 73 assemblies are under active CEA positions. The CEA fingers extend a short distance into the guide tube in these 73 assemblies at the all-rods-out (ARO) position which provides a substantial reduction in the guide tube bypass flow. The remaining eight assemblies were originally under the part length CEAs which have been removed. In these eight assemblies, the flow is unimpeded, since the last flow plugging devices were removed in Cycle 12. The assembly guide tubes of 91 assemblies project a short distance into close fitting sockets in the upper alignment plate. The resulting flow annulus represents a significant resistance to guide tube bypass flow in these assemblies. The remaining 45 core locations are instrument tube locations. In these locations, the peripheral guide tubes also project a short distance into close fitting sockets in the upper alignment plate. The center guide tube contains instrumentation which produces a flow annulus which in turn reduces the flow in the center guide tubes.

The guide tube model employed in the flow and heating calculations uses loss coefficients to determine the guide tube flow path hydraulic losses. The core pressure drop at rated power and flow is employed as the driving force for flow through the guide tube. The model permits calculation of the guide tube configurations described above. The guide tube thermal model includes the effects of coolant heating by gamma deposition and neutron deceleration. The effects of heating due to neutron absorption and gamma deposition in the inserted control rod are evaluated. Heat transfer through the guide tube wall to the coolant in the surrounding assembly is accounted for in the model.

Calculations were performed to assess the maximum expected guide tube bypass flow (Reference 3.5-6). At hot full power (HFP), ARO configuration was selected as that resulting in the greatest bypass flow. The total core bypass flow, including flow through the guide tubes in this

instance, was determined to be less than 4.0 percent of vessel flow. The result confirms that guide tube bypass flow does not unduly reduce core flow.

To assess the adequacy of guide tube cooling, a simulation was also performed for a single assembly with the CEA fully inserted at HFP conditions. The fully inserted CEA fingers substantially increase the hydraulic resistance in the guide tube, and also represent a significant heat source. The exit coolant temperature is well below saturation. Heat transfer through the guide tube wall provides a significant part of the cooling.

Based on the results described above, it is concluded that ample guide tube cooling is afforded by the current design, and that bypass flow remains within acceptable limits.

3.5.3.3.3 Control Element Assembly Insertion Time Analysis

A large data base of CEA insertion time measurements has been obtained at a CE plant similar to Millstone Unit 2, with fuel identical in pertinent guide tube design characteristics to the Millstone Unit 2 AREVA reload fuel. The measurements span a time period during which reload quantities of AREVA fuel resided in the core. Statistical analysis (Reference 3.5-6) of this data indicates that the CEA 90 percent insertion time is equal to or less than 2.5 seconds, which is well below the maximum acceptable 90 percent insertion time of 2.75 seconds specified in the Technical Specifications.

Over 500 CEA insertion time measurements from nine different tests were analyzed. The measurements reflect the time required to reach 90 percent insertion from interruption of power to the CEA drive mechanism. Approximately six standard deviations separate the mean of the measured CEA insertion time data from the 2.75 second maximum allowable for Millstone Unit 2.

With over 500 data points, higher order statistics may also be applied to the data to conclude that the rod drop time will be equal to or less than the greatest time measured in the tests with a probability of 99 percent at a 99 percent confidence level. The greatest rod drop time in the tests, as noted above, was 2.50 seconds. The AREVA assemblies are, therefore, expected to conform to the maximum CEA 90 percent insertion time of 2.75 seconds with a substantial margin.

3.5.3.3.4 Fuel Assembly Liftoff

The hydraulic lift force on the fuel assembly was calculated (Reference 3.5-6) using the drag coefficient for a 14 by 14 fuel assembly with bimetallic spacer grids. This value differed slightly for Reload Batches M, N, and P (Cycles 10, 11, and 12). The replacement of a bimetallic spacer with a debris resistant Inconel HTP spacer increased the drag while the thermal rounding of the leading edges of the remaining bimetallic spacers decreased the drag. The overall effect was a slight increase in drag force. The total of the buoyancy and hydraulic lift forces was calculated to be 1194 pounds. The assembly weight and spring force totals 1801 lbs, thus providing a 607 pound holddown margin. This margin, which is more than half of the worst case steady state lift force, will envelope any minor variation due to the spacer modifications. It will also provide holddown during and after a 20% pump overspeed resulting in a 44% lift force increase. For

Reload Batch R (Cycle 13) and Batch S, the fuel assembly weight increased by approximately 40 pounds and a bimetallic spacer replaced the Inconel HTP spacer, increasing the margin to liftoff. A similar analysis was performed for the Reload Batch T design. The use of HMP spacers beginning with Reload Batch Y has a negligible effect on lift. The introduction of the AREVA Standard CE14 HTP fuel with M5 cladding in Reload Batch EE has a negligible effect on lift. The AREVA Standard CE14 HTP fuel with M5 cladding is hydraulically equivalent to the HTP fuel with Zircaloy-4 cladding (Reload Batches Y through DD fuel).

The maximum shear stress of 84,062 psi in the holddown springs occurs in the cold reactor condition. This is below the design criterion of 100,000 psi. The stress at reactor operating conditions is 74,188 psi, which is below the criterion of 90,000 psi at operating temperature.

Irradiation may cause some stress relaxation of the Inconel X-750 holddown springs while causing irradiation induced growth of the fuel assemblies. The assembly growth results in higher spring deflection which offsets any radiation induced relaxation of the springs. The springs are partially shrouded in spring cups, which minimize flow-induced vibration of the springs and prevent potential fretting wear.

3.5.4 TESTS AND INSPECTIONS

3.5.4.1 Reactor Testing

Thermal-hydraulic design criteria are verified during plant startup testing. This is accomplished by measuring the primary intrinsic parameters (e.g., levels, pressures, temperatures, flows, neutron fluence and differential pressures) and calculating the non-measurable and extrinsic parameters (e.g., power level, core peaking factors). During the operating cycle, various thermal-hydraulic parameters are periodically monitored to ensure compliance with the Technical Specifications.

3.5.4.2 AREVA DNB and Hydraulic Testing

3.5.4.2.1 DNB Testing

Details of the testing supporting the HTP DNB correlation are contained in Reference 3.5-3.

3.5.4.2.2 Fuel Assembly Hydraulic Testing

Single-phase hydraulic characteristics of the AREVA Millstone Unit 2 fuel assembly were experimentally determined by hydraulic tests (Reference 3.5-5) performed in AREVA's Portable Hydraulic Test Facility (PHTF).

The pressure drop testing characterized the component loss/flow coefficients of the lower tie plate (including the inlet hardware), spacers, and the upper tie plate (including the exit hardware).

Differential pressure measurements were taken over a range of Reynolds Numbers (N_{Re}). These data were used to drive empirical relationships, which describe the single-phase pressure drops of the Millstone Unit 2 fuel assembly and its components.

These test data from Reference 3.5-5 were used to calculate the Batch M, N, and P lower tie plate, spacer, and upper tie plate pressure drop coefficients, and the bare rod friction factor. Additional test data and analyses were used to determine the Batch R lower tie plate pressure drop coefficient correlations. The loss/flow coefficients derived from these tests and calculations are all referenced to the bare rod Reynolds Number.

3.5.5 REFERENCES

3.5-1 XN-NF-81-58(P)(A), Revision 2, and Supplements 1 and 2, “RODEX2 Fuel Rod Thermal-Mechanical Response Evaluation Model,” March 1984.

3.5-2 XN-NF-75-21(P)(A), Revision 2, “XCOBRA-IIIC: A Computer Code to Determine the Distribution of Coolant During Steady-State and Transient Core Operation,” January 1986.

3.5-3 EMF-92-153(P)(A) Rev. 1, “HTP: Departure From Nucleate Boiling Correlation for High Thermal Performance Fuel,” Siemens Power Corporation, January 2005.

3.5-4 XN-75-32(P)(A), Supplements 1, 2, 3, and 4, “Computational Procedure for Evaluating Fuel Rod Bowing,” October 1983.

3.5-5 ANF-89-018(P), “Single-Phase Hydraulic Flow Test of ANF Millstone-2 Fuel Assembly,” January 1989.

3.5-6 ANF-88-088(P), Revision 1, “Design Report for Millstone Point Unit 2, Reload ANF-1,” August 1988.

3.5-7 BNWL-1695, “COBRA-IIIC: A Digital Computer Program for Steady-State and Transient Thermal-Hydraulic Analysis of Rod Bundle Nuclear Fuel Elements,” March 1973.

3.5-8 XN-NF-82-21(P)(A), Revision 1, “Application of Exxon Nuclear Company PWR Thermal Margin Methodology to Mixed Core Configurations,” September 1983.

3.5-9 EMF-2135, Revision 0, “Millstone Unit 2 Cycle 13 Extended Shutdown Safety Analysis Report,” January 1999.

3.5-10 J. A. Boure, A. E. Bergles, and L. S. Tong, “Review of Two-Phase Flow Instability,” ASME Paper 71-HT-42, August 1971.

3.5-11 S. Kakac et. al., “Sustained and Transient Boiling Flow Instabilities in a Cross-Connected Four-Parallel-Channel Upflow System,” Fifth International Heat Transfer Conf., pp. 235-239, Tokyo, Japan (September 1974).

3.5-12 S. A. Eide, “Instability Study for LOFT for L2-1, L2-2 and L2-3 Pretest Steady State Operating Conditions,” RE-A-78-096, Idaho National Engineering Laboratory, November 1978.

3.5-13 J. March-Leuba, “Density-Wave Instabilities in Boiling Water Reactors,” Oak Ridge National Laboratory Report ORNL/TM-12130 (September 1992).

3.5-14 Proceedings of the International Workshop on Boiling Water Reactor Stability, Committee on the Safety of Nuclear Reactors Installations, OECD Nuclear Energy Agency, Holtsville, NY (October 1990).

3.5-15 H. S. Kao, C. D. Morgan, and W. B. Parker, “Prediction of Flow Oscillation in Reactor Core Channel,” Trans. ANS Vol. 16, pp. 212-213 (1973).

3.5-16 A. E. Bergles and M. Suo, “Investigation of Boiling Water Flow Regimes at High Pressure,” Dynatech Corp. NYO-3304-8 (February 1966).

3.5-17 E. R. Hosler, “Flow Patterns in High Pressure Two-Phase (Steam-Water) Flow with Heat Addition,” 9th National Heat Transfer Conference, Chemical Engineering Progress Symposium Series, Number 82, Vol. 64, pp. 54-66 (August 1967).

3.5-18 Weisman et. al., “Experimental Determination of the Departure from Nucleate Boiling in Large Rod Bundles at High Pressure,” 9th National Heat Transfer Conference, Chemical Engineering Progress Symposium Series, Number 82, Vol. 64, pp. 114-125 (August 1967).

3.5-19 Reference Deleted

3.5-20 Letter, R. I. Wescott (SPC) to C. H. Wu (NU), “Transmittal of Bases for New Uncertainties in the Setpoint Analysis for Millstone Unit 2,” RIW:97:049, February 27, 1998.

3.5-21 Reference Deleted by FSARCR 06-MP2-016.

3.5-22 “Qualification of Exxon Nuclear Fuel for Extended Burnup,” XN-NF-82-06(P)(A) Revision 1 and Supplements 2, 4 and 5, Exxon Nuclear Company, October 1986.

3.5-23 EMF-2664, Rev. 0, “Millstone Unit 2 Thermal Hydraulic Compatibility Analysis,” January 2002.

3.5-24 XN-NF-621(P)(A) Revision 1, “Exxon Nuclear DNB Correlation for PWR Fuel Designs,” Exxon Nuclear Company, September 1983.

TABLE 3.5-1 NOMINAL REACTOR AND FUEL DESIGN PARAMETERS

Design and Operating Parameters	Value
Core Rated Power	2700 MWt
Fraction of Heat Generated in Fuel	0.975
Primary System Pressure	2250 psia
Core Inlet Temperature	549°F
Reactor Coolant Flow (Minimum)	360,000 gpm [a]
Assembly Pitch	8.18 inches
Bypass Flow Fraction (Best Estimate)	0.0303
Average Linear Heat Rate	6.206 kW/ft
Total Number of Assemblies	217

a. Flow reductions to 349,200 gpm are compensated for by reductions in the F_r^T and linear heat rate limits.

Fuel Parameters

Design and Operating Parameters	Value
Fuel Rod OD	0.440 inches
Guide Tube OD	1.115 inches
Rod Array	14 by 14
Rod Pitch	0.580 inches
Number of Fuel Rods/Assembly	176
Number of Guide Tubes/Assembly	5
Active Fuel Length	136.7 inches
Total Fuel Rod Assembly Length	146.67 inches (Batch EE and beyond)
Number of Spacers	9

TABLE 3.5-2 DESIGN OPERATING HYDRAULIC LOADS ON VESSEL INTERNALS

Component	Load Description	Load Value
Core Support Barre	Radial pressure differential directed inward opposite inlet duct	40 psi
Core Support Barrel and Upper Guide Structure	Uplift load	480,000 pounds
Flow Skirt	Radial pressure differential directed inward	6.0 psi average, 10.2 psi maximum, over 40° sector
Bottom Plate	Pressure differential load directed upward	43,400 pounds
Core Support Plate	Pressure differential load directed upward	43,100 pounds
Fuel Assembly	Uplift load	1194 lbs at 120% flow
Core Shroud	Radial load directed outward	20.8 psi at bottom, 0.0 psi at top
Upper Guide Structure	Pressure differential load directed upward	148,000 pounds
Fuel Alignment Plate	Pressure differential load directed upward	89,600 pounds
Upper Guide Plate	Pressure differential load directed downward	132,000 pounds
CEA Shrouds	Lateral drag load	4,200 pounds (dual CEA) 1,100 pounds (single CEA)

TABLE 3.5-3 UNCERTAINTY SOURCES FOR DNBR CALCULATIONS (DELETED)

3.A ANALYSIS OF REACTOR VESSEL INTERNALS

3.A.1 SEISMIC ANALYSIS

3.A.1.1 Introduction

Dynamic analyses of the reactor vessel internals for both horizontal and vertical seismic excitation were conducted to provide further bases for assessing the adequacy of their seismic design. These analyses were performed in conjunction with the dynamic seismic analyses of the reactor coolant system (RCS) which is discussed in Appendix 4.A. The following paragraphs provide a discussion of the analytical procedures used for the reactor internals, including a description of the mathematical models. Significant results are listed and compared to the results obtained from application of the design loads.

3.A.1.2 Method of Analysis

3.A.1.2.1 General

The procedure used in conducting the seismic analysis of the reactor internals consisted basically of three steps. The first step involved the formulation of a mathematical model. The natural frequencies and mode shape of the model were determined during the second step. The response of the model to the seismic excitation was determined in the third step. In this analysis, the horizontal and vertical components of the seismic excitation were considered separately and the maximum responses added to obtain conservative results.

3.A.1.2.2 Mathematical Models

For the dynamic analysis of the reactor internals, equivalent multi-mass mathematical models were developed to represent the system. Since the seismic input excitation of the reactor internals was obtained in the form of acceleration time history of the reactor vessel flange, only the internals are included in the model. The coupling effect of the internals' response on the vessel flange acceleration was accounted for by including a simplified representation of the reactor internals with the model of the RCS. This is discussed in Appendix 4.A. Since the horizontal and vertical responses were treated as uncoupled, separate horizontal and vertical models were developed to more efficiently account for the structural differences in these directions. A sketch of the internals showing the relative node locations for the horizontal model is presented in Figure 3.A–1. Figures 3.A–2 and 3.A–3 show the idealized horizontal and vertical models. Since the structural details provide for no vertical load transfer between the upper guide structure (UGS) and core or core shroud, the vertical response of the UGS is independent of the rest of the internals. Consequently, the vertical model was divided into two submodels. Model I consists of the core support barrel/thermal shield (CSB/TS), lower support structure, core shroud and core mass; Model II consists of the UGS.

The mathematical models of the internals are constructed in terms of lumped masses and elastic beam elements. At appropriate locations within the internals, points (nodes) are chosen to lump the weights of the structure. Between these nodes, properties are calculated for moments of

inertia, cross-section areas, effective shear areas, and lengths. The salient details of the models are discussed below.

3.A.1.2.2.1 Hydrodynamic Effects

The dynamic analysis of reactor internals presents some special problems due to their immersion in a confined fluid. It has been shown both analytically and experimentally (Reference 3.A-1) that immersion of a body in a dense fluid medium lowers its natural frequency and significantly alters its vibratory response as compared to that in air. The effect is more pronounced where the confining boundaries of the fluid are in close proximity to the vibrating body as is the case for the reactor internals. The method of accounting for the effects of a surrounding fluid on a vibrating system has been to ascribe to the system additional or "hydrodynamic mass."

This "hydrodynamic mass" decreases the frequencies of the system, but is not directly involved in the inertia force effects. The hydrodynamic mass of an immersed system is a function of the dimensions of the real mass and the space between the real mass and confining boundary.

Hydrodynamic mass effects for moving cylinders in a water annulus are discussed in References 3.A-1 and 3.A-2. The results of these references are applied to the internals structures to obtain the total (structural plus hydrodynamic) mass matrix which was then used in the evaluation of the natural frequencies and mode shapes for the model.

3.A.1.2.2.2 Fuel Assemblies

For the horizontal model, the fuel assemblies are treated as vibrating in unison. The member properties for the beam elements representing the fuel assemblies were derived from the results of experimental tests of the fuel assembly load deflection characteristics and natural frequency.

3.A.1.2.2.3 Core Support Barrel Flanges

To obtain accurate lateral and vertical stiffnesses of the upper and lower flanges, finite element analyses of these two regions were performed. As shown in Figures 3.A–4 and 3.A–5, the flanges were modeled with quadrilateral and triangular ring elements. Asymmetric loads, equivalent to lateral shear loads and bending moments, and symmetric axial loads were applied and the resulting displacements calculated. These results were then used to derive the equivalent member properties for the flanges.

3.A.1.2.2.4 Control Element Assembly Shrouds

For the horizontal model, the control element assembly (CEA) shrouds are treated as vibrating in unison and are modeled as guided cantilever beams in parallel. To account for the decreased lateral stiffness of the UGS due to local bending of the fuel alignment plate, a short member with properties approximating the local bending stiffness of the fuel alignment plate is included at the bottom of the CEA shrouds. Since the stiffness of the UGS support plate is large compared to that of the shrouds, the CEA shrouds are assumed to be rigidly connected to the UGS support plate.

3.A.1.2.2.5 Thermal Shield Supports

For the horizontal model, the thermal shield supports are modeled as horizontal members. The member properties of the beam elements representing the positioning pins were based on the radial stiffness of the circumferential set of pins. Likewise, the properties of the beam member representing the support lugs were based on the tangential stiffness of the circumferential set of lugs. For the vertical model, the equivalent cross-section area of the bar element representing the support lugs was based on the axial bending stiffness of the circumferential set of lugs. For both the horizontal and vertical models, the stiffness of the thermal shield supports includes the effect of local deformation of the core support barrel.

3.A.1.2.2.6 Upper Guide Structure Support Plate and Lower Support Structure Grid Beams

These grid beam structures were modeled as plane grids. Displacements due to vertical (out of plane) loads applied at the beam junctions were calculated through the use of the STRUDL computer code (Reference 3.A-3). Average stiffness values based on these results yielded equivalent member cross-section areas for the vertical model.

3.A.1.2.3 Natural Frequencies and Normal Modes

The mass and beam element properties of the models were utilized in STAR, a computer program from the MRI/STARDYNE Analysis System programs (Reference 3.A-4) to obtain the natural frequencies and mode shapes. This system utilizes the "stiffness matrix" method of structural analysis. The natural frequencies and mode shapes are extracted from the system of equations.

$$[\underline{K}-W_n^2\,\underline{M}]\underline{\phi}_n = 0$$

where:

$\underline{K}$ = Model stiffness matrix
$\underline{M}$ = Model mass matrix
W_n = Natural circular frequency for the n^{th} mode
$\underline{\phi}_n$ = Normal mode shape matrix for n^{th} mode

The mass matrix, $\underline{M}$, includes the hydrodynamic and structural masses.

The natural frequencies and mode shapes calculated for the first 3 modes for the horizontal model are presented in Figures 3.A–6 through 3.A–8. The natural frequencies calculated for the vertical model are presented in Table 3.A-1. The modal data shown is typical and is presented for illustrative purposes. The effect of additional higher modes was included in the response analyses.

3.A.1.2.4 Response Calculations

3.A.1.2.4.1 Horizontal Direction

The time history analysis technique was utilized to obtain the response of the internals for the horizontal seismic excitation. The horizontal excitation was specified as the acceleration time history of the reactor vessel flange, resulting from the operational basis earthquake (OBE) (OBE = 0.09g ground acceleration). The flange excitation resulting from the design basis earthquake (DBE) (DBE = 0.17g ground acceleration) was conservatively specified as 0.17/0.09 times that for the OBE.

The time history response analysis was performed utilizing the MRI STARDYNE System/ DYNRE 1 Computer Program. This program utilizes the "Normal Mode Method" to obtain time history response of linear elastic structure. Details of the program and the "Normal Mode Method" are presented in References 3.A-4, 3.A-5 and 3.A-6.

Input to DYNRE 1 consisted of the modal data as determined in Section 3A.2.3, the modal damping factors, and the forcing function time history. This analysis used the modal data for all modes with frequencies below 100 cps. This included the first 14 modes. Contributions from higher modes are negligible.

The modal damping factors were obtained by the method of "Mass Mode Weighting" which gives:

$$\beta_n = \frac{\Sigma M_i |\phi_{in}| \beta_i}{\Sigma M_i |\phi_{in}|}$$

where:

β_n = Modal damping factor
M_i = Structural mass of mass node i
$|\phi_i|$ = Absolute value of the mode shape as mass mode i
β_i = Damping associated with pass point i

The damping factor assigned to the nodes representing the fuel assemblies was 5 percent. This is a conservative value derived from proprietary experimental results. A value of 1 percent was used for the other nodes.

The output from the DYNRE 1 code consists of the nodal displacement, velocity, and acceleration time history relative to the base. The member bending moments and shears were obtained from the STAR code (Reference 3.A-5) and were derived from the DYNRE 1 nodal displacement vectors at the times of peak response.

3.A.1.2.4.2 Vertical Direction

The response of the reactor internals to the vertical excitation was obtained by the response spectrum technique. Because of the high natural frequencies and resulting low levels of responses for the vertical direction, the more conservative spectrum response analysis results were used instead of time history results. The response spectrum utilized was derived from the vertical acceleration time history at the reactor vessel flange. The spectrum curve is presented in Figure 3.A–9.

An acceleration level corresponding to the natural frequency of each mode was selected from the spectrum curve. The response spectrum technique uses these acceleration values to determine the inertia forces, accelerations, and displacements of each mode. The results for each mode were conservatively combined on the basis of absolute values. For the vertical models, the first seven modes were included in the results.

3.A.1.3 Results

Combined results for the horizontal and vertical dynamic seismic analyses are presented in Table 3.A-2 in terms of stresses at critical locations in the reactor internals for the DBE. Table 3.A-2 also lists the seismic stresses which result from application of the design loads specified for the DBE. A comparison shows the results of the dynamic analysis to be less severe.

3.A.1.4 Conclusion

It is concluded that the seismic loads specified for the design of the internals are adequate. All seismic loads calculated by the dynamic seismic analysis are less than the design loads specified by the DBE.

3.A.2 NORMAL OPERATING ANALYSIS

Design analyses were performed on the reactor internals for normal operating conditions to demonstrate that the mechanical design bases were satisfied. These design calculations included appropriate vibration analyses of the component assemblies. The flow induced vibration of the CSB/TS, during normal operation, was characterized as a forced response to deterministic and random pressure fluctuations in the coolant. Methods were developed for predicting the response of components to the hydraulic forcing functions.

Emphasis was placed on analysis and design of those components which were particularly critical and susceptible to vibratory excitation, such as the thermal shield. Using a top supported, as opposed to a bottom supported, thermal shield design improves stability as it eliminates a free edge in the flow path. Increasing the number of upper supports and lower jackscrews, in the specific manner chosen, provides a much stiffer structure and the use of an all-welded shield eliminates local flexibilities and relative motion at bolted joints. Analytical studies show the thermal shield to be stable on its support system when exposed to the axial annular flow encountered during normal operation. The snubber design is based upon limiting the motion of the core support barrel under conditions of hydraulically induced vibrations. The snubbers are at

the position of maximum amplitude for the fundamental lateral bending mode of the barrel, thereby restricting motion of the barrel at the most efficient position. The circumferential distribution of snubbers assures restraint regardless of the direction of response.

The random hydraulic forcing function was developed by analytical and experimental methods. An analytical expression was developed to define the turbulent pressure fluctuation for fully developed flow. This expression was modified, based upon the result of scale model testing, to account for the fact that flow in the downcomer was not fully developed. Based upon test results, an expression was developed to define the spatial dependency of the turbulent pressure fluctuations. In addition, experimentally adjusted analytical expressions were developed to define; the peak value of the pressure spectral density associated with the turbulence and; the maximum area of coherence, in terms of the boundary layer displacement, across which the random pressure fluctuations are in phase.

The natural frequencies and mode shapes of the CSB/TS system were obtained using the axisymmetric shell finite element computer program, ASHSD (Reference 3.A-7). This computer program is capable of obtaining natural frequencies and mode shapes of complex axisymmetric shells; e.g., arbitrary meridional shape, varying thickness, branches, multi-materials, orthotropic material properties, etc. To employ the ASHSD code, the CSB/TS were modeled as a series of conical shell frustrums joined at their nodal point circles. The length of each element, throughout the ASHSD model, was a fraction of the shell decay length. Since rapid changes in the stress pattern occur in regions of structural discontinuity, the nodal point circles were more closely spaced in such regions. The finite element model of the CSB/TS system included representation of the core support barrel upper and lower flanges, sections of different wall thickness, and thermal shield support lugs and jackscrews. Elements with orthotropic material properties were utilized to provide equivalent axisymmetric models of the structural stiffness and constraints to relative motion between the core support barrel and thermal shield provided by the thermal shield support lugs and jackscrews. Those modes which reflect the mass of the lower support structure, core shroud and fuel were simulated by the addition of concentrated masses at specific nodes in the core support barrel flange finite element model.

Applying Hamilton’s Variational Principle to the conical shell elements an equation of motion was formulated for each degree of freedom of the system. An inverse iteration technique was utilized in the program to obtain solutions to the characteristic equation, which was based on a diagonalized form of a consistent mass matrix and stiffness matrix developed using the finite element method. Four degrees of freedom — radial displacement, circumferential displacement, vertical displacement, and meridional rotation — were taken into account in the analysis, giving rise to coupled mode shapes and corresponding frequencies. Evaluation of the reduction of these frequencies for the system immersed in coolant was made by means of the “virtual mass” method outlined in Reference 3.A-2.

The random response analysis considers the response of the CSB/TS system to the turbulent downcomer flow during steady-state operation. The random forcing function is assumed to be a wide-band stationary random process with a pressure spectral density equal to the peak value associated with the turbulence. The rms vibration level of the CSB/TS system was obtained based upon a damped, single degree of freedom analysis assuming the rms random pressure fluctuation

to be spatially invariant. The analysis demonstrates that the anticipated rms response of the CSB⁄TS system is low. Snubber loads were derived using an analytical technique originally developed by a Combustion Engineering (CE) consultant using the random loads discussed above. Modeling the reactor vessel snubbers and core support barrel system as a single degree of freedom spring-mass system, the number and magnitude of snubber, core support barrel impacts was calculated based upon the response of the system to random excitation. The snubbers were designed, based upon this loading requirement, to meet the cyclic strength requirements specified in Section III of the ASME Boiler and Pressure Vessel Code.

The forced response of the reactor internals to deterministic loading was evaluated by classical analytical methods, using lumped mass and continuous elastic structural models. These calculated responses were used to verify the structural integrity of the reactor vessel internals to normal operating vibratory excitation. Components were design analyzed to assure that there were no adverse effects from dominant excitation frequencies, such as pump rotational and blade passing frequencies.

3.A.3 LOSS OF COOLANT ACCIDENT ANALYSIS

3.A.3.1 Discussion

A dynamic analysis (Reference 3.A-8) has been performed to determine the structural response of the reactor vessel internals to the transient loss of coolant accident (LOCA) loading. The analysis determined the shell, beam and rigid body motions of the internals using established computerized structural response analyses. The finite-element computer code, ASHSD (Reference 3.A-7) was used to calculate the time-dependent beam and shell response of the CSB/TS system to the transient LOCA loading. The finite-element computer code SAMMSOR-DYNASOR (Reference 3.A-9) was used to evaluate the core support barrel's potential for buckling when loaded by a net external radial pressure resulting from an outlet line break. The structural response of the reactor internals to vertical and transverse loads resulting from inlet and outlet breaks, was determined using the spring-mass computer code, SHOCK (Reference 3.A-10).

The time and space dependent pressure loads used in the above analysis were the result of a detailed hydraulic blowdown analysis. The pressure fluctuations were determined for each node in the hydraulic model for inlet and outlet line breaks. The pressure time histories at these nodal locations were then decomposed into the Fourier harmonics which define the circumferential pressure distribution at the nodal elevations. Where the hydraulic model nodes did not correspond to those of the structural model, the hydraulic model pressure components were interpolated to provide the required loading information.

The finite element computer code, ASHSD, was used to calculate the dynamic response of the CSB/TS to transient LOCA loading resulting from an inlet break. To employ the ASHSD code, the CSB/TS were modeled as a series of conical shell frustrums (elements) joined at their nodal point circles. Applying Hamilton's Variational Principle to the conical shell elements a damped equation of motion was formulated for each degree of freedom of the system. Four degrees of freedom — radial displacement, circumferential displacement, vertical displacement and meridional rotation — were taken into account in the analysis, giving rise to coupled modes. The

differential equations of motions were solved numerically using a step integration procedure. To ensure computational stability of the numerical solution, the integration time step was chosen such that it is small compared to the shortest period of the finite element system. The model developed for the CSB/TS system is shown in Figure 3.A–10. The length of each element, throughout the analytical model, was a fraction of the shell decay length. Since rapid changes in the stress pattern occur in regions of structural discontinuity, the nodal point circles were more closely spaced in such regions. The finite element model of the CSB/TS system included representation of the core support barrel upper and lower flanges, sections of different wall thickness, and thermal shield support lugs and jackscrews. Elements with orthotropic material properties were utilized to provide equivalent axisymmetric models of the structural stiffness and constraints to relative motion between the core support barrel and thermal shield provided by the thermal shield support lugs and jackscrews. Those modes which reflect the mass of the lower support structure, core shroud and fuel were stimulated by the addition of concentrated masses at specific nodes in the core support barrel flange finite element model.

In performing the dynamic analysis of the CSB/TS system, the transient load harmonics were applied in two successive phases to account for time-dependent boundary conditions at the snubbers. The first phase used those harmonics which excite the beam modes, whereas the second phase used those harmonics which excite the shell modes. During the first phase, the lower end of the core support barrel was unrestrained. Within a very few milliseconds, the clearances between the core support barrel and reactor vessel snubbers were closed and for the remainder of the LOCA transient, the core support barrel was restrained radially at the snubber level. Transient responses were computed throughout each loading phase.

The ASHSD code computed the nodal point displacement, resultant shell forces, shell stresses and maximum principle stresses as functions of time. The maximum principle stresses at the internal and external surfaces of the CSB/TS were determined from the bending and membrane components during each phase of transient loading. Stress intensity levels calculated from the principle stresses were combined with normal operating and seismic induced stresses for comparison with design criteria.

Accurate representation and analysis of the CSB/TS shell structures was obtained through use of the finite element code ASHSD. Accurate representation of the remainder of the internals (i.e., fuel, core shroud, CEAs, UGS, lower support structure, etc.) was obtained using the SHOCK code.

The SHOCK code determines the response of structures which are represented as lumped-mass systems and subjected to arbitrary loading functions. The code solves the differential equations of motion for each mass by a numerical step-integration procedure. The lumped mass model can represent a vertically or laterally responding system subject to arbitrary loading functions and initial conditions. Options are available for describing steady state loads, preloads, input accelerations, linear and nonlinear springs (including tension and compression only springs) gaps, and structural and viscous damping.

The reactor internals were developed in terms of a spring-mass system for both vertical and lateral directions; see Figures 3.A–11 and 3.A–12. For both models, the spring rates were generally

evaluated using strength of material techniques. However, in complex areas such as at the core support barrel flanges and UGS support flange, the stiffness was derived from finite element model analyses. The lumped mass weights were generally based upon the mass distribution of the uniform support structures, but included at appropriate nodes, local masses such as snubber blocks, fuel end fittings, thermal shield lugs, etc. The net result was a lumped-mass system having the same distribution of mass as the actual structure. To simulate the effect associated with the internals oscillating laterally in the water filled vessel, a distributed virtual mass was calculated based upon the procedure outlined in Reference 3.A-8 (which includes the annulus effect) and was added to the structural lumped-mass system, to provide an analytical model with a dynamic response quantitatively similar to the actual internals. In the case of the vertical model, the hydraulic effect is notably one of reducing the effective weight of the reactor internals and this effect was included in the structural lumped-mass system.

The SHOCK code provided excellent facility for modeling clearances, preloads and component interfaces. In the lateral model, the core support barrel, reactor vessel snubber clearance was simulated by a nonlinear spring which accounted for the increased resistance to core support barrel motion when snubbing occurred. In the vertical model, nonlinear springs in the form of compression only springs, were used extensively to simulate preload and interface conditions, such as exist between the UGS support plate and core support barrel upper flange; at the fuel hold-down spring; at the fuel, core support plate interface and at the core shroud, core support plate interface. Tension only springs were used to simulate the effect of the core shroud tie rods.

In both the vertical and lateral SHOCK models, damping was varied throughout the system to simulate structural and hydraulic frictional effects within the reactor internals. The effect of hydraulic drag in the vertical model was simulated by a force time-history applied to the fuel lower end-fitting. Vertical loads were used directly from the detailed hydraulic analysis, whereas lateral loads were obtained by integrating those harmonics which excite the beam modes to obtain the net lateral load on the CSB/TS system.

The SHOCK code calculated the vertical and lateral response of the system in terms of displacements, velocities and accelerations and internal force, moments and shears as related to each model. These quantities were sufficient to permit calculation of membrane and where appropriate bending stresses for comparison with design criteria.

The finite-element code SAMMSOR-DYNASOR was used to determine the dynamic response of the core support barrel, with initially imperfect geometry, to a net external radial pressure resulting from an outlet line break. The above analysis has the capability of determining the nonlinear dynamic response of axisymmetric shells with initial imperfections subjected to arbitrarily varying load configurations.

Since SAMMSOR-DYNASOR is a finite-element program, a model was developed, Figure 3.A–13, of the core support barrel using axisymmetric finite-elements similar to those used for the ASHSD analysis. As was for the ASHSD model, the SAMMSOR-DYNASOR finite-element lengths were considerably less than the decay length of the core support barrel. The boundary condition at the core support barrel flange was considered fixed, whereas at the core support barrel lower flange radial displacements were restrained. These boundary conditions represented

the restraint due to the expansion compensating ring and pressure vessel head at the top and the snubbers and lower support structure at the bottom. For conservatism, the stiffening effects of the fuel alignment plate, core shroud and core support plate were neglected.

Since the basic phenomenon in buckling is nonlinear instability, the initial deviation of the structure from a perfect geometry greatly affects its response. The initial imperfection was applied to the core support barrel by means of a pseudo-load so developed to provide the maximum imperfection over each of the desired number of circumferential harmonics. The actual transient loading in terms of its harmonics was applied to the initially “imperfect” geometry core support barrel and the response obtained for each of the imperfection harmonics for the combined loading harmonics.

3.A.3.2 Analysis Codes

ASHSD (Reference 3.A-7) is a structural finite-element computer code developed at the University of California, Berkeley, and supported in part by the National Science Foundation. It performs dynamic analyses of complex axisymmetric structures subjected to arbitrary dynamic loadings or base accelerations. The frequencies of free vibrations as calculated by ASHSD compare well to those calculated by the equations of Hermann-Mirshy and Flugge, References 3.A-11 and 3.A-12, respectively. The authors also make comparisons with available experimental results (Reference 3.A-13) of free vibrations of cylindrical shells. The resulting comparison is good. Comparison of the numerical solution (Reference 3.A-14) of the dynamic response of a shell to suddenly applied loads and the finite-element (ASHSD) solution of the same problem are in good agreement. The response of a shell to a moving axisymmetric pressure load was evaluated by ASHSD and analytically (Reference 3.A-15) with the results being in good agreement.

SAMMSOR-DYNASOR (Reference 3.A-9) is a finite-element computer code developed at Texas A&M University and supported in part by a NASA grant from the Manned Spacecraft Center, Houston, Texas. This code has the capability of determining the nonlinear dynamic response of axisymmetric shells subjected to arbitrary dynamic loads. Asymmetrical dynamic buckling can be investigated using this program. The program has been extensively tested, using problems the solutions to which have been reported by other researchers, in order to establish the validity of the codes. Among these are a shallow shell with axisymmetric loading as described in Reference 3.A-16. Identical results are obtained with those of Reference 3.A-17 for the analytical evaluation of blast loadings on a cylindrical shell. Calculations made by SAMMSOR-DYNASOR for the symmetric buckling of a shallow spherical cap is in good agreement with the analyses of References 3.A-18 and 3.A-19 and the experimental data of References 3.A-20 and 3.A-21.

SABOR-5 - DRASTIC, (Reference 3.A-22) is a structural finite-element computer code developed at the Aeroelastic and Structures Research Laboratory, Department of Aeronautics at the Massachusetts Institute of Technology. The work was administered by the Air Force Systems Command with technical monitoring by the Aerospace Corp. SABOR 5 - DRASTIC is the end result of combining a finite-difference solution procedure and a finite-element program to permit predicting the transient response of complex shells of revolution which are subjected to arbitrary transient loadings. Comparisons with reliable independent analytical predictions (notably finite-

difference transient response solutions submitted by AVCO) confirm the accuracy and reliability of the SABOR 5 -DRASTIC dynamic response predictions. An experiment and accompanying analysis were performed by the Aerospace Corp. (Reference 3.A-23) to verify the ability of the code to account for a complex geometry shell of revolution subjected to transient asymmetric loads. Loads were applied by means of well-defined explosive charges. Based upon the results of dynamic strain measurements made on the test structure, it is evident that the SABOR 5 - DRASTIC code is capable of solving complex dynamic shell structure problems successfully.

In developing the above finite-element computer codes, (i.e., ASHSD, SAMMSOR-DYNASOR, SABOR 5 - DRASTIC) the authors have independently verified their codes with respect to the results of other established structural programs, classical solutions and as possible to experimental data. The correlations demonstrate that the above programs are capable of solving complex dynamic shell structure problems successfully and that the finite-element method of modeling provides accurate representation of the structural phenomena. The SABOR 5 - DRASTIC code, which has had extensive and successful analytical and experimental correlation (Reference 3.A-6) for transient (explosive) asymmetric loading, was used to analyze a core support barrel structure with short-term loading. The results of this well-verified program are identical to these of the finite-element codes ASHSD and SAMMSOR-DYNASOR (which are used in the LOCA analysis) for the same core support barrel problem, demonstrating the ability of these programs to adequately represent and evaluate the effect of a transient load on an axisymmetric structure like the core support barrel.

3.A.4 EFFECTS OF THERMAL SHIELD REMOVAL

Following the discovery of the thermal shield support degradation at the end of Cycle 5 in July, 1983, the thermal shield was removed. A detailed inspection of the core barrel revealed damage at two thermal shield support lug locations. Repairs to the core barrel comprised of drilling crack arrestor holes at the ends of through-wall cracks and removal by machining of non through-wall cracks.

Analytical evaluations and assessments were performed to demonstrate continued structural adequacy of the reactor internals without the thermal shield for all design loading conditions. Special attention was paid to the core barrel to justify the repairs. A description of the repairs to the core barrel, analyses, and significant results is given in Reference 3.A-24.

In conclusion, there was no significant change in the loads and the stresses in the internal structures remained within the ASME Code allowables.

3.A.5 LEAK-BEFORE-BREAK ANALYSIS

Leak-Before-Break (LBB) analyses for the reactor coolant system (RCS) main coolant loops, for the pressurizer surge line, and unisolable RCS portions of the safety injection and shutdown cooling piping, which demonstrated that the probability of fluid system piping rupture was extremely low, was reviewed and approved by the commission. (See References 3.A-25 through 3.A-29.) Subsequent to the commission review and approval, weld overlays were applied to dissimilar metal welds (DMWs) at the shutdown cooling, the safety injection and the pressurizer

surge nozzles. A revised LBB analysis was performed for these nozzles (see Reference 3.A-30). Accordingly, pursuant to revised GDC 4, the dynamic effects associated with pipe ruptures in the above piping segments, including the effects of pipe whipping and discharging fluids have been excluded from the design basis of the following reactor vessel and reactor internals components:

Core barrel snubbers, core barrel stabilizer blocks
Reactor vessel core support ledge
Reactor Cavity Seal Plate, Neutron Shielding

3.A.6 REFERENCES

3.A-1 Fritz, R. J., and Kiss, E., "The Vibration Response of a Cantilevered Cylinder Surrounded by an Annular Fluid," KAPL-M-6539, February 1966.

3.A-2 Kiss, E., "Analysis of the Fundamental Vibration Frequency of a Radial Vane Internal Steam Generator Structure," ANL-7685, Proceedings of Conference on Flow-Induced Vibrations in Reactor System Components, May 1970, Argonne National Laboratory, Argonne, IL.

3.A-3 ICES STRUDL-II, The Structural Design Language Engineering Users' Manual.

3.A-4 "MRI/STARDYNE - Static and Dynamic Structural Analysis System: User Information Manual," Control Data Corporation, June 1, 1970.

3.A-5 MRI/STARDYNE User Manual, Computer Methods Department, Mechanics Research, Inc., Los Angeles, California, January 1, 1970.

3.A-6 Hurty, W. C., and Rubinstein, M. F., "Dynamics of Structures," Chapter 8, Prentice Hall, Inc., Englewood Cliffs, New Jersey, 1964.

3.A-7 Ghosh, S., Wilson, E., "Dynamic Stress Analysis of Axisymmetric Structures Under Arbitrary Loading," Dept. No. EERC 69-10, University of California, Berkeley, September 1969.

3.A-8 CENPD-42, "Topical Report on Dynamic Analysis of Reactor Vessel Internals Under Loss of Coolant Accident Conditions with Application of Analysis to C-E 800 Mw(e) Class Reactors," August 1972.

3.A-9 Tillerson, J. R., Haisler, W. E., "SAMMSOR II - A Finite Element Program to Determine Stiffness and Mass Matrices of Shells-of- Revolution," Texas A&M University, TEES-RPT-70-18, October 1970. "DYNASOR II - A Finite Element Program for the Dynamic Nonlinear Analysis of Shells-of-Revolution," Texas A&M University, TEES-RPT-70-19, October 1970.

3.A-10 Gabrielson, V. K., "SHOCK - A Computer Code for Solving Lumped-Mass Dynamic Systems," SCL-DR-65-34, January 1966.

3.A-11 Hermann, G., Mirshy, I., "Three Dimensional Shell Theory Analysis of Axially Symmetric Motions of Cylinders," Journal of Applied Mechanics, Trans. ASME, Vol. 78, P. 563-568, 1956.

3.A-12 Flugge, W., "Stresses in Shells," Third Printing, Springer-Verlag, New York, 1966.

3.A-13 Koval, L. R., Cranch, E. I., "On the Free Vibrations of Thin Cylindrical Shells Subjected to Initial Torque," Proceedings of the U. S. National Congress of Applied Mechanics, P. 11, 1962.

3.A-14 Reismann, H., and Padloy, J., "Forced, Axisymmetric Motions of Cylindrical Shells," Journal of the Franklin Institute, Vol. 284, Number 5, November 1967.

3.A-15 Tang, Sing-Chih, "Response of a Finite Tube to Moving Pressure," Journal Engineering Mechanics Division, ASCE, Vol. 93, Number EM3, June 1967.

3.A-16 Klein, S., and Sylvester, R. J., "The Linear Elastic Dynamic Analysis of Shells of Revolution by the Matrix Displacement Method," Air Force Slight Dynamics Laboratory, TR-66-80, 1966, P. 299-329.

3.A-17 Johnson, D. E., Grief, R., "Dynamic Response of a Cylindrical Shell: Two Numerical Methods," AIAA Journal, Vol. 4, Number 3, March 1966, P. 486-494.

3.A-18 Huang, N. C., "Axisymmetric Dynamic Snap-through of Elastic Clamped Shallow Spherical Shells," AIAA Journal, Vol. 7, Number 2, February 1969, P. 215-220.

3.A-19 Stephen, W. B., and Fulton, R. E., "Axisymmetric Static and Dynamic Buckling of Spherical Caps due to Centrally Distributed Pressures," Paper 69-89, AIAA Journal, 1969.

3.A-20 Lock, M. H., Okrebo, S., and Whittier, J. S., "Experiment of the Snapping of a Shallow Dome Under a Step Pressure Loading," AIAA Journal, Vol. 6, No. 7, July 1968, P. 1320-1326.

3.A-21 Stricklin, J. A., and Martinez, J. E., "Dynamic Buckling of Clamped Spherical Caps Under Step Pressure Loadings," AIAA Journal, Vol. 7, Number 6, June 1969, P. 1212-1213.

3.A-22 Kotanchik, J. J., et al., "The Transient Linear Elastic Response Analysis of Complex Thin Shells of Revolution Subjected to Arbitrary External Loadings, by the Finite-Element Program SABOR 5 - DRASTIC," AD-709-189, Massachusetts Institute of Technology, April 1970.

3.A-23 Klein, S., "A Static and Dynamic Finite Element Shell Analysis with Experimental Verification," International Journal for Numerical Methods in Engineering, Vol. 3, P. 299-315, 1971.

3.A-24 “Thermal Shield Damage Recovery Program - Final Report,” Northeast Nuclear Energy Company, Millstone Nuclear Power Station, Unit Number 2, Docket No. 50-336, License No. DPR-65, December, 1983.

3.A-25 NRC Letter from D. G. McDonald, Jr. to M. L. Bowling, Jr., “Revised Evaluation of the Primary Cold Leg Piping Leak - Before-Break Analysis for the Millstone Nuclear Power Station, Unit Number 2,” dated November 9, 1998.

3.A-26 NRC Letter from D. G. McDonald, Jr. to M. L. Bowling, Jr., “Application of Leak - Before-Break Status to the Portions of the Safety Injection and Shutdown Cooling System for the Millstone Nuclear Power Station, Unit Number 2,” dated November 9, 1998.

3.A-27 NRC Letter from B. Eaton to R. P. Necci, “Staff Review of the Submittal by Northeast Nuclear Energy Company to Apply Leak-Before-Break Status to the Pressurizer Surge Line, Millstone Nuclear Power Station, Unit 2,” dated May 4, 1999.

3.A-28 NRC Letter from G.S. Vissing to J.F. Opeka, “Application of Reactor Coolant System Leak-Before-Break Analysis,” dated September 1, 1992.

3.A-29 Federal Register/Volume 53, No. 66/April 6, 1988, “10 CFR Part 50 Leak Before Break Technology Solicitation of Public Comment on Additional Applications.”

3.A-30 Structural Integrity Associates Report: 0901238.401, Revision 0, dated: December 2010, Updated Leak-Before-Break Evaluation of Weld Overlaid Hot Leg Surge, Shutdown Cooling and Safety Injection Nozzles for Millstone Nuclear Power Station, Unit 2.

TABLE 3.A-1 NATURAL FREQUENCIES FOR VERTICAL SEISMIC ANALYSIS MATHEMATICAL MODEL

Mode Number	Sub-Model I Frequency, cps	Sub-Model II Frequency, cps
1	21.60	72.98
2	67.75	404.09
3	124.59	-

TABLE 3.A-2 SEISMIC STRESSES IN CRITICAL REACTOR INTERNALS COMPONENTS FOR THE DESIGN BASIS EARTHQUAKE

Structural Component	Location	Stress Mode	Design Load Stress	Dynamic Analysis Stress
Core Support Barrel	Upper Section of Barrel	Tension & Bending	1,129 psi	746 psi
Lower Core Support	Beam Flange	Bending	5,278 psi	929 psi
CEA Shrouds: Single	End of Shroud	Tension & Bending	3,548 psi	1,295 psi
CEA Shrouds: Dual	End of Shroud	Tension & Bending	2,762 psi	697 psi
Upper Grid Beams	Center of Beam	Bending	1,652 psi	127 psi
Upper Guide Structure Flange	Junction of Flange & Barrel Cylinder	Tension & Bending	2,823 psi	146 psi

FIGURE 3.A–1 REPRESENTATIVE NODE LOCATIONS - HORIZONTAL MATHEMATICAL MODEL

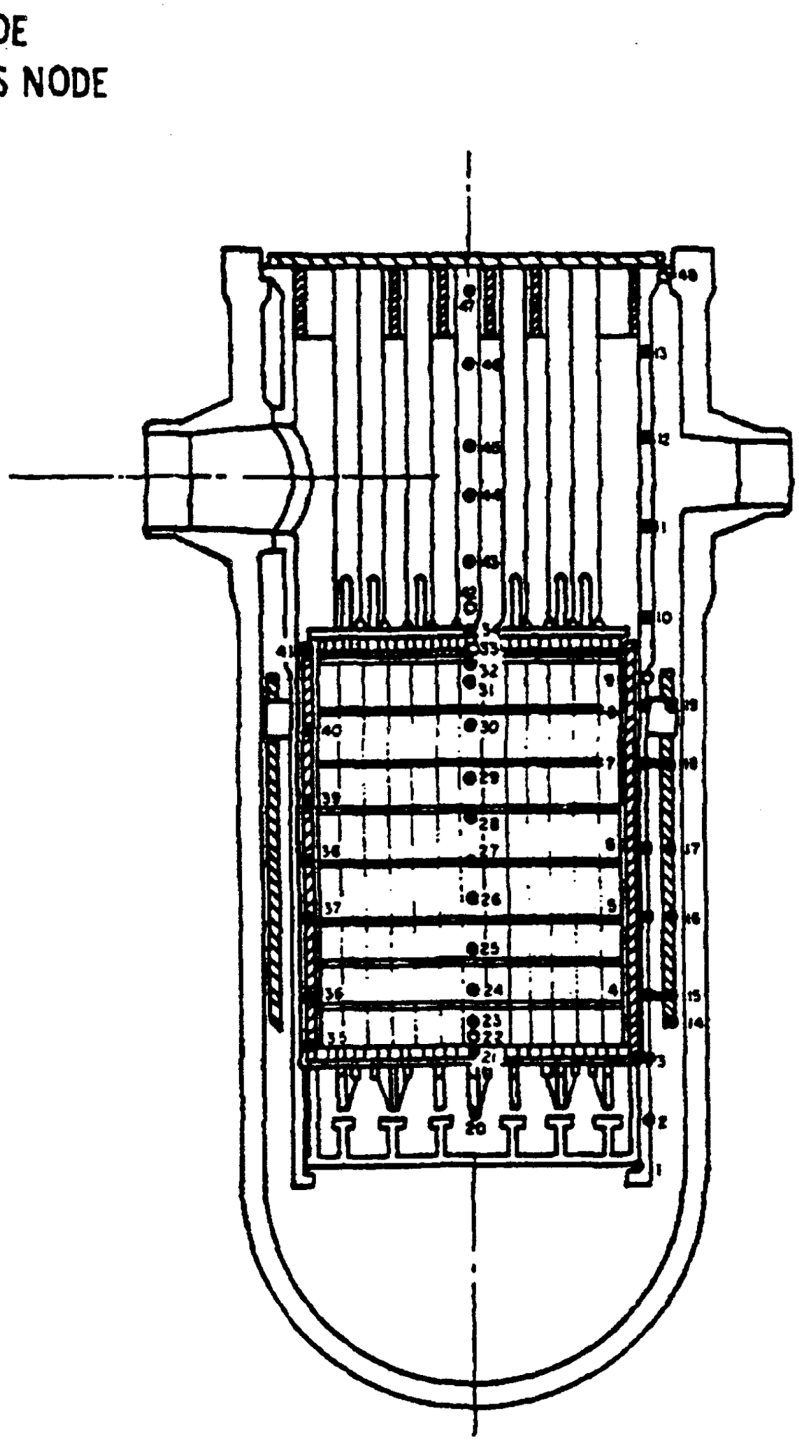

FIGURE 3.A–2 MATHEMATICAL MODEL - HORIZONTAL SEISMIC ANALYSIS

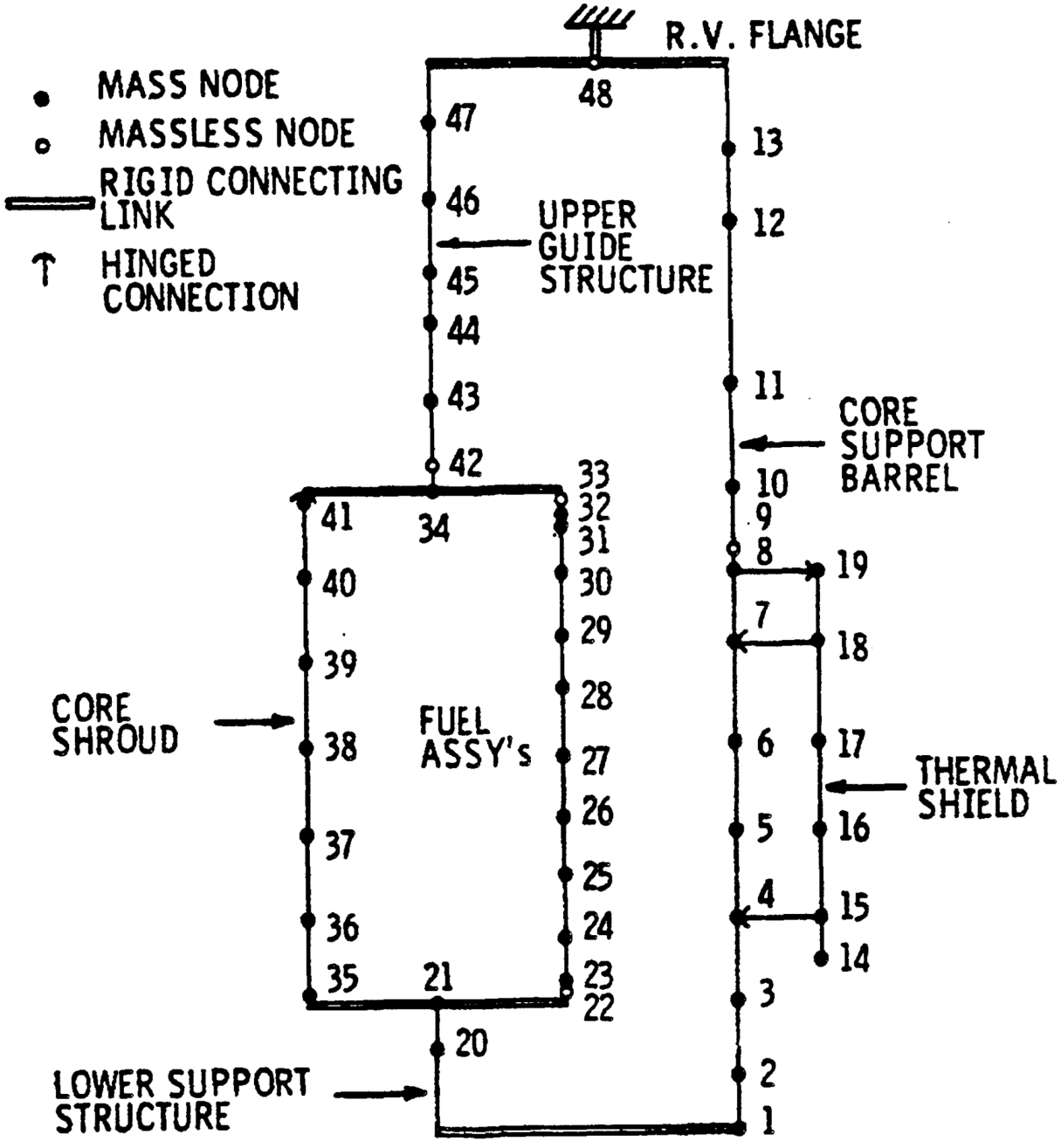

FIGURE 3.A–3 MATHEMATICAL MODEL - VERTICAL SEISMIC ANALYSIS

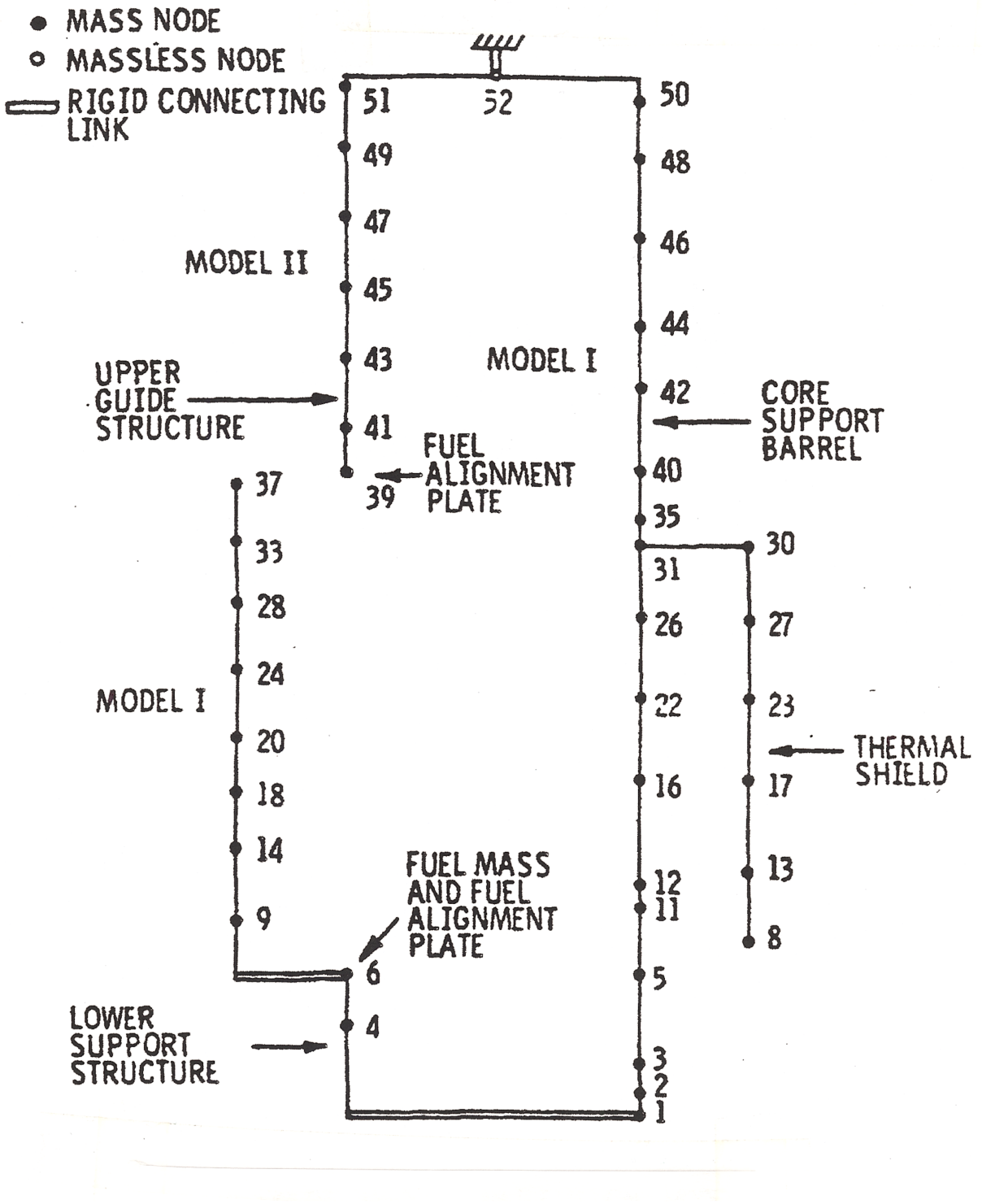

FIGURE 3.A–4 CORE SUPPORT BARREL UPPER FLANGE - FINITE ELEMENT MODEL

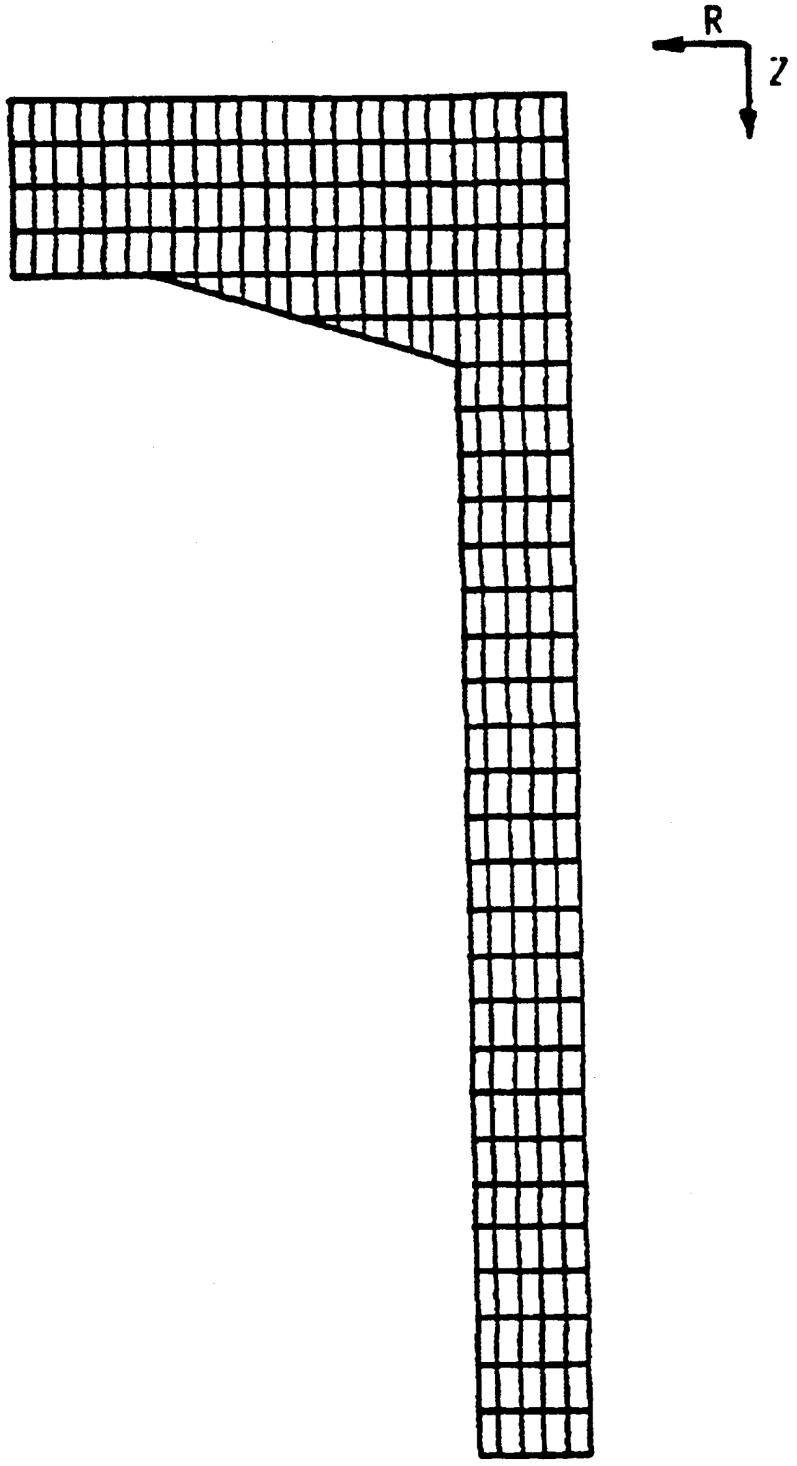

FIGURE 3.A–5 CORE SUPPORT BARREL LOWER FLANGE - FINITE ELEMENT MODEL

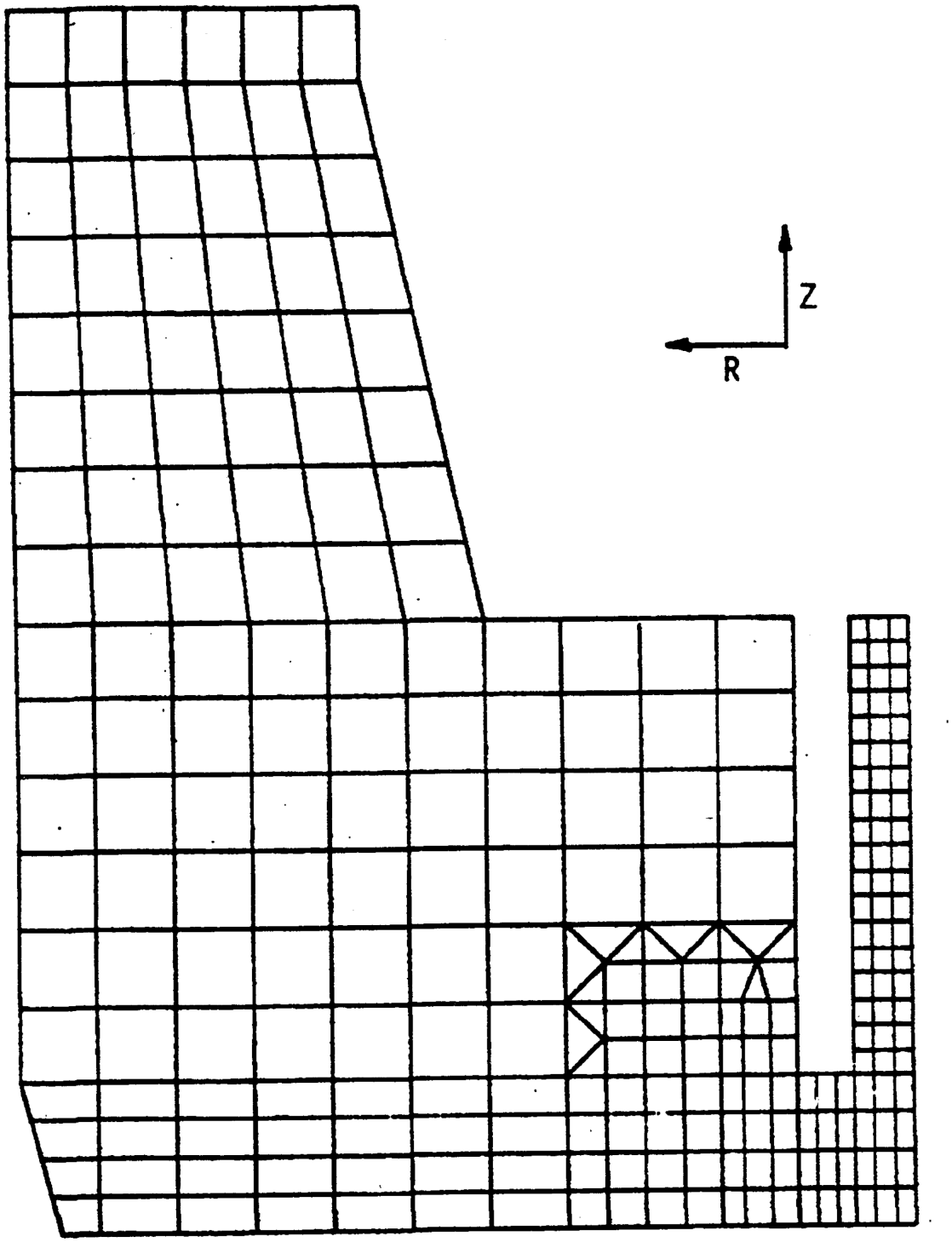

FIGURE 3.A–6 LATERAL SEISMIC MODEL - MODE 1, 3.065 CPS

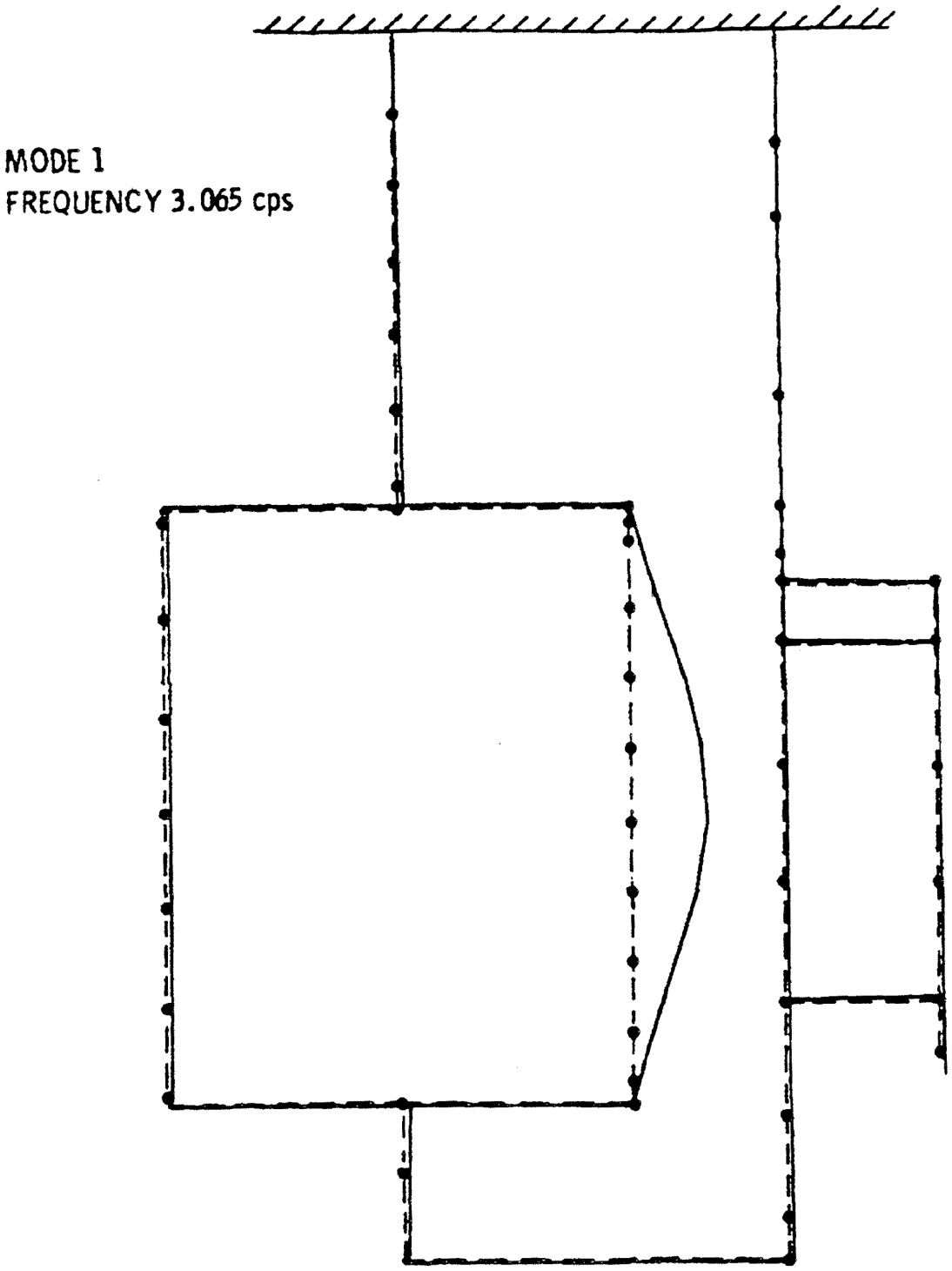

FIGURE 3.A–7 LATERAL SEISMIC MODEL - MODE 2, 5.118 CPS

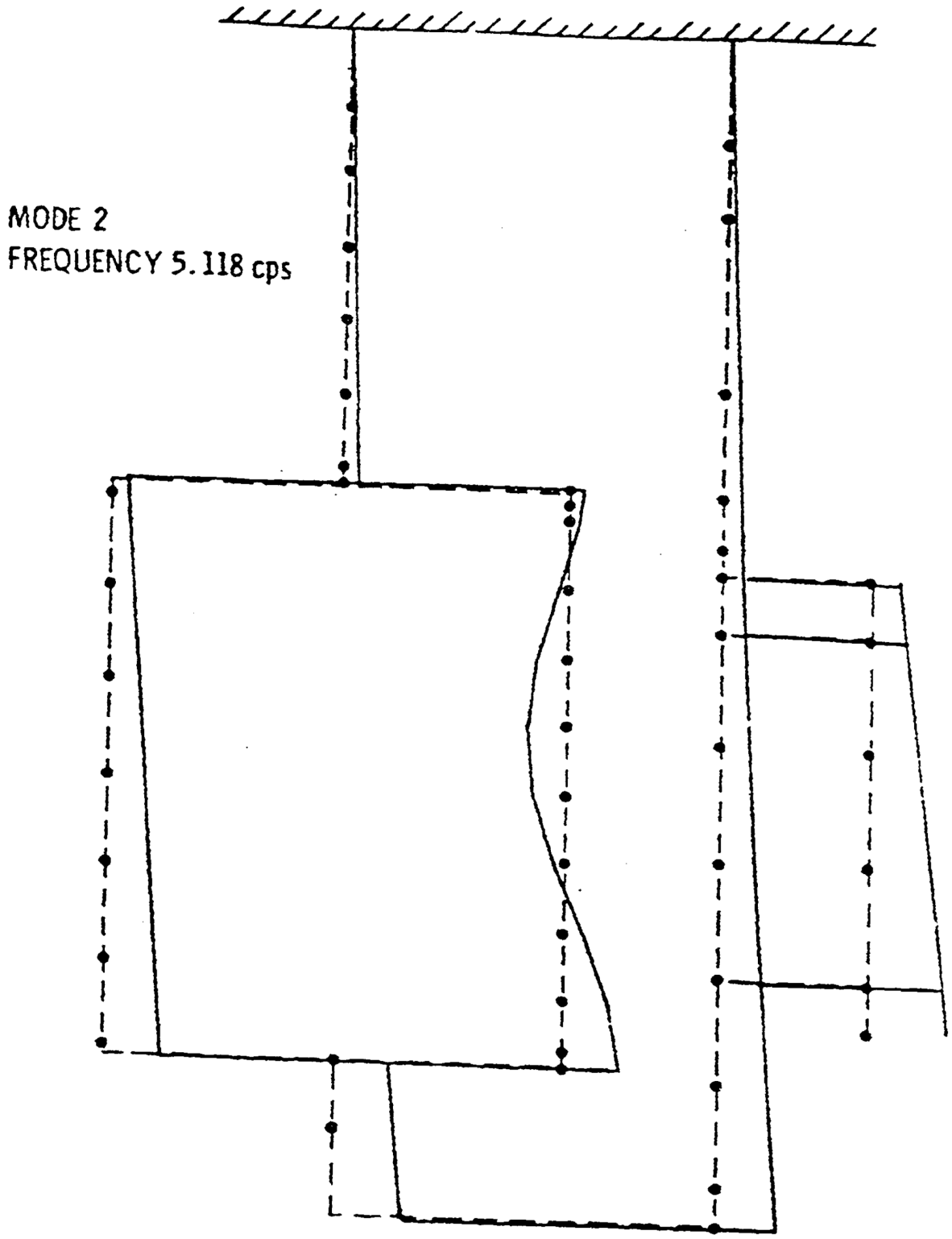

FIGURE 3.A–8 LATERAL SEISMIC MODEL - MODE 2, 5.118 CPS

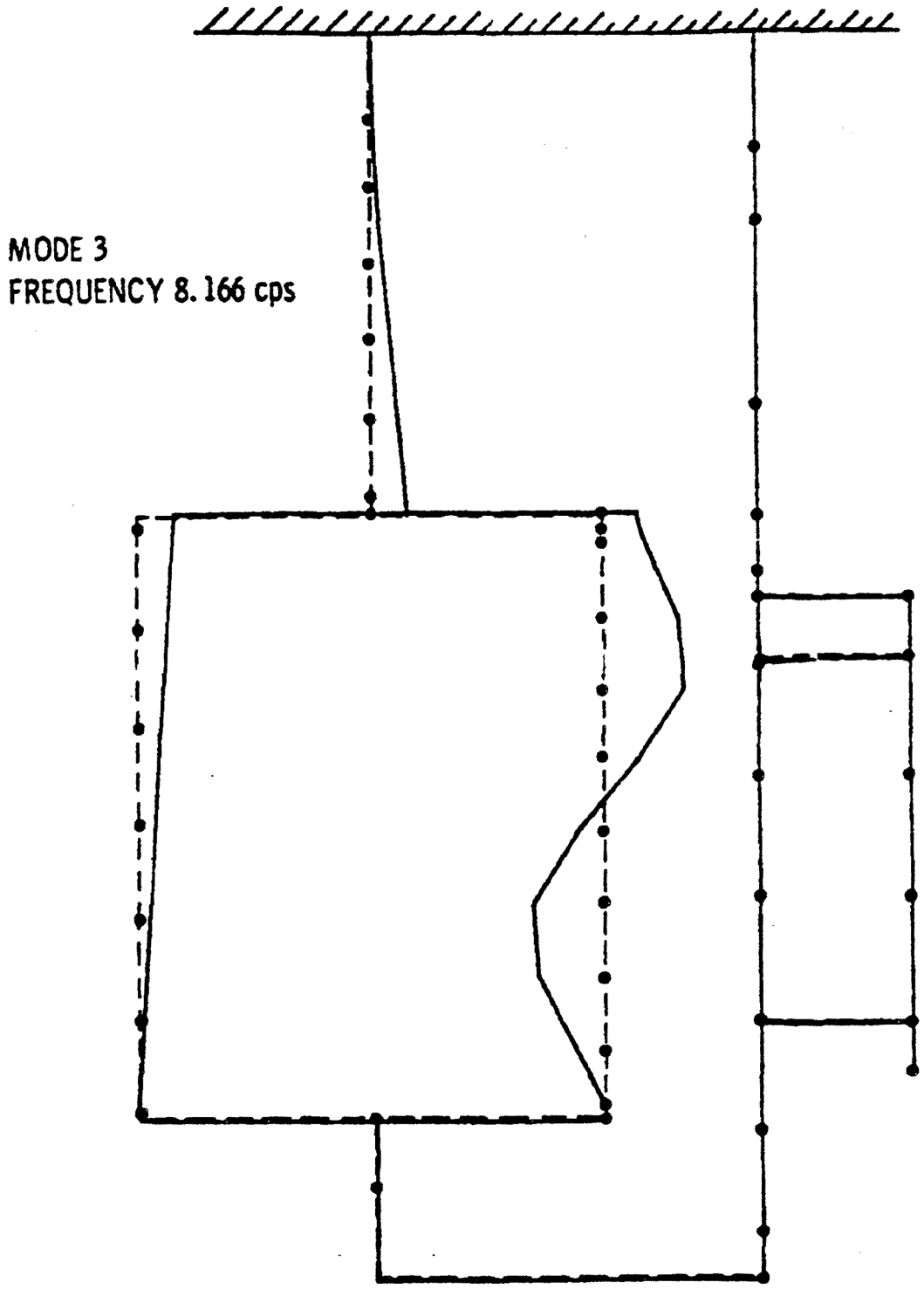

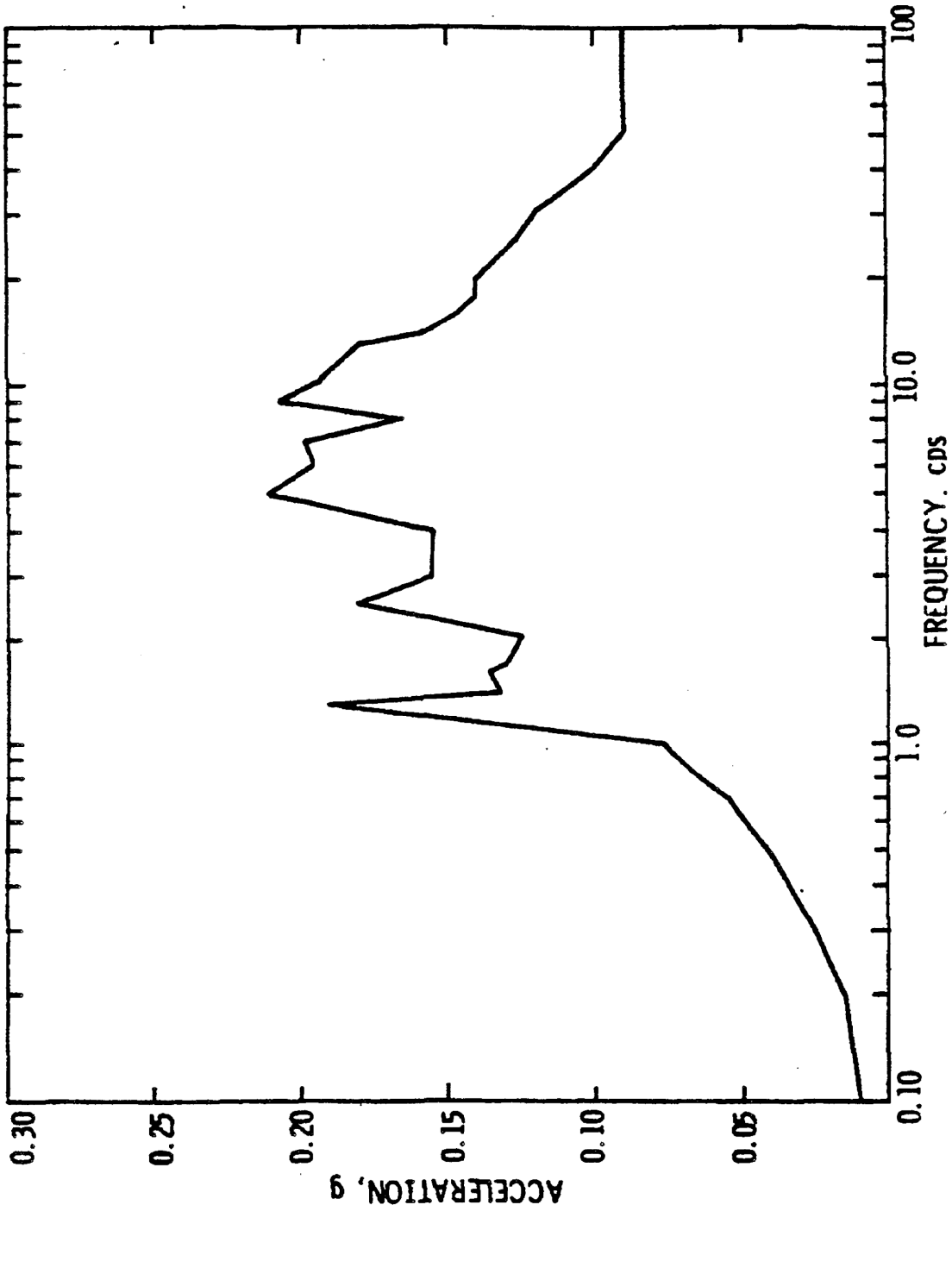

FIGURE 3.A–9 REACTOR VESSEL FLANGE VERTICAL RESPONSE SPECTRUM (1% DAMPING)

FIGURE 3.A–10 ASHSD FINITE ELEMENT MODEL OF THE CORE SUPPORT BARREL/THERMAL SHIELD SYSTEM

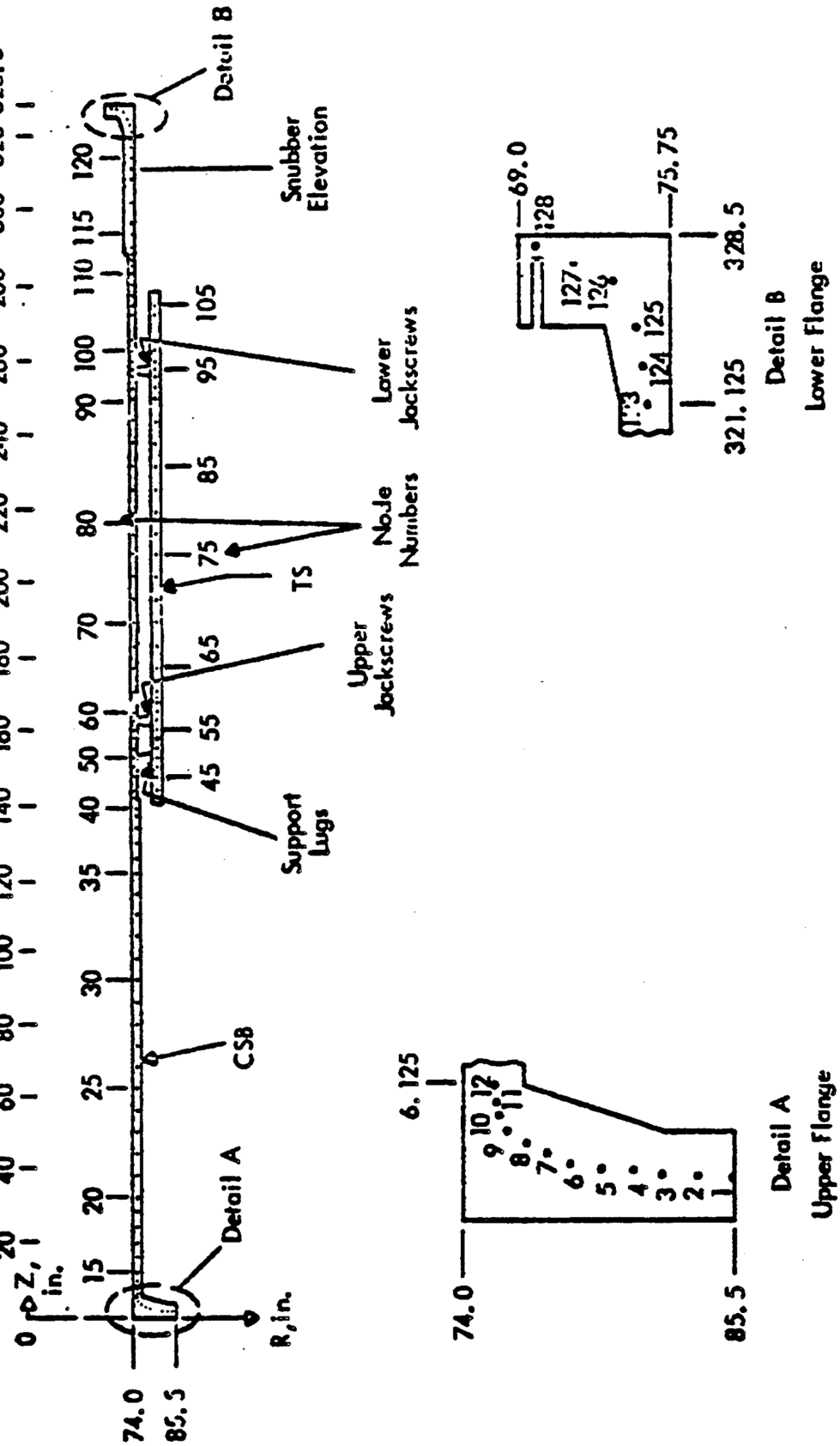

FIGURE 3.A–11 VERTICAL SHOCK MODEL

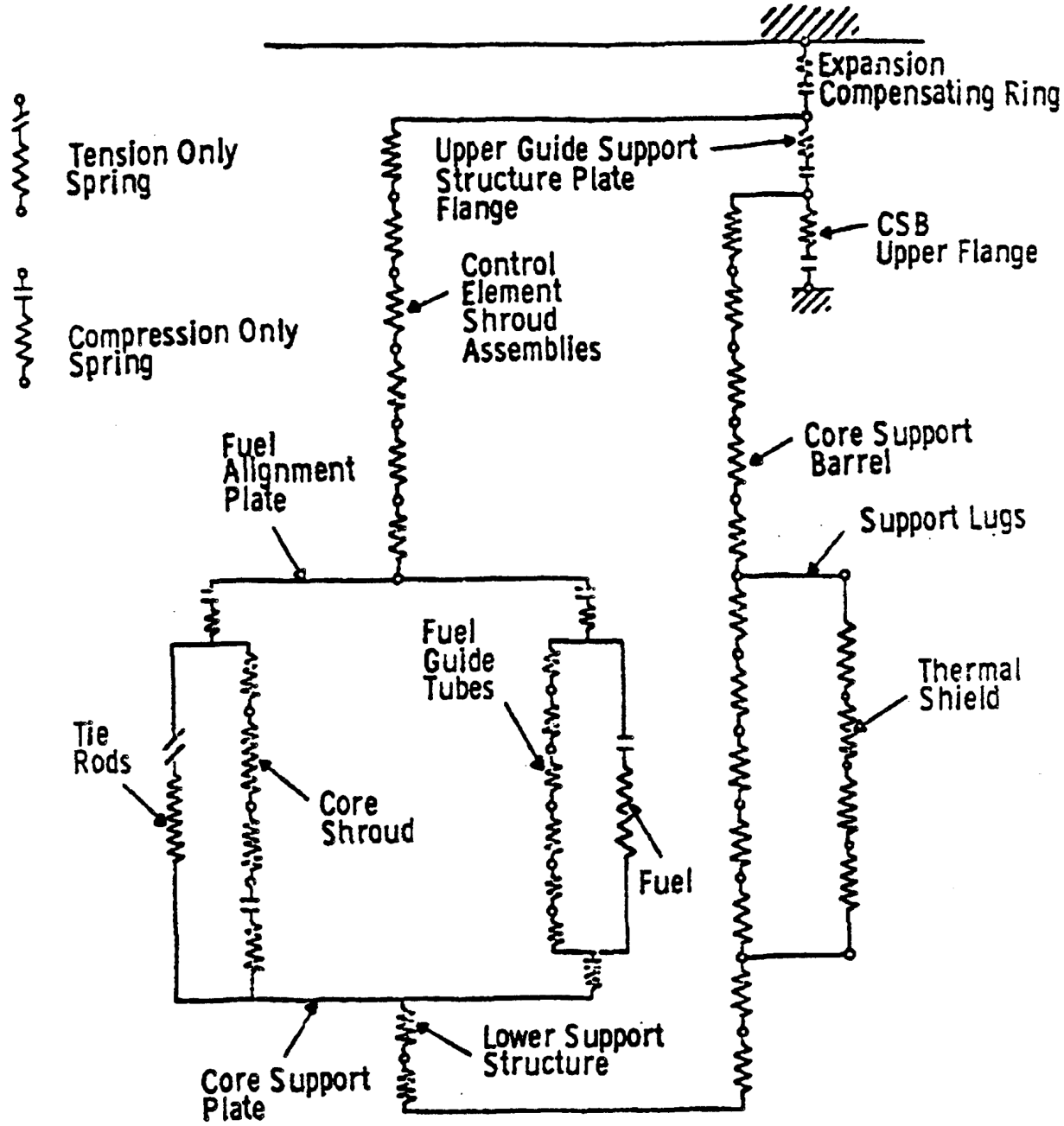

FIGURE 3.A–12 LATERAL SHOCK MODE

APRIL, 199(

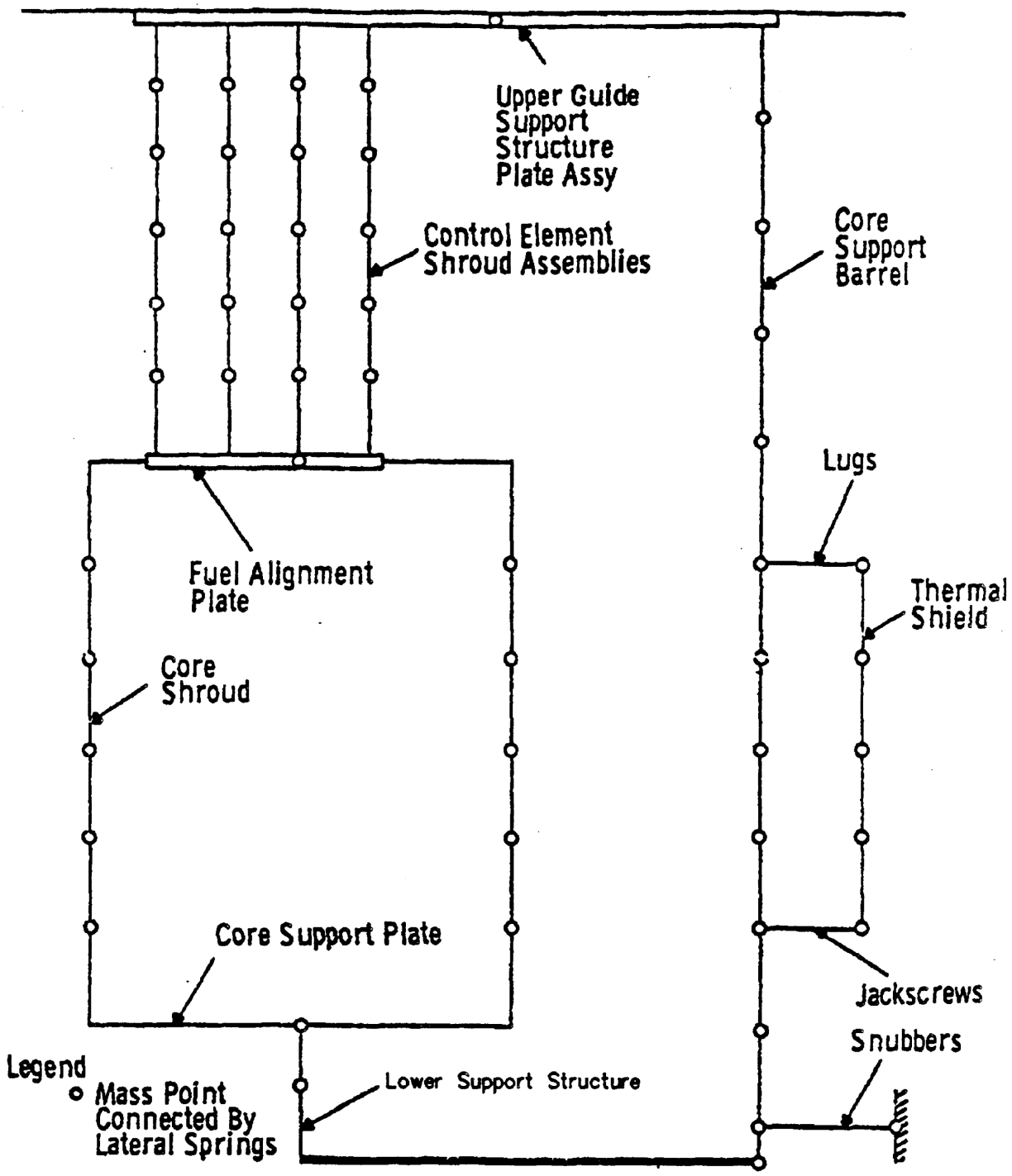

FIGURE 3.A–13 SAMMSOR DYNASOR FINITE ELEMENT MODEL OF CORE SUPPORT BARREL